PRESSURE-INDUCED GROWTH AND REMODELING OF ARTERIES IN A PORCINE AORTIC COARCTATION MODEL

A Dissertation

by

JIN-JIA HU

Submitted to the Office of Graduate Studies of
Texas A&M University
in partial fulfillment of the requirements for the degree of

DOCTOR OF PHILOSOPHY

December 2005

Major Subject: Biomedical Engineering

PRESSURE-INDUCED GROWTH AND REMODELING OF ARTERIES IN A PORCINE AORTIC COARCTATION MODEL

A Dissertation

by

JIN-JIA HU

Submitted to the Office of Graduate Studies of
Texas A&M University
in partial fulfillment of the requirements for the degree of

DOCTOR OF PHILOSOPHY

Approved by:

Chair of Committee,	Jay D. Humphrey
Committee Members,	John C. Criscione
	Christopher Quick
	Emily Wilson
Head of Department,	Gerard L. Coté

December 2005

Major Subject: Biomedical Engineering

ABSTRACT

Pressure-induced Growth and Remodeling of Arteries in a Porcine Aortic Coarctation Model. (December 2005)

Jin-Jia Hu, B.S., National Taiwan University;

M.S., National Taiwan University

Chair of Advisory Committee: Dr. Jay D. Humphrey

Hypertension is a risk factor for many cardiovascular and cerebrovascular diseases such as atherosclerosis and stroke. It is therefore important to understand the effect of hypertension on temporal growth and remodeling of arteries. In this study, experimental hypertension was induced in the mini-pig by aortic coarctation. Basilar arteries and aortas were collected for analysis over an eight week period of hypertension with specimens from normotensive animals serving as controls. Changes in mechanical properties of the basilar artery were evaluated by in vitro pressure-diameter tests on intact cylindrical segments at their in situ length. The basilar arteries from hypertensive animals became less distensible, reflecting increases in both structural and material stiffness, compared to their normotensive counterparts. The circumferential stress rapidly returned toward its homeostatic value by increasing the wall thickness within two weeks. Immunohistochemistry, which is capable of illustrating the localization and distribution of protein expression, was performed to examine changes in wall constituents in the aorta. The increased medial thickness observed in hypertensive pigs compared to normotensive pigs was due to hyperplasia of smooth muscle cells (SMCs) and accumulation of extracellular matrix proteins, which were accompanied by the

phenotypic modulation of SMCs. The increased interlamellar thickness, collagen fibers, and the thickness of elastic lamina found in the inner media of hypertensive animal may be associated with the gradient of stress decreasing into the outer media. SMC proliferation, if any, was found evenly distributed across the media, however. In cases showing increased proliferation and matrix protein synthesis, the SMC contractile markers were down-regulated whereas the SMC synthetic markers were up-regulated. While the aortic intima appeared normal in the normotensive animals, neointima formation, which may predispose the vessel to atheroma formation, was found in the hypertensive animals. Immunohistochemistry of Hsp47 and procollagen revealed that the endothelial cells (ECs) may produce collagen, specifically type I collagen in response to hypertension and contribute to the thickened intima. In addition, lectin staining for ECs markers and immunostaining for eNOS suggested that endothelial cells may transdifferentiate into intimal SMCs. These findings suggested an alternative role that ECs may play in hypertension-induced atherogenesis.

DEDICATION

To my parents

ACKNOWLEDGMENTS

And we know that in all things God works for the good of those who love him.

—Romans 8:28

I am grateful to have joined Dr. Theresa Good's group in Chemical Engineering when I first came to Texas A&M University, where I learned and built up experimental techniques proven to be useful later. She is extremely intelligent and full of creative ideas and definitely has had a great impact on my thoughts in research. Her moving to University of Maryland, however, led to my transferring to Biomedical Engineering. Since then, I have been abundantly blessed by the guidance of my advisor, Dr. Jay Humphrey, who brought me into and stimulated my passion for this rapidly expanding field (biomechanics). He is so intelligent, knowledgeable, and practical that I can always learn something from him. I thank him for his trust, understanding, and supports in many respects.

It is a special pleasure to thank Dr. Emily Wilson for her support in the immunohistochemical study. Establishment of the staining station could not be possible without her full support; I am enormously grateful for that. I am also grateful to Dr. John Criscione for the idea of least square solutions for strain analysis and Dr. Christopher Quick for insights from the hemodynamics perspective. Their willingness to serve on my committee and to give me comments and suggestions for my dissertation are greatly appreciated.

Of course, this clinical investigation could not be done without the outstanding

surgical expertise provided by the world-class investigators at the College of Veterinary Medicine: Drs. Theresa Fossum, Matthew Miller, Michelle McDonald, David Nelson, Brian Saunders, and Mr. Galen Pahl. I appreciated their full support; it is their hard work that made this dissertation possible.

I would like record my gratitude to Drs. Saravanan Umakanthan and Seungik Baek, with whom I had many insightful discussions, Zachary Bujnoch, who efficiently digitalized the enormous amount of images, and Hai Xu, who has helped in image analysis. I would also like to thank Dr. Sandy Ambrus and Rosemary Vollmar for advice and assistance in immunohistochemistry and histology, respectively.

I appreciated all my brothers and sisters in the College Station Chinese Church for their prayers when I was in need. Special thanks are due to Dr. Lih Kuo, who has been my spiritual reminder and encouragement provider. His generosity of sharing his laboratory space and experimental experience is also gratefully acknowledged.

I wish to take this opportunity to acknowledge the true-blue friendship of Drs. Jun-Yen Tewg and Won-Hyouk Jang for they had made this journey more unforgettable.

Finally, I would like to thank my parents Ray-Yuan and Jing-Yuh; they respected my decision to pursue my Ph.D. abroad and were always concerned about me during these six years, to which I am indebted very much. I love them.

Financial support from the National Institute of Health is gratefully acknowledged.

TABLE OF CONTENTS

CHAPTER Page

LIST OF TABLES

LIST OF FIGURES

FIGURE Page

FIGURE Page

CHAPTER I

INTRODUCTION

The vasculature is capable of diverse morphological and functional changes in response to a variety of biochemical and biomechanical stimuli. Vascular adaptations, such as normal changes during development and aging, and pathological changes in atherogenesis, hypertension, and aneurysms, have caught much attention due to their importance in understanding the treatment of diseases and developing strategies for engineered vascular grafts. Among the stimuli, mechanical forces (stress and strain) are believed to play a major role in most of these adaptations. This thesis focuses on growth and remodeling (G&R) of arteries in a hypertension animal model.

Changes in arterial mechanical properties can deteriorate the local functionality of the artery and lead to global vascular diseases. The passive mechanical property of an artery is determined mainly by its constituents (i.e., smooth muscle cells, collagen, and elastin). In the progression of hypertension, however, the spatial and temporal changes in these constituents remain largely unknown.

A combination of histological, immunohistochemical, and mechanical analysis was employed in this study. Immunohistochemistry, which is capable of illustrating the localization and distribution of protein expressions, was performed to examine in situ changes of the constituents in the aorta. The mechanical properties of the basilar artery were evaluated by in vitro pressure-diameter tests on intact cylindrical segments at their

---

This dissertation follows the style of *Hypertension*.

in situ length.

Chapter II reviews the histology of arteries and our current understanding of hypertension, it provides a brief introduction to differentiation markers for examining smooth muscle cell (SMC) phenotypic heterogeneity, and it summarizes the experimental model we used in this study.

Chapter III focuses on histo-mechanical changes of the porcine basilar artery due to hypertension over 8 weeks of development. There have been few studies on the mechanical properties of cerebral arteries despite their importance in understanding the physiology of the cerebral circulation and investigating the pathogenesis of cerebrovascular lesions. Surprisingly, therefore, the effects of hypertension on mechanical properties in cerebral arteries remain unknown despite hypertension being a leading risk factor for stroke and aneurysms.

In Chapter IV, a combined histological and immunohistochemical analysis was used to characterize G&R of the aorta in hypertension. Specifically collagen and elastin deposition, phenotypic changes of SMCs, and their turnover were analyzed. Medial SMCs bear part of the initially increased circumferential stress in hypertension. These cells may undergo hypertrophy and/or hyperplasia and may abnormally synthesize and release matrix proteins as well as matrix metalloproteinases (MMP) and tissue-inhibitors of MMPs (TIMP), which further regulate matrix protein turnover. Each of these processes plays an active role in G&R in the arterial wall. Despite controversial debates on SMC heterogeneity, it is essential to know the phenotype locally, specifically, the effect of altered stress on phenotypic change before we can better understand its functions.

In Chapter V we used immunohistochemistry to trace the source of matrix proteins accumulated in the neointima. Hypertension is one of many causes leading to neo-intimal thickening and a risk factor for atherosclerosis; how hypertension induces or aggravates atherosclerosis is still unknown, however. An understanding of how intimal thickening happens may provide clues to prevent atherosclerosis.

Chapter VI introduces a uni-axial stretcher which was built for future investigation of G&R of the aorta subjected to tensile stress. This design excludes the influences of radial stress and distribution of tensile stress across the vessel wall.

Finally, Chapter VII summarizes the major contributions of this study.

CHAPTER II

BACKGROUND AND SIGNIFICANCE

HISTOLOGY OF ARTERIES

Arteries can be categorized primarily into two types based on their relative size and/or morphological characteristics: elastic arteries and muscular arteries.

Elastic arteries are characterized by concentric elastic lamina occupying much of the tunica media; Verhoeff van Giesion (VVG) or elastic van Giesion (EVG) staining is most commonly used to demonstrate the elastic lamina *in situ*. Elastic arteries are relatively large in diameter and located close to the heart. The aorta, major trunks originating from the aortic arch and the terminal bifurcation of the abdominal aorta, and the pulmonary trunk belong to this type. The primary characteristic of muscular arteries is a relatively thick media composed of mainly smooth muscle cells (SMCs). These areteries are the main distributing branches of the vascular tree (e.g., the radial, femoral, coronary, and cerebral arteries). There is a gradual transition in structure and function between two types of arteries; some arteries exhibit features of both types. Nevertheless, the ratio of elastic fibers to the smooth muscle component decreases as the arteries become smaller.

Regardless of type, all arteries consist of three concentric layers, called from the luminal side outward: the tunica intima, tunica media, and tunica adventitia. The tunica intima of elastic arteries consists of a single layer of flattened endothelial cells, which rest on basal lamina and line the lumen of the vessel, plus an underlying subendothelial

connective tissue whose thickness increases during aging and disease progression. The tunica intima in muscular arteries is generally thinner than that in elastic arteries. In healthy arteries, the intima probably offers negligible mechanical strength. The tunica media of elastic arteries consists of many fenestrated lamellae of elastin, known as elastic laminae, alternating with circularly oriented layers of SMCs. The number of elastic laminae increases during development. The elastic laminae also increase in thickness because of the continued deposition of elastin, which constitutes much of the tunica media[1]. The tunica media of muscular arteries is mainly composed of SMCs oriented concentrically around the lumen, but it also contains abundant collagen and elastin. The tunica adventitia is largely composed of collagen, with sparse elastic fibers, that remain slack at physiological pressures; however, it appears to protect the artery from overstretching at high pressure [2].

Despite its heterogeneity in some cases, the arterial wall can be modeled as a mechanically homogeneous body probably because of the interlocked structure of elastin, muscle, and collagen. Indeed, by tracking the deformation of each elastic lamina at different locations across the wall thickness, Dobrin found that the media behaves mechanically as if its material properties were homogeneous[3].

HYPERTENSION

Hypertension is a common disease in developed countries. Twenty-eight percent of Americans from 20 to 74 years of age are hypertensive[4] and there were 35 million office visits for hypertension in 2000 alone[5]. It is a leading risk factor for many

cardiovascular diseases, including atherosclerosis, stroke, and aneurysms. It also leads to cardiac hypertrophy with heart failure, aortic dissection, and renal failure, and thus is a leading cause of death.

Hypertension is defined as a persistent elevation of blood pressure. The vessel walls subject to high blood pressure undergo tremendous structural and functional changes. Specific manifestations may include wall thickening[6], smooth muscle cell (SMC) hypertrophy and/or hyperplasia[7], abnormal matrix protein turnover[8], increased viscoelasticity[9], increased vascular tone[10], and altered reactivity and sensitivity to pharmacologic stimulation[11]. Changes in structural and mechanical properties of the vessel wall turn out to contribute to the persistence and progression of hypertension. Although pharmacologic treatment can control the blood pressure, reduction of blood pressure to its normal level does not usually reverse the structural changes. In order to prevent and cure hypertension, it is crucial to understand the mechanism by which the elevated pressure leads to these permanent structural and functional changes.

The vasculature responds quickly to acute changes of physiological conditions such as blood flow or pressure. When the endothelium is subject to an acute change of blood flow, it releases many substances including vasoactive materials such as nitric oxide (NO) and endothelin (ET-1). Acting on SMCs, these vasoactive materials not only regulate the caliber of the vessel, they also act as growth promoters or inhibitors for long-term adaptation. Less is known about the mechanism underlying pressure-induced arterial responses although a myogenic response, which is pronounced in arterioles, can be demonstrated occasionally in arteries[12]. In addition to the direct effect of mechanical

strain on SMC growth[13], it is believed that the paracrine/autocrine growth factors released during the early stage of pressure elevation trigger G&R if the pressure sustains. Many growth factors, including PDGF[14], TGF-β[15], IGF-I and IGF-I binding proteins[16,17], and their associated receptors have been shown to be involved in the G&R of hypertensive vessels.

Growth of SMCs has been found in human hypertension and experimental hypertension models, thus contributing to the wall thickening. Depending on the model of hypertension, however, the growth response of SMC in terms of hypertrophy and/or hyperplasia can be different within a given blood vessel[7,18]. Studies suggest that the increased turnover of endothelial cells in a coarctation model causes SMC hyperplasia but not hypertrophy[18].

Extracellular matrix remodeling is another adaptation process leading to wall thickening in hypertension. In a blood vessel, collagens and elastin are the two main extracellular matrix proteins, the absolute and relative quantities of which mainly determine the passive mechanical properties of the vessel[2]. In addition to causing wall thickening, the abnormal turnover of elastin and collagen changes the mechanical properties of the vessel, which further influence vascular physiology and the development and progression of vascular disease. In an aortic coarctation rabbit model [19,20], the gene expression for both collagen and elastin was found to increase in the adventitia and the outer media, which may be correlated to a differential distribution of stress across the vessel wall. Enzymes involved in the degradation of matrix proteins are called matrix metalloproteinases (MMPs). These enzymes have natural inhibitors called tissue

inhibitors of metalloproteinases (TIMPs), which tightly regulate the activity of MMPs. In an uninjured vessel, the turn-over of collagen and elastic fibers is low. When the balance between MMPs and TIMPs is altered in some pathology, however, matrix remodeling is triggered. Studies show that at least two MMPs increase their activity under high transmural pressure and the local distribution and activity of the MMPs may be more relevant to vessel wall remodeling than changes in the overall levels of MMPs[21].

SMC DIFFERENTIATION MARKERS

SMCs are generally classified as in either a contractile or synthetic phenotype. Recent evidence, however, suggested that there exists a spectrum of phenotypically distinct SMCs in arterial media. Supported by different evidence, at least two hypotheses have been proposed to explain SMC heterogeneity in diseased arteries. Some suggest that smooth muscle cells retain remarkable plasticity even in mature animals and are capable of modulating their phenotypes in response to the environmental stimuli[22]; others claim that there are subpopulations of different SMC phenotypes coexisting in the media, and altered mechanical or chemical stimuli have different effects on different subpopulations[23] (e.g. cause the expansion of a specific subpopulation).

Generally, the appropriate phenotypic expression is essential for SMC to maintain and regulate vascular tone, and to repair the injured vessel wall. In hypertension, growth response of SMCs in terms of hyperplasia and/or hypertrophy and their matrix protein deposition play central roles in arterial G&R. These reactions are believed to be closely dependent on their phenotypes.

An increasing list of cell markers for SMC differentiation has been identified to study the functional and structural changes of SMC associated with its phenotypic changes in pathophysiological conditions[24,25]. The contractile markers include calponin, caldesmon, sm22, and myosin heavy chain isoforms and the cytoskeletal markers include desmin, vinculin, and meta-vinculin[26,27]. Since our focus is on how altered mechanical stress influences the SMC phenotypic heterogeneity in a time course, below I only briefly introduced the markers applied in this study.

Calponin is a 34-kDa myofibrillar thin filament, actin-binding protein; it is implicated in an auxiliary regulatory role of SMC contraction. Calponin expression is restricted to SMCs and has been shown to be a marker of the contractile phenotype of developing smooth muscle[28,29].

Caldesmon is an 120-kDa actin binding protein and has been detected in smooth muscle and in a number of non-muscle cells[30,31]. In comparison to some traditional smooth muscle markers, it may be more sensitive and specific in differentiating tumors with different origins[32,33].

Smooth muscle myosin heavy chains (MHCs) exist in multiple isoforms. At least three types of MHC isoforms have been identified in rabbit: SM1(204 kDa), SM2 (200 kDa), and Smemb (200 kDa)[34]. Due to the unavailability of antibodies to SM1 and SM2, in this study, we only performed immunohistochemistry for MHC and Smemb.

Smoothelin is a 59-kDa cytoskeletal protein exhibiting a filamentous organization and uniquely expressed in fully differentiated (contractile) SMC[35,36]. Smoothelin shows up very late during differentiation in chick gizzard (ED 18) compared to SM α-actin (ED

2.5), sm22α (ED 4), calponin (ED 6), caldesmon (ED 6), and SM α-tropomyosin (ED 6)[22,37]. It can be used to discriminate between SMCs and other SMC-like cells such as myofibroblasts and myoepithelial cells[35]. It does not belong to any classes of structural proteins previously described and may be a valuable addition to markers used for the assessment of the stage of SMC differentiation[35,36].

ANIMAL MODEL

Because of the unclear etiology of hypertension, several animal models have been established to study hypertension, as, for example, spontaneously hypertensive rat (SHR) and aortic coarctation models; each model provides valuable but different insights into the mechanism of hypertension. Unfortunately, some results from past studies are controversial probably due to species-, tissue-, or model-related differences of the animal models. It is therefore challenging to compare findings in each study and also difficult, if not impossible, to derive a correlation among the structural, functional, and mechanical changes. Moreover, most studies only focus on changes at one time-of-development, not its time-course. There is a need for data of these changes during the progressing of hypertension (i.e., the kinetics).

Since many observations of experimental hypertension are species-, tissues- and model- dependent, therefore, it is essential to study G&R of a specific artery in the same experimental model. It is equally important to correlate G&R with the altered mechanics of the same artery in the same experimental model. The novel mini-pig coarctation model developed by Dr. Fossum et al.[38] was used in this study.

We choose to induce hypertension in the Yucantan micro-pig, which is more similar genetically to humans than rodents but less expensive than primates. Whereas blood pressure tends to increase with increasing weight gain in domestic pigs, using the micro-pig avoids this complication. The thoracic aortic coarctation model is chosen based on three reasons: First, the coarctation model admits a primary mechanical hypertension by gradually increasing the constriction with or without a simultaneous application of ACE-inhibitors. Second, the development of hypertension induced by aortic coarctation undergoes three phases: an acute mechanically-induced phase, a sub-acute rennin-dependent phase, and a chronic G&R phase; the time-course adaptation in each phase and the transition between phases can be delineated. Three, the hypertension develops at different rates in the vasculature distal and proximal to the occluder, again providing additional data on time-courses and stimuli. Additionally, the observed enlargement of the intercostal arteries after aortic constriction provides an opportunity to study arteriogenesis, a type of flow-induced G&R *in vivo*.

CHAPTER III

HISTO-MECHANICS OF THE PORCINE BASILAR ARTERY IN HYPERTENSION

INTRODUCTION

Hypertension afflicts nearly 50 million Americans and is a significant risk factor for many cardiovascular diseases, including aneurysms, atherosclerosis, heart failure, stroke, and end-stage renal failure. It is well known that hypertension induces, and is exacerbated by, significant changes in the structure and function of both conduit and resistance vessels. It is remarkable, therefore, that data are scant on the potential time-course of changes in the biomechanical properties of arteries of the brain and heart, two organs often affected by hypertension-induced alterations. Knowledge of arterial properties is essential for correlating changes in wall mechanics with mechanobiologically-induced changes in cell activity and modification of the extracellular matrix; likewise, arterial properties are essential for understanding changes in hemodynamics, particularly the propagation of pulse waves. In this paper, we report data on the histo-mechanics of the basilar artery throughout the development of hypertension over 8 weeks in a novel mini-pig model. Despite considerable biological variability, we show that significant biomechanical changes manifest rapidly (within 2 weeks) in both the structural and material stiffness of the basilar artery.

METHODS

Animal Model. Our aortic coarctation model for studying hypertension in the mini-pig is described in detail elsewhere[38]. Briefly, a balloon-expandable occluder is pre-filled with a 50% dextrose solution, placed over a Gor-Tex soft tissue patch sheet, and secured with suture around the aorta proximal to the diaphragm. The occluder is connected via stiff tubing to a vascular access port that is placed subcutaneously in the neck, which allows the occluder to be inflated or deflated in the conscious animal. An indwelling pressure transducer is placed within the internal thoracic artery or right carotid artery and connected to an implanted telemetry unit. Arterial pressure and heart rate can then be recorded continuously, but are typically recorded for 30 s every 2 h. The mean arterial pressure is defined as the diastolic pressure plus one-third the difference between systolic and diastolic pressure, and a daily average mean arterial pressure is used to track the condition of each animal.

To initiate hypertension, the aorta was coarcted approximately 1 week after surgery by adding small amounts of dextrose to the occluder over a 7 to 10 day period until the mean arterial pressure reached or exceeded 150 mmHg. Data were collected from a total of 37 mature (7 to 16 month old) male mini-pigs: 14 normotensive (NT) controls and 23 hypertensives (HT). Specifically, basilar arteries were harvested from true controls (n = 4) without an occluder, from normotensive animals at 2 (n = 2), 4 (n = 2), 6 (n = 2), and 8 (n = 4) weeks following a sham surgery wherein an occluder was implanted but not inflated, and from hypertensive animals at 2 (n = 6), 4 (n = 5), 6 (n = 5), and 8 (n = 7) weeks after the animal reached its target mean arterial pressure (> 150

mmHg). All animal care and use was approved by the University Laboratory Animal Care Committee at Texas A&M University.

TABLE III-1. Number of Basilar Artery Data Available

Number of data	2-week	4-week	6-week	8-week
Hypertensive	6	5	5	7
Normotensive	2	2	2	4
Control		4		

Biomechanical Tests. Our biaxial test system is a modified version of one reported earlier[39]; it is well suited for performing cyclic pressurization tests on small vessels at multiple fixed axial extensions. Briefly, the basilar artery is excised from the isolated brain, perforating branches are ligated with 9-O or 11-O silk, and the vessel is cannulated with blunt-ended 26 G needles (Figure III-1). The cannulated vessel (~ 0.8 mm dia and 1.2 cm long from left suture to right suture) is then placed within a test chamber filled with normal saline at room temperature and coupled to the loading frame, which consists of precision x-y-z stages mounted on sub-micron resolution x-translation stages that can extend the vessel under computer control (Figure III-2A). The vessel is pressurized under computer control using a syringe pump, and luminal pressure and axial load are measured on-line; resolution is 0.001 mmHg and 0.25 grams, respectively. Surface strains in the central region are inferred from the motions of multiple 50 micron diameter microspheres (Figure III-2B), which were affixed to the superior surface of the artery with glue and

tracked on-line at 30 Hz using a frame grabber board and custom correlation-based software. This approach allows circumferential and axial strains to be inferred equally, thus avoiding problems with edge detection when trying to track the diameter in the presence of loose adventitia or ligated perforating branches. Current video resolution for marker tracking is 4.75 micron/pixel.

Figure III-1. Photograph of a porcine brain stem. The black-ink gel infusing into the basilar artery facilitated the identification and ligation of the perforating branches along the trunk.

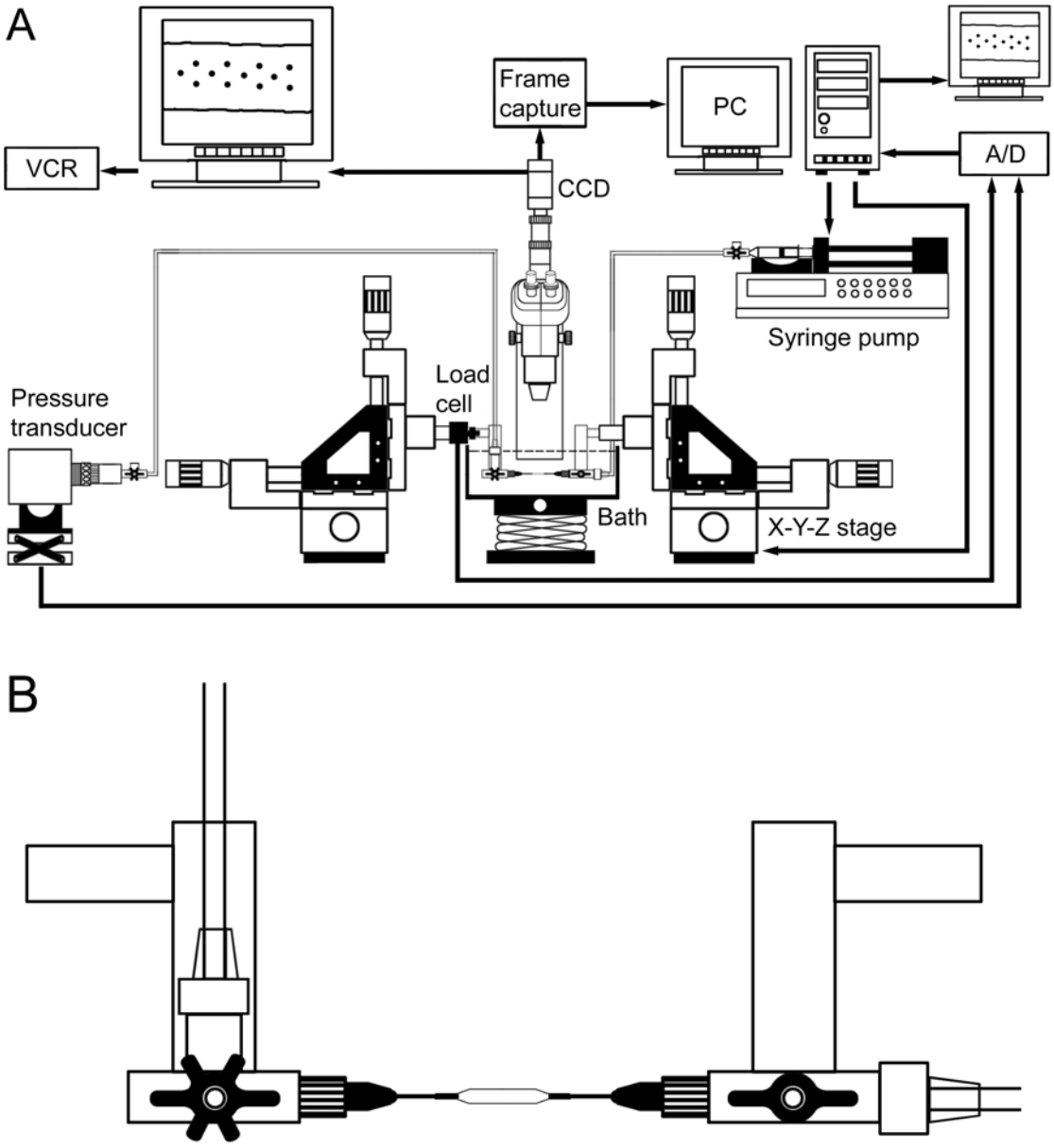

Figure III-2. Schematic drawing of the experimental system. Panel (A) shows the entire setup, which consists of two x-y-z stages atop computer controlled translation stages, a syringe pump, a pressure transducer and load cell, and a CCD mounted on a dissection microscope to allow on-line imaging of microspheres that are affixed to the surface of the artery in a central region. Panel (B) illustrates the details of the canulation of the artery.

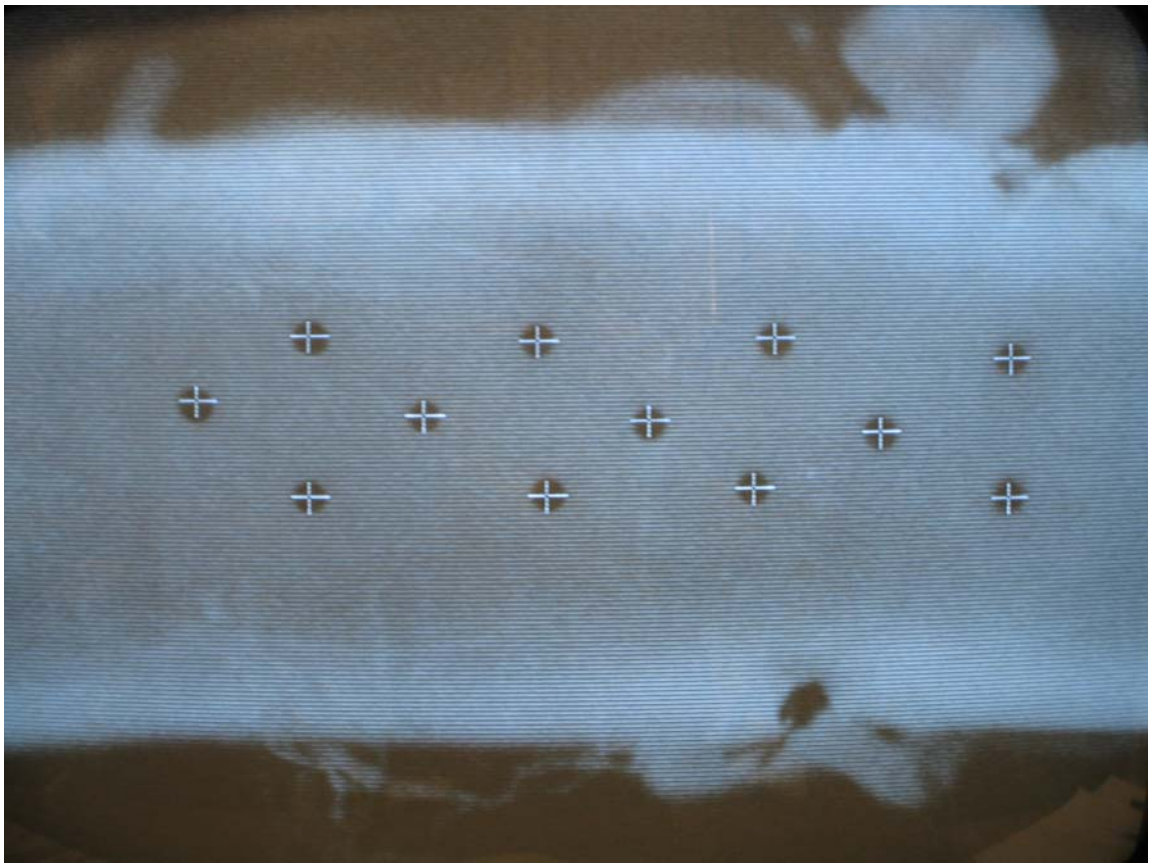

Figure III-3. A representative video image of a basilar artery with surface markers that are tracked on-line (note: the crosshair shows the computer-determined centroid of each marker).

Two types of reference configurations were employed: the unloaded reference wherein the vessel was at zero pressure and zero axial force, and an initial reference wherein the vessel was stretched longitudinally to a prescribed length at zero pressure. Vessels were preconditioned by cyclic pressurization 5 times from 0 to either 80 or 120 mmHg at the prescribed axial length. Data (pressure, axial load, and marker positions) were then collected for slow cyclic inflation tests at 2-3 different fixed axial lengths including the *in situ* length which was near the shortest length at which the vessel did not

bend when pressurized at 80 mmHg. Typically axial extensions were about 1.15, 1.2, or 1.25 relative to the overall unloaded reference length.

Histology. Following biomechanical testing, arteries were immersed and fixed in a fresh 4% paraformaldehyde solution for 1 to 2 hours at room temperature. The artery was then dehydrated through a series of graded alcohols overnight, embedded in paraffin, and sectioned at 5 microns using a Leitz 1512 microtome. Sections were then mounted on Superfrost Plus slides and dried overnight. After being deparaffinized in pure xylene and rehydrated through a series of graded alcohols, sections were stained with either Verhoeff van Giesion (VVG) or picrosirius red (PSR) for measurement of wall dimensions and collagen content, respectively.

Data Analysis. Biomechanical data were studied in terms of both the structural stiffness (i.e., pressure-strain relation) and the material stiffness (i.e., stress-stretch relation). Whereas the structural stiffness accounts for changes in wall thickness and is that stiffness which resists the distension pressure in vivo, the material stiffness addresses directly the stiffness of the constituents of the wall. Because of the finite deformations, Green strain at the adventitial surface was used to assess distensibility whereas the mean Cauchy (true) stress and left stretch were used to assess material behavior in the current configuration. Assuming locally homogeneous strain fields, Green strains can be estimated from the motions of 3 markers defining a triplet, but because of potential heterogeneities introduced by the ligated perforating branches, mean values of strain were determined at each pressure state based on a pseudo inverse (least squares) fit to the chosen surface markers; the markers, which introduced significant shear strain were

discarded in analysis assuming that the pressure inflation causes no shear. Once the motions are known, the deformation gradient and Green strain are determined easily (see Appendix A). Mean Cauchy stresses were computed as

$$\sigma_{\theta\theta} = \frac{Pa}{h} \quad \text{and} \quad \sigma_{zz} = \frac{f}{\pi h(2a+h)}, \tag{1}$$

where P is the distending pressure, a is the deformed inner radius, h is the deformed wall thickness, and f is the applied axial load. Herein, however, we focus on the mean hoop stress.

The inner radius, wall thickness, medial cross-sectional area, and luminal area were also calculated in a fixed unloaded configuration using a custom image analysis program that objectively determines boundaries of interest in the histological sections. Briefly, image processing techniques such as threshold, median filter and a morphology remove algorithm, were used to determine the medial boundaries. The unloaded inner radius was then calculated by $A = \textbf{Inner Perimeter}\ /2\pi$ assuming that luminal surface is circular in vivo. The number of pixels surrounded by specific boundaries was used to calculate the medial cross-sectional area, *MCSA*. Units in pixels were converted to metric units (1.25 μm/pixel). Assuming that the vessel wall is incompressible, the inner radius and wall thickness at any pressure can be calculated respectively as

$$a = \sqrt{(\lambda_r B)^2 - \frac{MCSA}{\pi\lambda_z}} \quad \text{and} \quad h = \lambda_r B - a, \tag{2}$$

where λ_r is the radial stretch ratio on the outer surface of the vessel, λ_z is the uniform axial stretch ratio, and B is the undeformed outer radius.

The collagen content was quantified from the PSR-stained specimens using an Olympus BX-51 microscope customized for circularly polarized illumination[40]. Briefly, one quarter-wave plate was mounted into the strain-free polarizing condenser (between the condenser and the polarizer) and oriented at 45^{o} to the transmission axis of the polarizer. The other quarter-wave plate was inserted into the compensator slot in the nosepiece. Under circularly polarized light, which removes the dependence of brightness on fiber orientation, only fibrillar collagen (I & III) is visible due to its natural birefringence; other tissue components, including non-fibrillar collagen appears dark. The relative fibrillar collagen content was determined as the ratio of the bright area to the total area of the media, the latter determined under non-polarized illumination. A threshold was applied to the converted grey-scale image to obtain the collagen region. Sections from normal hearts, in which collagen content is reported to be 2-3% were used as a standard to determine independently the threshold[41,42].

Differences between groups (e.g., hypertension HT or normotension NT, and 2, 4, 6 or 8 weeks of hypertension) were assessed via an Analysis of Variance (ANOVA) or an unpaired student t-test, with $p < 0.05$ at the 0.05 level deemed as significant. Results are reported as means ± standard deviation.

RESULTS

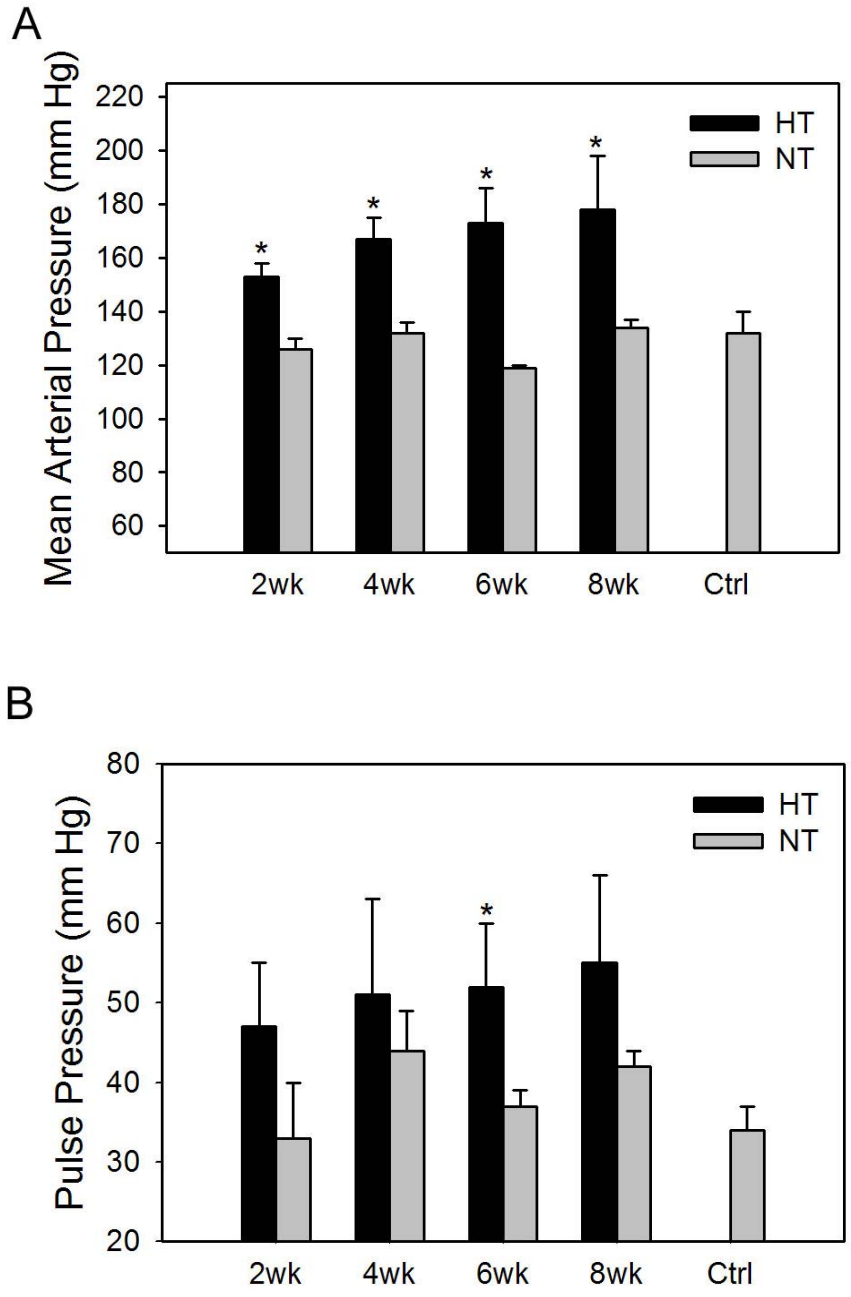

Figure III-4. Telemetry-based 24-hour average mean arterial pressures (A) and pulse pressures (B) in the internal thoracic artery for the normotensive (NT) and hypertensive (HT) groups at each end-point: 2, 4, 6, and 8 weeks. The asterisks denote statistically significant differences ($p < 0.05$) at a given end-point. Total numbers are $n = 10$ (NT) and $n = 24$ (HT).

The 24-hour average mean arterial pressure was significantly different ($p < 0.05$) between the hypertensive and normotensive animals at each of the desired end-points: 2, 4, 6, and 8 weeks (Figure III-4A). Notwithstanding a gradual, but significant, increase in pressure over time during hypertension, note that the overall averaged mean arterial pressures were 168 ± 16 for the HT animals and 129 ± 7 for the NT animals, which were significantly different ($p < 0.05$). The pulse pressure in the NT and HT animals differed significantly only at 6 wks ($p = 0.015$); however, if we grouped all NT and HT together the overall averaged pulse pressures were 40 ± 5 in NT and 51 ± 10 in HT, which were also significantly different ($p=0.0012$) (Figure III-4B). Recall that all pressures were measured in the internal thoracic artery or right carotid artery in conscious, unrestrained animals.

Figure III-5 shows representative pressure-strain and pressure-axial force data from one NT basilar artery. Specifically, panel (B) reveals a characteristic nonlinear behavior and that there was only slight hysteresis following preconditioning. Although modest increases in axial extension (from 1.0 to 1.23) reduced the diameter at zero pressure, relative to the unloaded intact reference configuration, the pressure-strain responses were otherwise similar over this range of stretches. Panel (D) reveals that the axial force tended to be nearly constant during pressurization at the lower axial stretch, which suggests that this stretch is near the in vivo value (cf. Humphrey[43]; pp. 281-284). Subsequent results are presented for axial extensions near the in vivo value, which varied slightly from animal to animal and between NT and HT (albeit not a consistent, statistically significant difference).

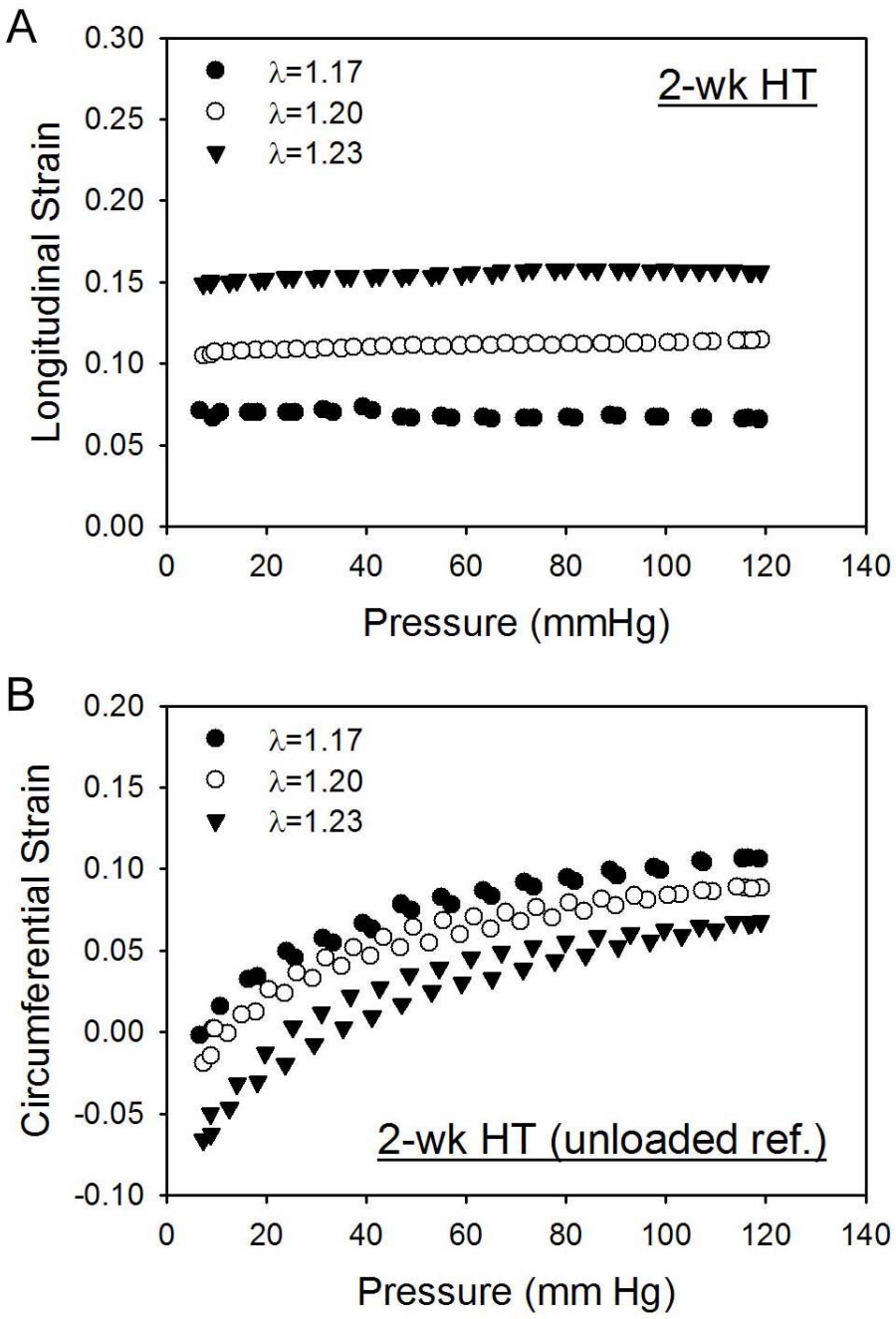

Figure III-5. Representative pressure-strain (A, B, and C) and pressure-axial force (D) data from a single basilar artery from a 2 week hypertensive animal. Note the characteristic nonlinear response, slight hysteresis following preconditioning, and constancy of the axial force during pressurization at (near) the in vivo axial extension.

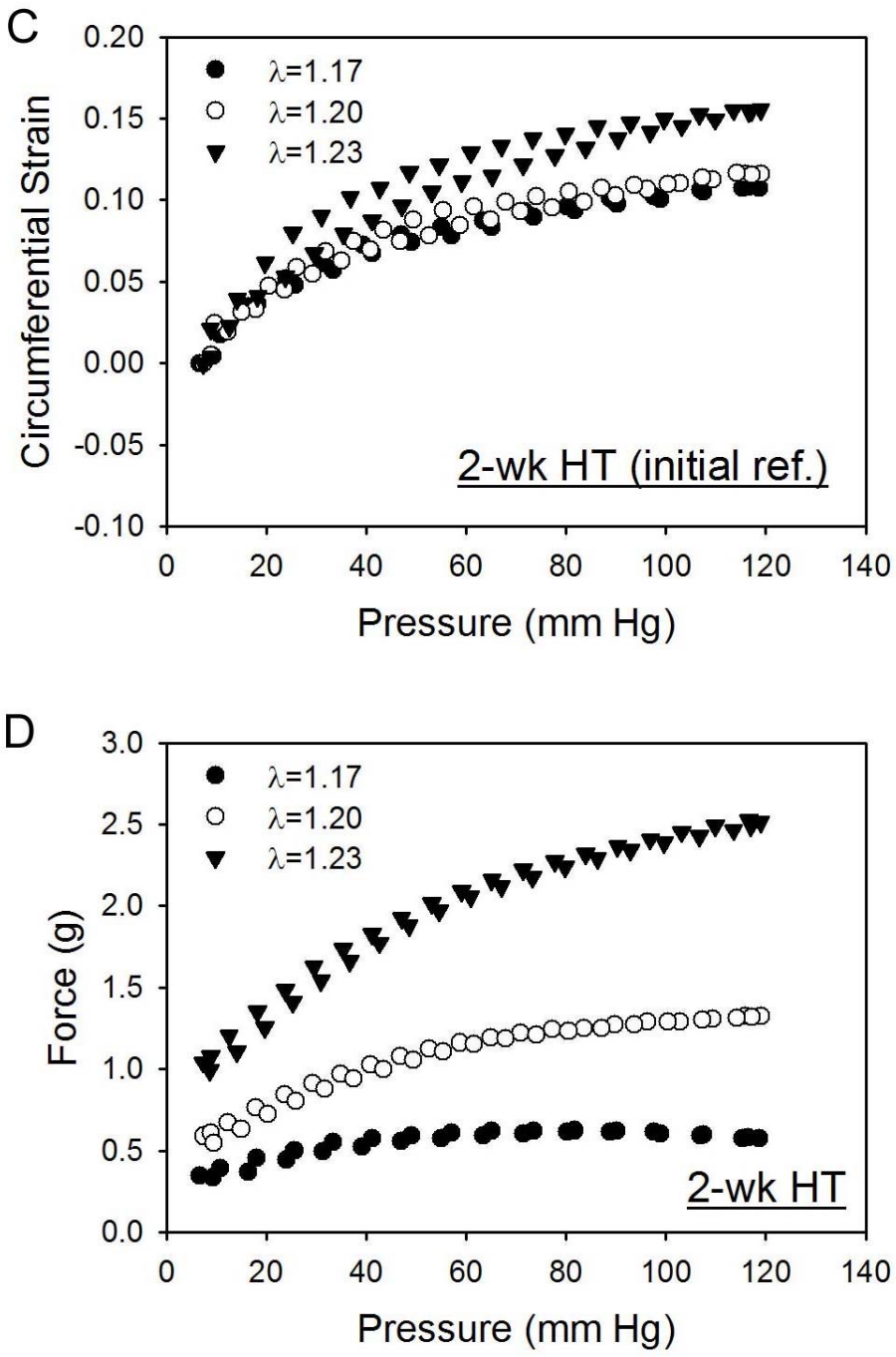

Figure III-5 (Continued)

Hypertension induced significant structural stiffening at each end-point, which is appreciated by comparing circumferential Green strains at in vitro distending pressures of 20 to 80 mmHg at 2, 4, 6, and 8 weeks (e.g., Figure III-7A shows results at 80 mmHg). An ANOVA showed no significant differences in strain, at a common pressure, across the various end-points for either the NT or HT groups, hence we separately pooled the NT and HT data (Figure III-4B). Statistical comparisons showed significant differences in distensibility at all pressures except those less than 10 mmHg. Whereas the structural stiffness may depend on both wall properties and wall thickness, traditional stress-stretch curves reflect material stiffness independent of geometry.

Basilar arteries represent a special class of muscular artery – the media consists primarily of smooth muscle cells, collagen fibers, and sparse elastin; there is a prominent internal elastic lamina but no external elastic lamina (Figure III-11). Whereas wall thickening in the aorta of HT animals was accompanied by marked neo-intimal thickening (see Chapter V), no such neo-intimal involvement was seen in the basilar arteries. Rather, thickening appeared to be primarily due to enhanced collagen deposition, particularly in the adventitia (Figure III-12), as well as increased collagen and cell hypertrophy or hyperplasia in the media. Indeed, quantification of the birefringence in sections stained with PSR revealed a 1.4 fold increase in medial collagen due to HT, which was statistically significant ($p < 0.05$). The internal radii and cross sectional area of media and lumen did not change significantly in HT pigs, however.

Plots of circumferential Cauchy stress versus stretch reveal that there was also a marked increase in the material stiffness due to hypertension (Figure III-8A). Again,

however, it was not possible to delineate potential trends due to the increased duration of hypertension. Thus, similar to Figure III-7B, NT and HT data were separately pooled across end-points and compared (Figure III-8B). There was a significant increase in the material stiffness at all but the lowest pressures as well. Also note from Figure III-8 that the maximum achieved stresses were higher in the NT than in the HT vessels at a common distension pressure (e.g., 80 mmHg) because of an increase in wall thickness in

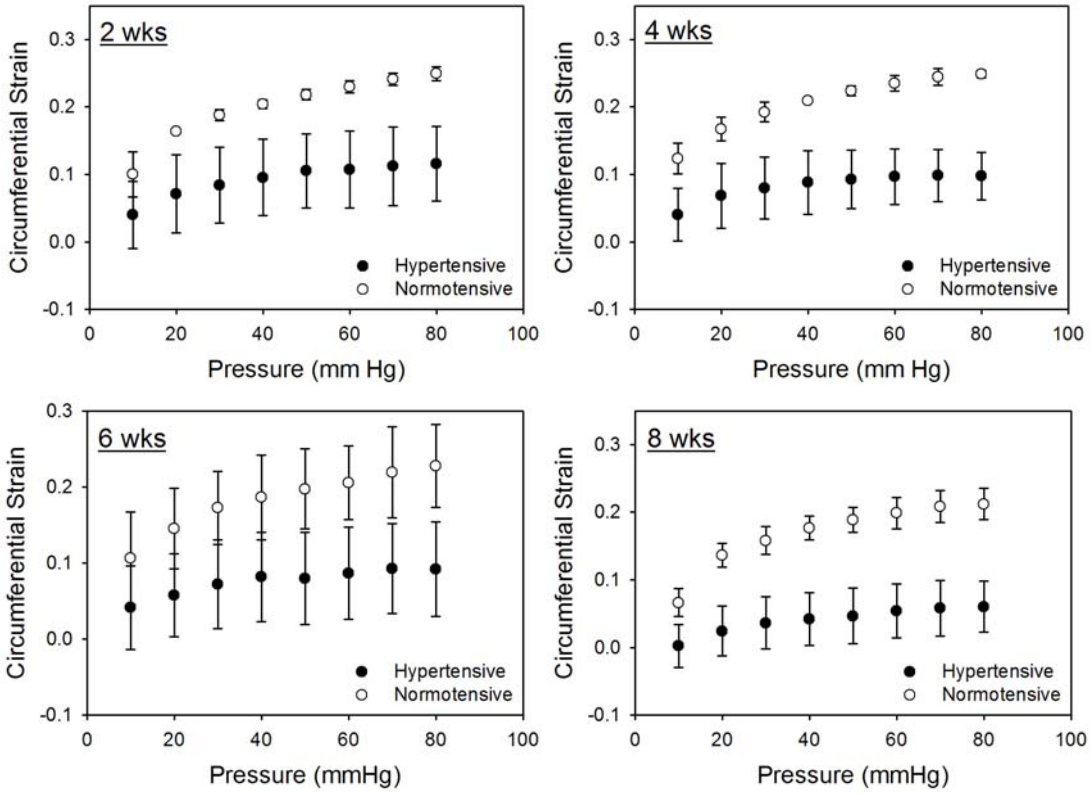

Figure III-6. The circumferential strain-pressure curves of the basilar arteries at four time points (2, 4, 6, and 8 week), which illustrates the significant change in the structural stiffness due to hypertension.

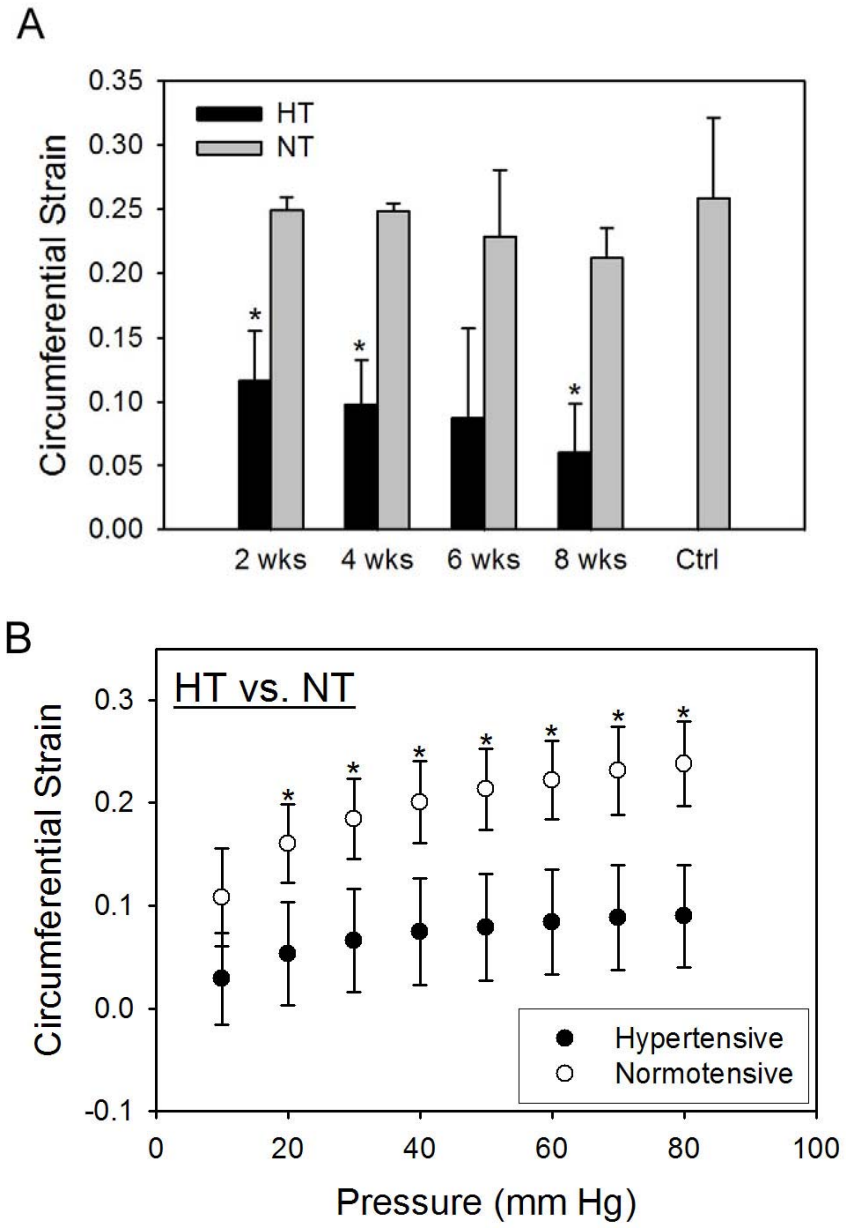

Figure III-7. Comparisons of circumferential structural stiffness in normotensive (NT) and hypertensive (HT) vessels based on the distensibility (i.e., Green strain) at comparable pressures (A). Whereas distensibility is markedly less in HT than NT at each end-point (albeit not reaching significance at 6 weeks at $p < 0.05$ due to high variability), the trend towards a slight decrease in distensibility with increased duration of hypertension is not significant (panel a; data at 80 mmHg). Hence, consistent with Figure III-4, data are simply grouped as NT versus HT and shown to be significantly different at all pressures above 20 mmHg (B).

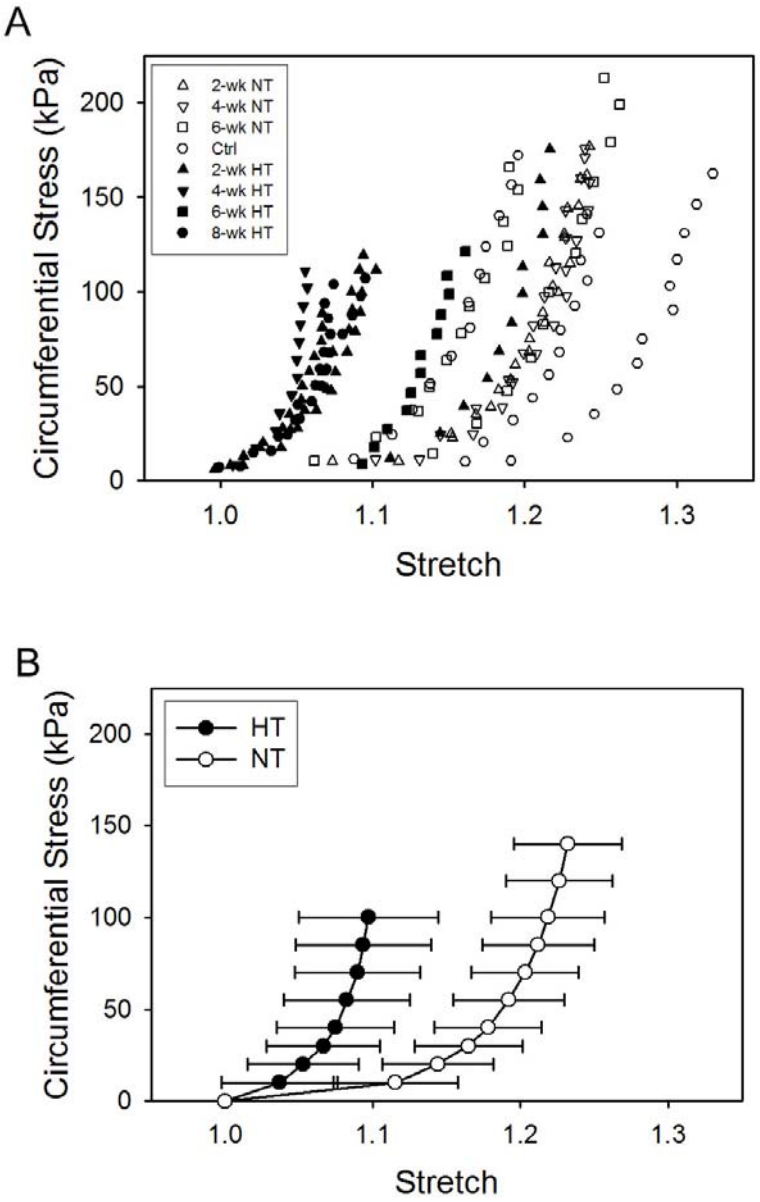

Figure III-8. Cauchy stress versus stretch for representative specimens at 2, 4, 6 and 8 weeks, both normotensive control (NT) and hypertensive (HT). Despite considerable biological variability (A), these differences were statistically significant when contrasted between NT and HT independent of the end-point (B), consistent with Figure III-7B.

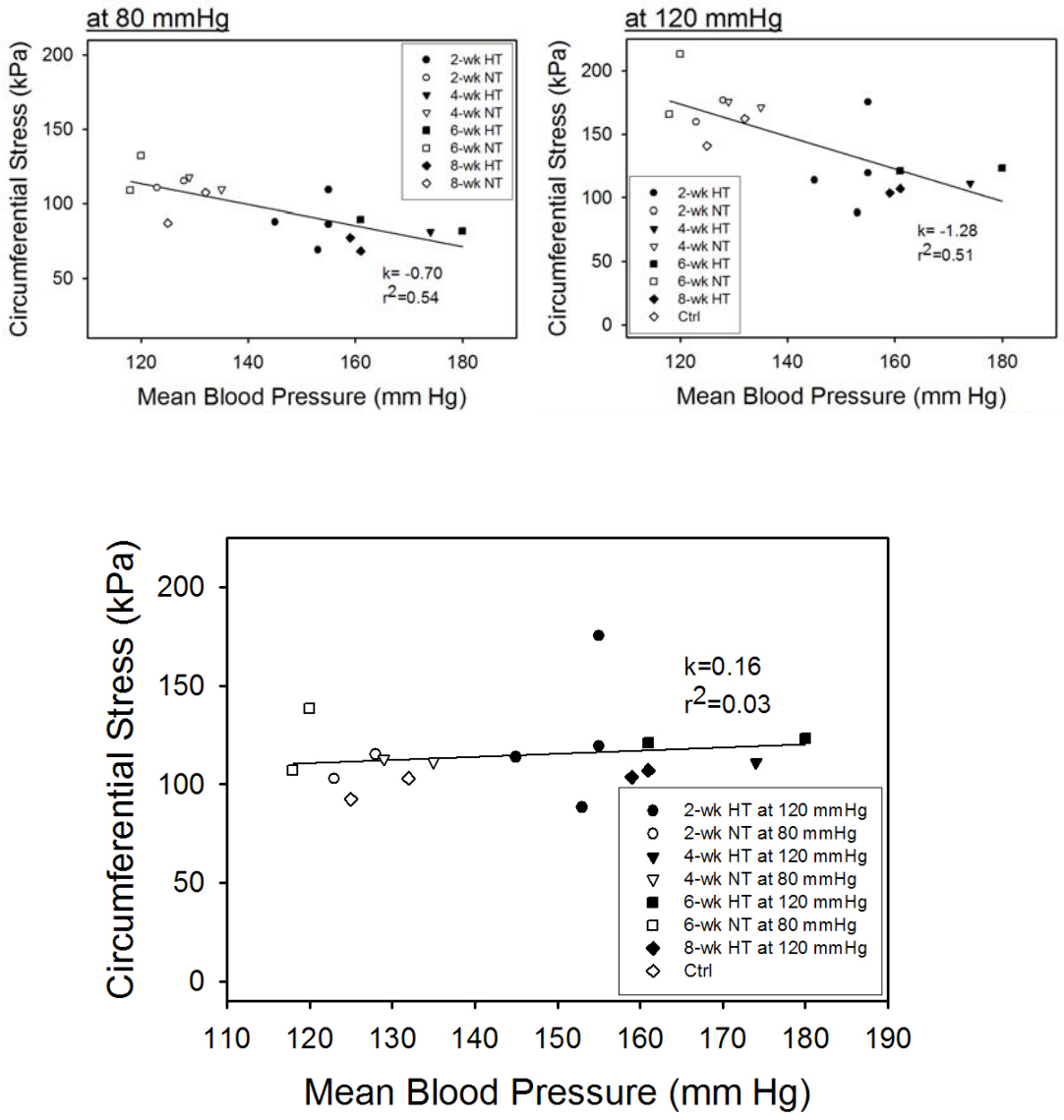

Figure III-9. Cauchy stresses at comparable pressures (e.g., 80 or 120 mmHg) differed between NT and HT ($p < 0.05$), but they did not differ between NT at 80 mmHg and HT at 120 mmHg during in vitro testing. This suggests that structural and morphological adaptations during hypertension tended to restore the stresses back towards normal values.

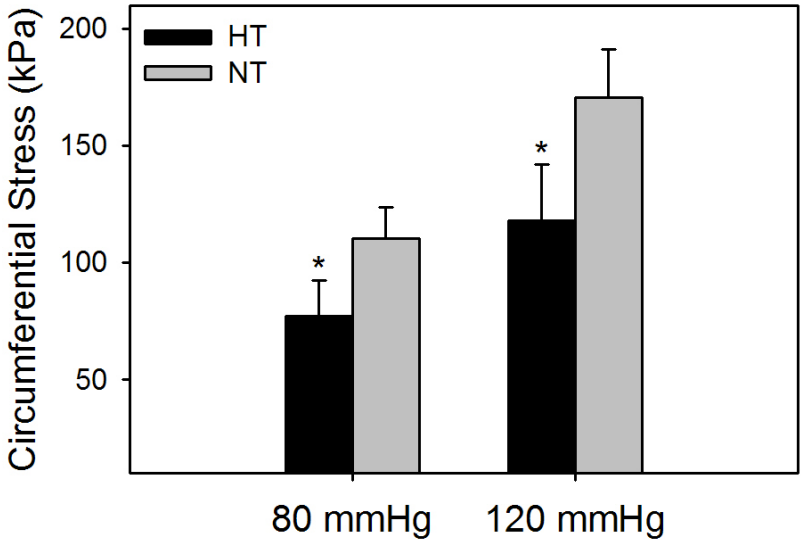

Figure III-9 (Continued)

hypertension (see below). Comparisons of hoop stresses at 80 and 120 mmHg (Figure III-9) suggested however that wall stress were statistically similar ($p = 0.06$) between NT vessels at 80 mmHg (perhaps close to an in vivo working pressure) and HT vessels at 120 mmHg (perhaps close to their in vivo working pressure). This observation was due, in part, to the increased thickness of the wall in HT, which resulted in a lower value of luminal radius:wall thickness *a/h* in HT at a given in vitro pressure (Figure III-10).

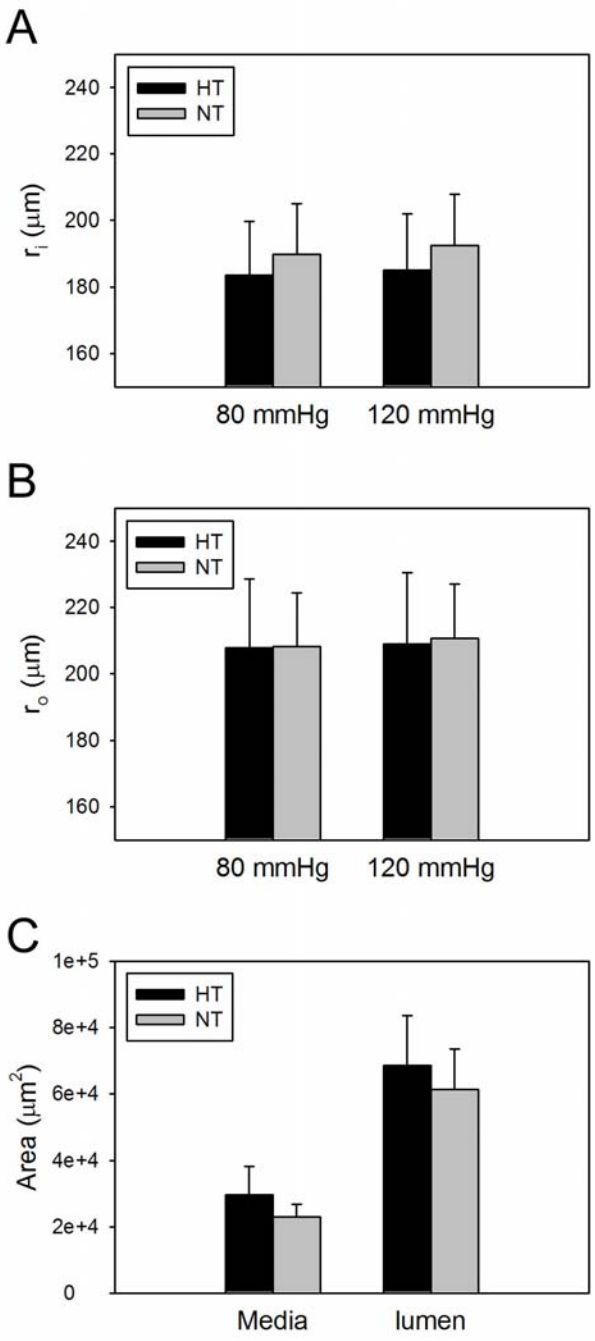

Figure III-10. Wall dimensions of the basilar artery from NT and HT pigs with pressure-dependent deformation taken into consideration (80 and 120 mmHg). The internal radius r_i (A), external radius r_o (B), and cross section area of media and lumen (C) did not change significantly in HT whereas wall thickness h (D) and ratio of internal radius to wall thickness r_i/h (E) were increased and decreased in HT, respectively.

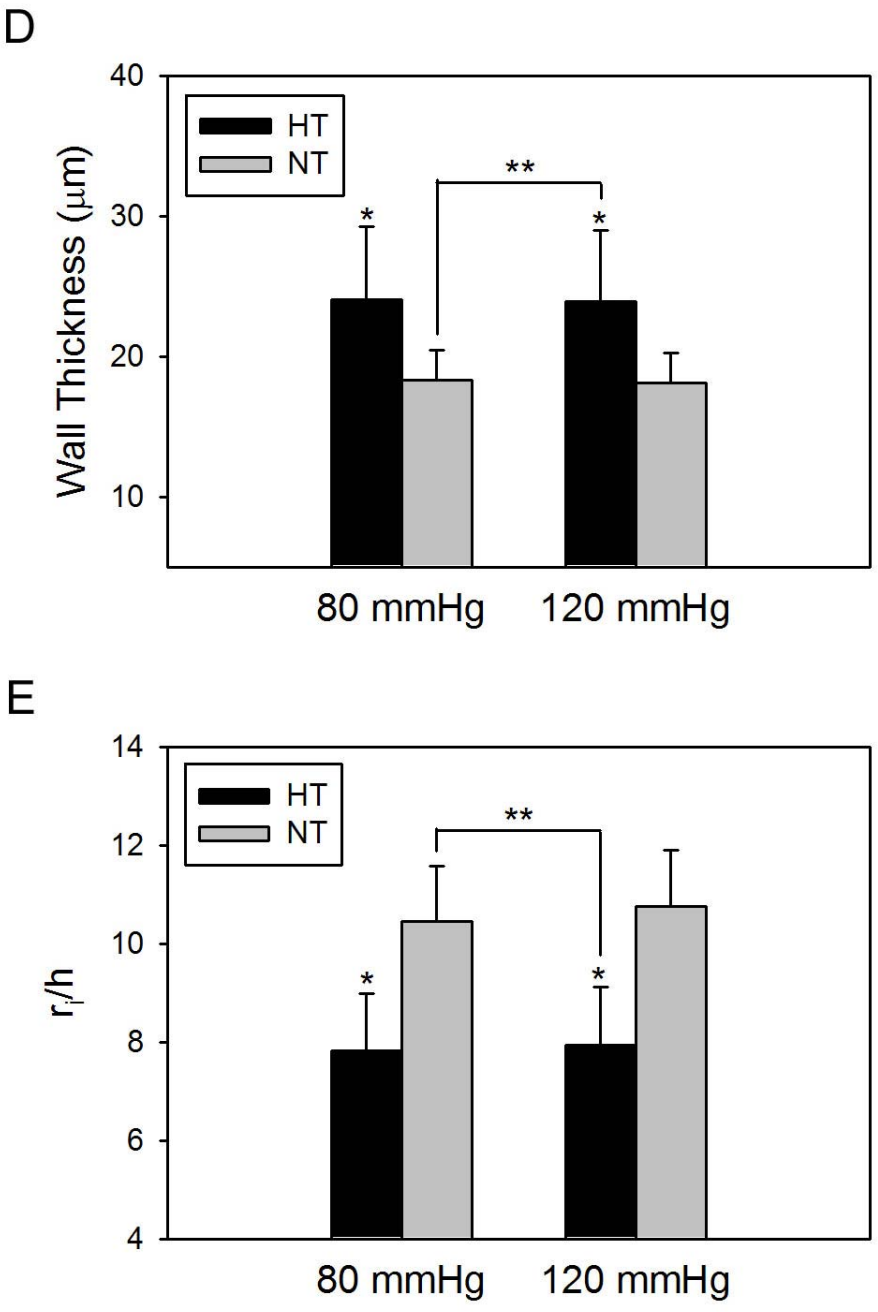

Figure III-10 (Continued)

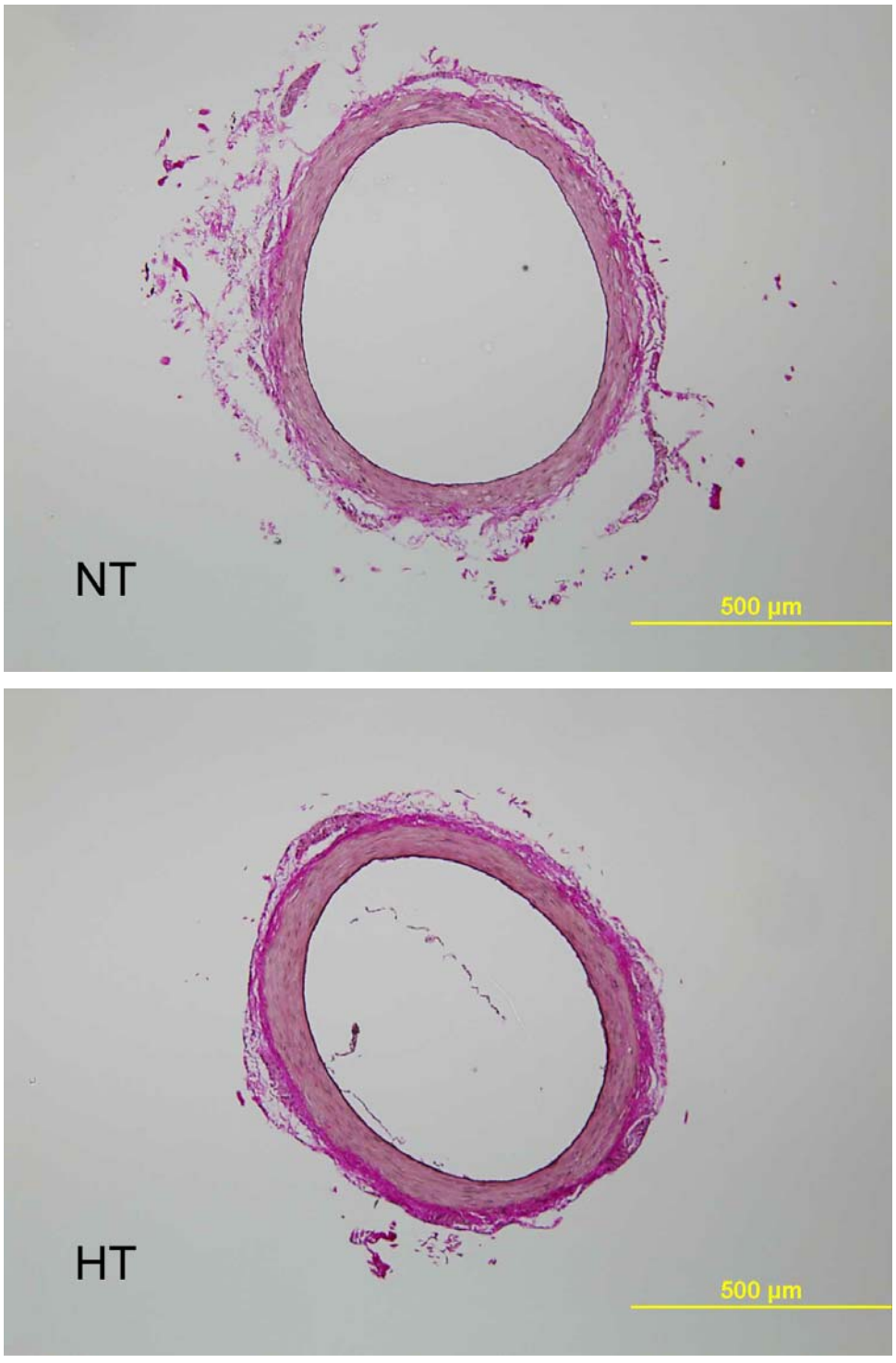

Figure III-11. VVG-stained cross sections of basilar arteries from NT and HT pigs; fixed in unloaded condition. Note the prominent presence of internal elastic lamina and absence of external elastic lamina.

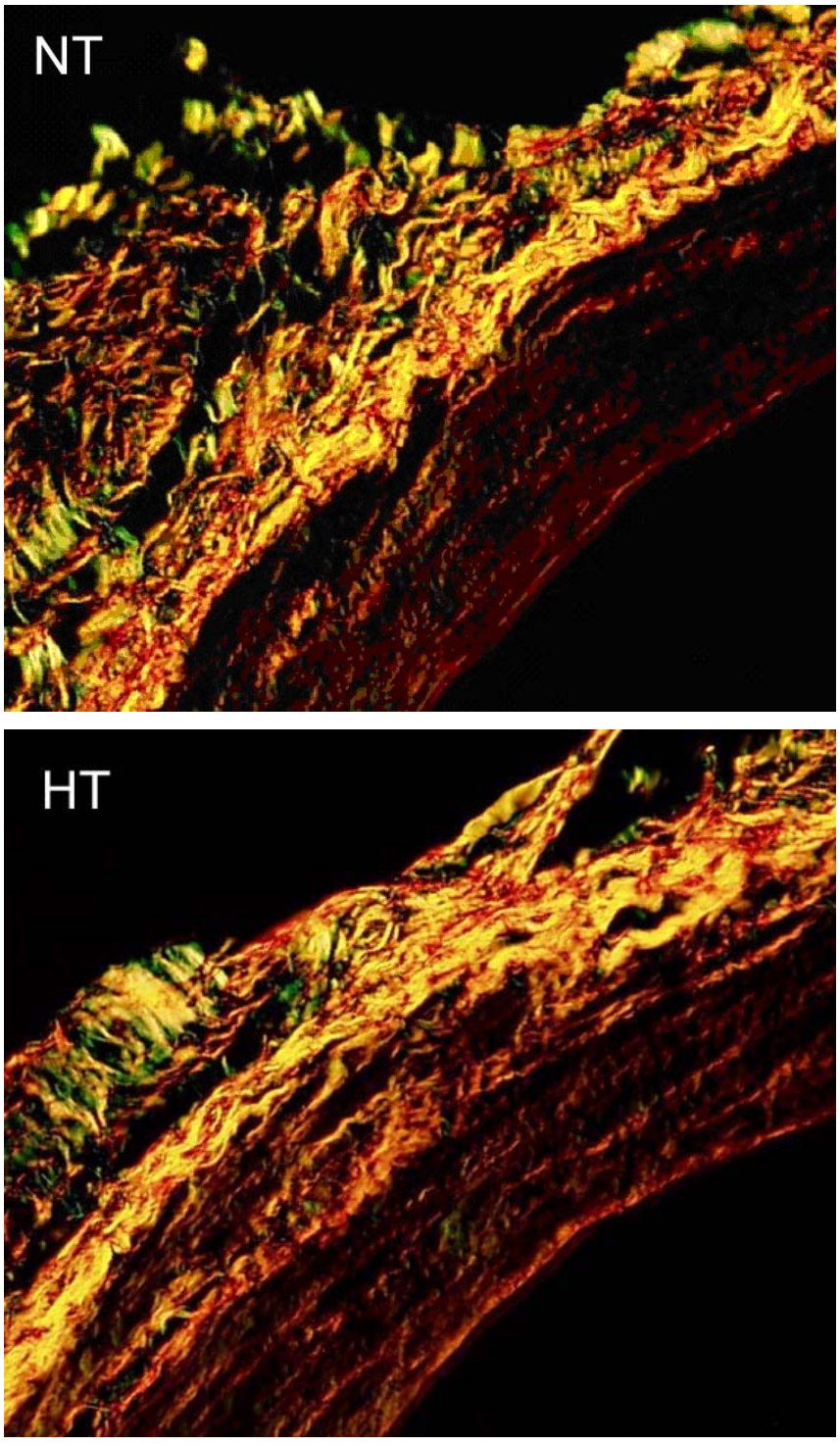

Figure III-12. PSR-stained cross sections of basilar arteries from NT and HT pigs under circularly polarized light; fixed in unloaded condition.

TABLE III-2. Wall Dimensions of Basilar Arteries in Unloaded Condition

	2 week		4 week		6 week		8 week		Ctrl(n=3)
	NT(n=2)	HT(n=4)	NT(n=2)	HT(n=1)	NT(n=2)	HT(n=2)	NT	HT(n=3)	
R_{inner}(μm)	135.9±17.7	137.8±11.3	131.4±17.6	128.3	134.3±13.8	130.5±11.8	n/a	153.4±4.2	121.8±10.0
H(μm)	25.8±2.6	29.3±6.6	25.5±1.5	25.2	25.9±6.6	27.6±0.9	n/a	35.6±2.6	27.6±5.2
R_{inner}/H	5.3±0.2	4.8±0.6	5.2±0.4	5.1	5.8±0.5	4.7±0.3	n/a	4.32±0.20	4.6±1.3
A_{sec}(μm^2)	15510±3498	28543±9297	23145±4320	22343	21359±6150	25084±2962	n/a	38294±4038	23338±3235
A_{lum}(μm^2)	67561±18763	67123±12983	54528±17989	60251	61058±11205	58243±19062	n/a	84152±5245	55230±9614

DISCUSSION

Although hypertension is a major risk factor for various neurovascular diseases, including saccular aneurysms and stroke, there is surprisingly little information in the literature on changes in the biomechanical properties of cerebral arteries due to hypertension. Without information on wall properties, one cannot perform the stress analyses that are needed to study the associated vascular cell mechanobiology – we know, for example, that increased wall stress alters the production and degradation of extracellular matrix as well as the proliferation and apoptosis of vascular smooth muscle cells[43]. One reason for this lack of data may be due to the presence of many small perforating vessels and the associated difficulty of isolating cerebral arteries suitable for in vitro pressure-diameter tests. That is, whereas "ring tests" have proven useful in certain classes of pharmacologic studies (e.g., Winquist and Bohr[44]), pressure-diameter tests at in vivo axial extensions are preferred for biomechanical testing[45,46]. Excellent early papers by Nagasawa et al.[47] and Hayashi et al.[48] showed that human intracranial arteries tend to be stiffer than their extracranial counterparts, consistent with their higher collagen:elastin ratio. Yet, these investigators focused on the effects of age, not hypertension.

The best study available on changes in the mechanical properties of cerebral arteries, measured via in vitro tests at the in situ length, is that by Hajdu and Baumbach[49]. Briefly, they compared pressure-diameter and circumferential stress-strain behaviors of the posterior cerebral artery in normotensive (Wistar-Kyoto) and spontaneously hypertensive (stroke-prone SHR) rats at 6 to 8 months of age. Very similar to findings herein (cf. their Figures 2a and 3a to the present Figures III-7B and III-8B), they report

significant decreases in distensibility at all but the lowest pressures and significant increases in the material stiffness due to hypertension. Indeed, if one accounts for differences in reference configurations (they appear to have used the in situ length at zero pressure whereas we use the unloaded reference), even the degree of changes are very similar. What is remarkable in comparing these two reports, therefore, is that their findings are for 6 to 8 month old spontaneously hypertensive rats, which presumably begin arterial adaptations early on in maturation, whereas our results show tremendous structural and material changes within 2 weeks of onset of hypertension in maturity. That is, although one might suggest that our findings imply a trend towards a gradual decrease in distensibility with duration of hypertension (Figure III-7A), there was a gradual increase in pressure at 6 and 8 weeks (Figure III-4A) – hence, it appears that the mechanical adaptations exhibited by the basilar artery were rapid and that once adapted, both structural and material properties tended to change little thereafter. It is of note, therefore, that similar rapid and sustained changes in structural stiffness were shown by Matsumoto and Hayashi[50] in rat aorta over 2 to 16 weeks of hypertension in a Goldblatt model. This is, to our knowledge, the first such demonstration in maturity in an intracranial vessel within a strong autoregulatory system (Strandgaard and Paulson[51]).

Although the contractile behavior of cerebral arteries is fundamental to autoregulatory control, most of such control resides in the smaller resistance vessels. Moreover, given that "Chronic hypertension is characterized by impairment in maximal dilator capacity of cerebral blood vessels" (Hajdu and Baumbach[49]), we focused on the passive properties. Consistent with prior results on extracranial conducting arteries (see

Matsumoto and Hayashi[50]; Rachev et al.[52]; Gleason and Humphrey[53]), our data suggested that wall adaptations tend to restore the mean hoop stress back towards a target value. For example, Figure III-9 reveals that circumferential wall stress in the hypertensive vessels at a higher pressure (say 120 mmHg) was similar to the stress in the normotensive vessels at lower pressure (say 80 mmHg); indeed, it is interesting that this value of comparable stress is ~120 kPa, which is not too different from that calculated in Humphrey and Wilson[54] as a possible target value. A similar finding was not true with respect to circumferential wall strain, however, for the hypertensive vessels were significantly less distensible than the normotensive controls; that is, it does not appear that hypertension-induced adaptations tend to restore to normal the values of cyclic strain (relative to updated unloaded configurations) or the structural stiffness. It is, of course, the structural stiffness that governs the hemodynamics, thus despite the renormalization of wall stress due to structural changes, it would be expected that the hemodynamics would remain altered. In this regards, it is important to note that our selection of 80 mmHg for NT and 120 mmHg for HT was arbitrary and meant only to be provocative; selection of other pairs of pressures could reveal an even closer result, but it is not clear what pressures should be compared. For example, do arterial adaptations correlate best with the diastolic, systolic, or mean blood pressure? Although there is a need for research into this issue, correlations should be based on the transmural pressure, not the luminal pressure. Unfortunately, determination of effects of perivascular tissue on the overall biomechanics of an artery remains a significant challenge. In the case of cerebral vessels, this issue is simplified slightly when vessels are surrounded largely by cerebrospinal fluid

(CSF); the pressure in the CSF is typically reported to be 5 to 10 mmHg[55]. Yet, it was because of the continuing lack of information on perivascular constraints that we restricted our attention to modest ranges of transmural testing pressures (up to 120 mmHg) in the passive state despite the much higher luminal pressures measured in vivo in the internal thoracic artery.

Similar to other extracranial arteries, the media of the basilar artery appears to bear most of wall tensile stress during normalcy. Therefore, changes in mechanical properties were predictably due to significant changes in structure and composition of the media. Indeed, histological analysis showed that wall thickness, which contributes significantly to the structural stiffness, was increased in the media of HT pigs. Under the circularly polarized light, PSR-stained cross sections revealed the increased collagen deposition in terms of thickening of the fibers. In addition, the cell number per unit area of media increased in HT. This is consistent with a morphometrical study of cerebral arteries from rats (SHR and SHRSP), in which the wall hypertrophy was characterized by increased SMC layers in comparison to wild type controls (WKY)[56]. The complementary work on the histology elucidated the mechanics underlying the increased stiffness and may provide information on strategies of treating such mal-adaptation.

In closing, we present here the first data on the time-course of changes in the histo-mechanical properties of a large cerebral artery during the early development of hypertension in maturity. In contrast to prior studies that employed rat models wherein hypertension initiates during development, our model examined adaptations during maturity that are more relevant to the human disease. Rapid and sustained changes

occurred in both the structural and material stiffness, due largely to an increased wall thickness and increased matrix deposition. There is a now a pressing need to determine if such changes can be reversed by lowering the blood pressure and, if so, how long does such reversal take or is there a narrow window of opportunity wherein reversal can be achieved.

CHAPTER IV

PHENOTYPIC MODULATION OF AORTIC SMOOTH MUSCLE CELLS IN HYPERTENSION: AN IMMUNOHISTOCHEMISTRY STUDY

INTRODUCTION

In both human and experimental hypertension, the arterial walls subjected to elevated blood pressure undergo tremendous growth and remodeling (G&R), the most conspicuous manifestation being thickening of the wall. Albeit adaptive, which is to say favorable by reducing circumferential wall stress towards normal values despite the persistence of the elevated pressure, such G&R may contribute to the progression of hypertension.

The altered circumferential stress in early hypertension is often hypothesized to be a key initiator of G&R[57-59]. Medial smooth muscle cells (SMCs), embedded in an abundant extracellular matrix consisting of elastin, collagen, and many other proteins and proteoglycans, bear part of the initially increased circumferential stress in hypertension. These cells may undergo hypertrophy and/or hyperplasia and may abnormally synthesize and secrete/deposit matrix proteins (e.g. collagen and elastin) as well as matrix metalloproteinases (MMP) and tissue-inhibitors of MMPs (TIMP), which further regulate matrix turnover. Each of these processes plays an active role in G&R of the arterial wall and is believed to be closely associated with the phenotype of the SMCs. Nonetheless, the mechanism underlying stress-induced phenotypic changes is largely unknown. It is thus essential to know the phenotype locally, specifically, the effect of altered stress fields on

phenotypic change before we can better understand its functions.

Marked spatial and temporal changes in the expression of multiple smooth muscle cell differentiation markers (e.g., myosin heavy chain isotypes[60,61], calponin[62], SM 22[63], 1E12[64], smoothelin[65]) has been reported in arterial development. These changes reflect, in part, the transition from a developing vessel, with strongly proliferative and synthetic SMCs, to a mature vessel, with a contractile and quiescent character. Spatial variations in the expression of the connective tissues proteins (e.g. collagen and elastin) across the vessel wall have been demonstrated in experimental hypertension model[19-21,66]. Similarly, we hypothesize that the localization of phenotypically differential SMCs may exhibit pattern that may correlate with the altered stress/strain gradient or the growth factor concentration gradient due to hypertension.

Because of the different growth responses of SMCs as well as the different deposition patterns of matrix proteins associated with animal models of hypertension and vascular bed[18], it is essential to study G&R of a specific artery in the same animal model. In our hypertension model, the in situ expression of several standard SMC differentiation markers was investigated by immunohistochemistry. Temporal changes of SMC differentiation with advancing hypertension were evaluated. Finally, the spatial and temporal expressions of collagen and elastin were also examined by observation of picrosirius red-stained and VVG-stained sections under polarized and normal light, respectively.

METHODS

Animal Model. Our aortic coarctation model for studying hypertension in the mini-pig is described in detail elsewhere[38]. Briefly, a balloon-expandable occluder is pre-filled with a 50% dextrose solution, placed over a Gor-Tex soft tissue patch sheet, and secured with suture around the aorta proximal to the diaphragm. The occluder is connected via stiff tubing to a vascular access port that is placed subcutaneously in the neck, which allows the occluder to be inflated or deflated in the conscious animal. An indwelling pressure transducer is placed within the internal thoracic artery or right carotid artery and connected to an implanted telemetry unit. Arterial pressure and heart rate can then be recorded continuously, but are typically recorded for 30 s every 2 h. The mean arterial pressure is defined as the diastolic pressure plus one-third the difference between systolic and diastolic pressure, and a daily average mean arterial pressure is used to track the condition of each animal.

To initiate hypertension, the aorta was coarcted approximately 1 week after surgery by adding small amounts of dextrose to the occluder over a 7 to 10 day period until the mean arterial pressure reached or exceeded 150 mmHg. Data were collected from a total of 46 mature (7 to 16 month old) male mini-pigs: 20 normotensive (NT) controls and 26 hypertensive (HT). Specifically, aortas were harvested from true controls ($n = 5$) without an occluder, from normotensive animals at 2 ($n = 4$), 4 ($n = 4$), 6 ($n = 3$), and 8 ($n = 4$) weeks following a sham surgery wherein an occluder was implanted but not inflated, and from hypertensive animals at 2 ($n = 7$), 4 ($n = 7$), 6 ($n = 6$), and 8 ($n = 6$) weeks after the animal reached its target mean arterial pressure (> 150 mmHg). All

animal care and use was approved by the University Laboratory Animal Care Committee at Texas A&M University.

Preparation of Paraffin Sections. Segments of aorta 3+ cm proximal and distal to the occluder that was used to induce the coarctation, and hence hypertension, were dissected free of perivascular tissue. The segments were fixed by immersing in 4% fresh paraformaldehyde for one hour at room temperature, dehydrated through a series of graded alcohols overnight, and embedded in paraffin to enable examination of cross sections. Five micron serial sections were cut using a microtome. Finally, control tissues (e.g. spleen and skeletal muscle from normotensive pigs) where handled and processed in a similar way.

Histology and Immunohistochemistry. Sections were deparaffinized in pure xylene, rehydrated through a series of graded alcohols and rinsed in phosphate buffered saline (PBS). Sections were stained with standard H&E for general morphology, Verhoeff-van Gieson (VVG) for elastin (Appendix D), and picro-sirius red (PSR) for collagen (Appendix E), or immuno-stained for a panel of antibodies (Table IV-1). Immunohistochemistry was carried out at room temperature in a humidity chamber to reduce evaporation. To unmask the antigen site, heat-induced epitope retrieval or enzymatic digestion was applied (Appendix F). The optimal retrieval methods were found for each antibody. After antigen retrieval, the slides were incubated with 3% H_2O_2 for twenty minutes to block endogenous peroxidase and rinsed in PBS. Slides were incubated in blocking serum for 30 minutes to prevent non-specific staining. Optimal dilution for each antibody was found by titering. Sections were incubated with

appropriately diluted primary antibody for 1 hour at room temperature. After washing in PBS, the diluted biotinylated secondary antibody was applied to the sections, incubated for 30 minutes, and again washed in PBS. Sections were then incubated with streptavidin-peroxidase conjugate for 30 minutes, washed, and incubated with DAB substrate (Vector laboratories) for 3-5 minutes in dark until achieving the desired staining intensity. For simultaneous demonstration of two antigens in the same section, the section was incubated with the first primary antibody followed by ABC procedures with the addition of 0.02% $NiCl_2$ to the DAB substrate. This stains the first antigen black. The section was then incubated with the second primary antibody followed by ABC procedures using the DAB reaction without $NiCl_2$, giving a brown product. The slides were rinsed in tap water, couterstained with hematoxylin, dehydrated, and finally coverslipped with Permount (Fisher Scientific). Concerning the standardization and reproducibility for future image analysis, the sections were cut in the same thickness and stained in the same batch (or the same day if the former is not possible).

Antibodies: Table IV-1 shows the antibodies, the vendors, the pretreatment needed to unmask the epitope, and the optimal dilutions.

TABLE IV-1. Primary Antibodies Used in Medial Immunohistochemistry

Antibody	Source	Pretreatment	dilution
SMC differentiation markers			
SM myosin heavy chain (SMMS-1)	Dako	1 mM EDTA, pH 8, MW 30%, 5 min*2	1:1000
Desmin (DE-R-11)	Dako	1 mM EDTA, pH 8, MW 30%, 5 min*2	1:200
Calponin (CALP)	Dako	1 mM EDTA, pH 8, MW 30%, 5 min*2	1:500
Caldesmon (N5/22)	Chemicon	1 mM EDTA, pH 8, MW 30%, 5 min*2	1:2500
Smoothelin (R4A)	Abcam	1 mM EDTA, pH 8, MW 30%, 5 min*2	1:50
SMemb (3H2)	Abcam	None	1:25,000
Cell proliferation			
Ki-67 (MIB-1)	Dako	1 mM EDTA, pH 8, MW 30%, 5 min*2	1:200
Collagen synthesis			
Hsp47 (M16.10A1)	Stressgen	1 mM EDTA, pH 8, MW 30%, 5 min*2	1:4000
Carboxyl-terminal propeptide of type I collagen (SP1.D8)	DSHB	Trypsin, 20 min, RT	1:300
Amino-terminal propeptide of type I collagen (PCIDG10)	Chemicon	Pronase, 20 min, RT	1:750

DSHB: Developmental Studies Hybridoma Bank, University of Iowa

Apoptosis assay. The terminal deoxynucleotidyl transferase (TdT)-mediated deoxyuridine triphosphate (dUTP)-biotin nick end-labeling (TUNEL) was performed on paraffin sections for labeling of DNA fragmentation according to manufacturer's instructions (DeadEnd colorimetric TUNEL kit, Promega) with modifications[67]. Briefly, after deparaffinization and rehydration, slides were placed in a plastic jar containing 200 ml EDTA solution (1 mM, pH=8). Following a brief period of equilibrium, the jar was irradiated in a microwave power-set at 20% for five minutes, which increased the temperature to 85-90^{o}C. An extra 80 ml of distilled water at room temperature were

added to the jar immediately after the irradiation to cool the solution. Then the slides were transferred to another plastic jar containing 250 ml PBS at room temperature (rapid cooling). An EDTA solution (1 mM, pH=8) was superior to a citrate buffer (0.01 M, pH=6), which is recommended by various references in terms of background staining and strength of specific positive staining; this may be due to differences in fixation and processing procedures. Endogenous peroxidases were quenched by incubation with 3% H_2O_2 for twenty minutes and rinsed in DDW. The sections were immersed in TDT buffer (30mM Trizma base, pH 7.2, 140 mM sodium cacodylate, 1 mM cobalt chloride). TDT (0.3 e.u./ μl) and biotinylated dUTP in TDT buffer were then added to cover the sections, which were then incubated in a humid chamber at 37°C for 60 min. The reaction was terminated by transferring the slides to TB buffer (300 mM sodium chloride, 30 mM sodium citrate) for 15 min at room temperature. The sections were rinsed with DDW, covered with 2% bovine serum albumin (BSA) for 10 min at room temperature, rinsed in DDW, and immersed in PBS for 5 min. Sections were then incubated with streptavidin-peroxidase conjugate for 30 minutes, washed, and incubated with DAB substrate (Vector laboratories) for 5-10 minutes in the dark until desired staining intensity was reached. The exact same protocol was used on sections of lymph node as a positive control.

RESULTS

Collagen and Elastin. Viewed under circularly polarized light, the PSR-stained sections revealed the lamellar structure of collagen in the media. Its thickness and the interlamellar distance increased in hypertensive media in comparison to that of the sham-operated or non-operated controls, which indicated more collagen deposition occurring in hypertension. This feature was more prominent in the inner media than in the outer media, however (Figure IV-1). Similarly, VVG staining (Figure IV-2) revealed that both the thickness of elastic lamina and interlamellar distances increased in the inner media of hypertensive animals in comparison to their counterparts in control animals. In the hypertensive intima and inner media, the intense elastin staining could be due to synthesis of elastin or fragmentation of existing elastin, and in these cases the internal elastin lamina was hardly defined.

Apoptosis and Cell Proliferation. The antigen Ki-67 is present during all active phases of the cell cycle (G_1, S, G_2, and M), but absent in resting cells (G_0); it is thus an excellent marker for cell proliferation activity. We found an increased number of nuclei staining for Ki-67 in the intima and media proximal to the occluder in many hypertensive pigs (Table IV-2, IV-3) compared to the sham-control or un-operated control animals. The TUNEL assay, which demonstrates in situ DNA fragmentation, a hallmark for apoptosis, similarly showed positive reaction in many hypertensive intima and some of adventitia (Figure IV-7) but no staining was found in the media. Together, therefore, immunostaining of Ki-67 and TUNEL indicated an increased turnover rate of endothelial cells. Note that in 8-week HT, there is still apoptosis undergoing in the endothelial cell

layer.

On the other hand, in the media that showed significant amount of Ki-67 staining, the stained nuclei appeared to be distributed evenly across the vessel wall. The peak of cell proliferation seemed to appear in the early phase of hypertension (2-4 weeks). It is worth noting that proliferation of cells in media and intima appeared to be independent in most cases of the hypertensive animals, which suggested that the intimal cells may be from different cell types than the medial SMCs. However, Ki-67-stained cells can be found in the neointima whenever there is a neointima development (Figure IV-6B).

The aortic SMC responded to hypertension by proliferating and increasing their deposition of ECM proteins. These seem to be independent of the radial position within the wall.

Expression of SMC differentiation markers. Because of variations in animal size, the slightly different positions of the occluder, the degree of hypertension (average MAP = 168 ± 16, n=37) and their associated influences on the SMC phenotypes, it was challenging to compare the immuno-stained sections from animal to animal; i.e. larger animals have a larger aorta with a thicker aortic wall, and the relative composition of elastin and collagen changes as the aorta tapers. Therefore to evaluate the phenotypic changes of SMCs due to hypertension, I chose to focus on the area that showed marked changes in cell proliferation and collagen production, which were demonstrated by immunostaining for Ki-67 and procollagen, respectively (Figure IV-3). Serial sections of the same area immuno-stained for a battery of SMC differentiation markers were then compared to counterparts for the controls.

In cases showing increased medial SMC proliferation and collagen synthesis, the SMC contractile markers – calponin, caldesmon, and smoothelin – were down-regulated; in contrast, non-muscle MHC, the SMC synthetic marker, was up-regulated. Smoothelin was the only SMC contractile markers among the five that did not stain all the medial SMC (i.e., some medial SMCs were positive whereas others remained unstained), which suggested that there were distinct populations of medial SMCs.

Desmin is an intermediate filament, a large family of cytoskeletal components. Immunohistochemistry for desmin revealed an inhomogeneous expression across the aortic wall. Generally, SMC from the inner media and sometimes from near the boundary of media and adventitia stained positive for desmin. In addition, the expression pattern of desmin along the circumference showed significant differences, which were most prominent when comparing anterior and posterior portions of the aorta. The staining intensity of desmin was also found to be less in the HT than in the NT.

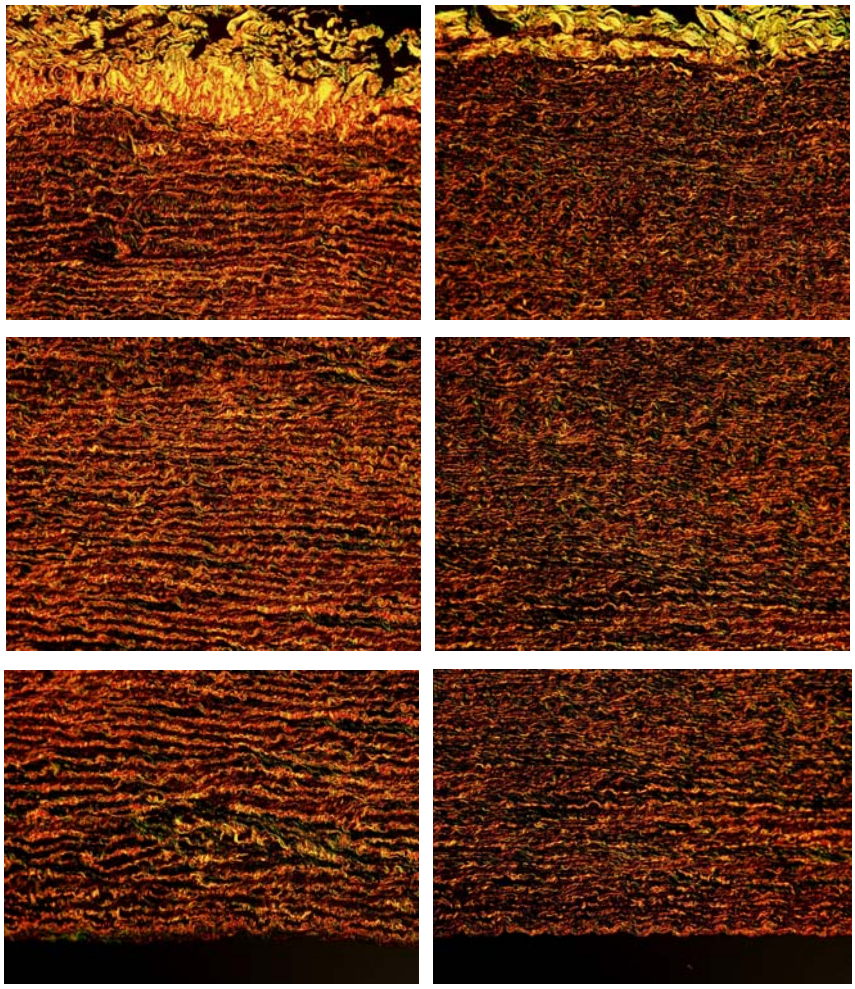

Figure IV-1. Representative microphotography of PSR-stained aortic sections under circularly polarized light. The thickness of the collagen "layer" increased in the HT animal (left panel) compared to the sham-control animal (right panel).

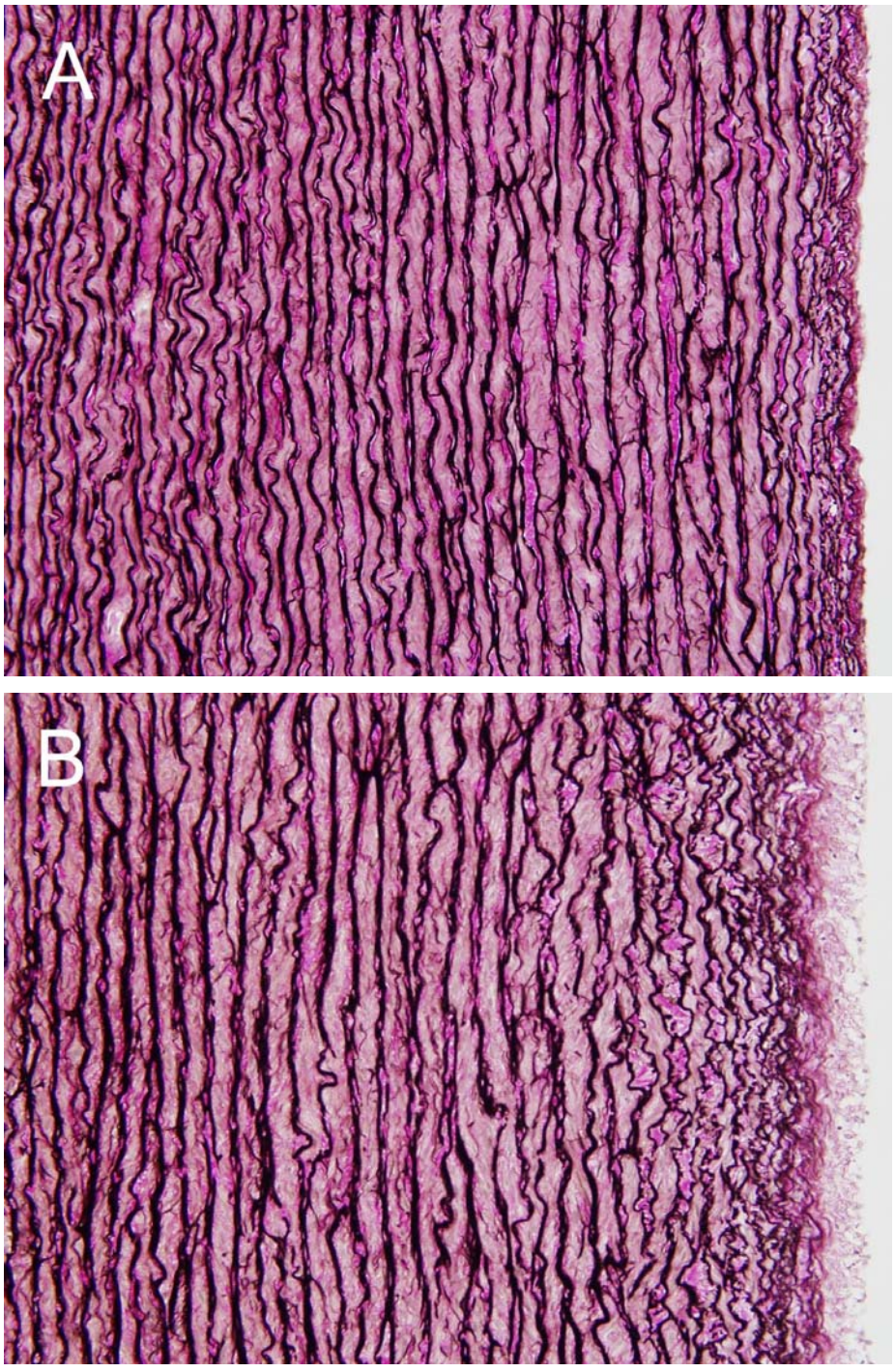

Figure IV-2. Representative microphotography of VVG-stained sections of the aorta. Note the increased interlamellar spacing and elastic lamina thickness in the inner media of HT animals and lose of organization of elastic lamina possibly due to fatiquing effects[68].

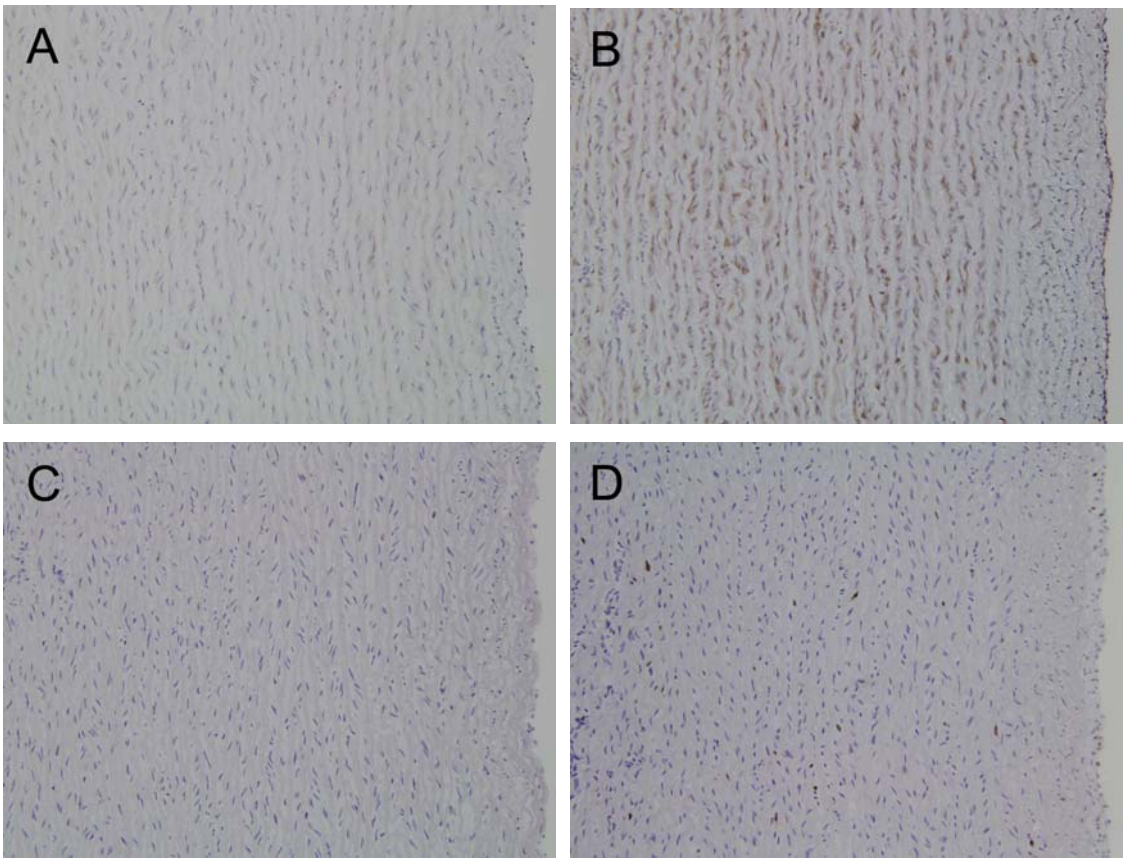

Figure IV-3. Immunohistochemical staining of formalin-fixed, paraffin-embedded (FFPE) porcine aorta with anti-procollagen (I) (A and B) and anti-Ki-67 (C and D) using ImmPRESS. Serial sections from HT animals (B and D) and NT animals (A and C). The lumen is at the right of the micrographs.

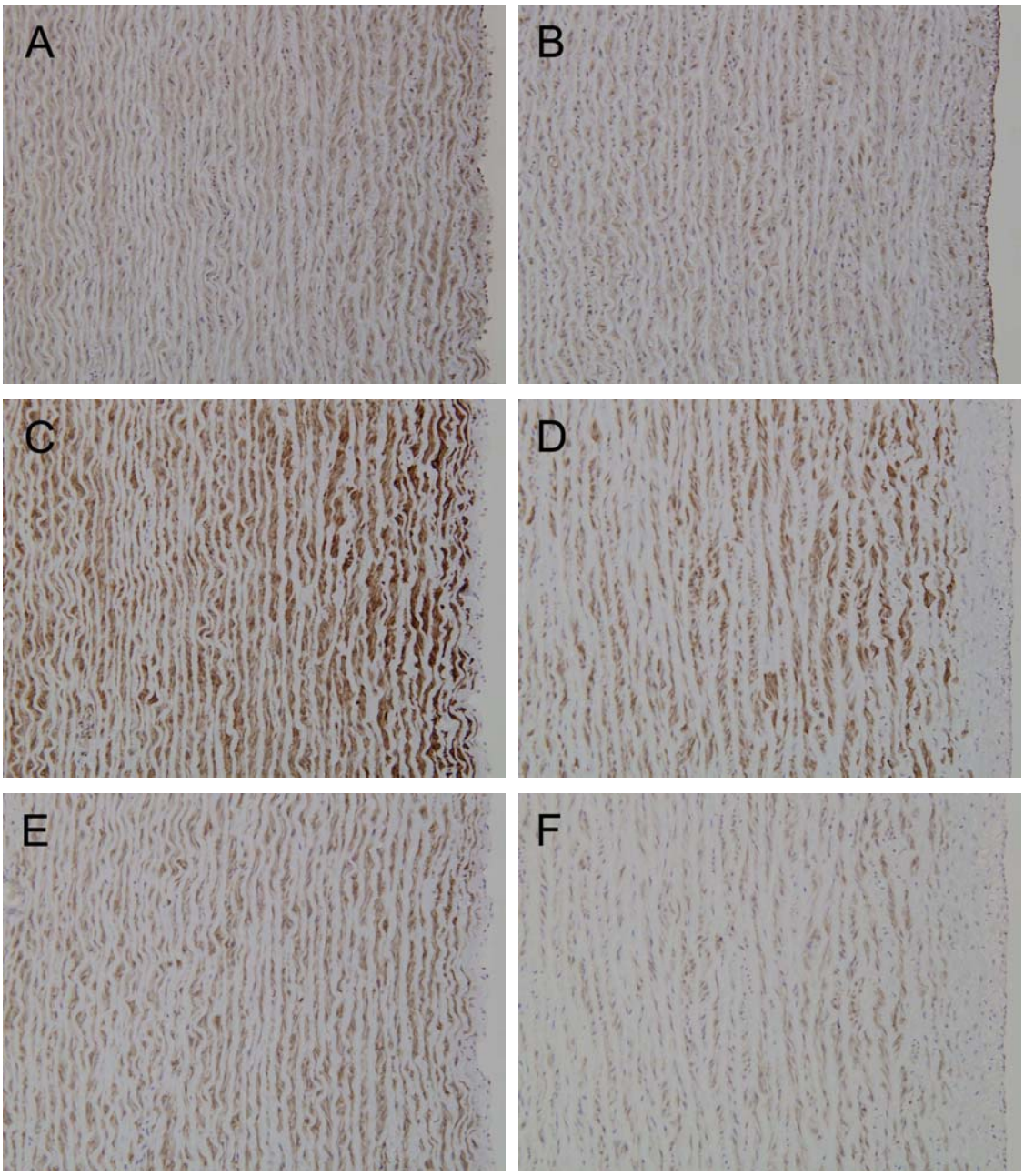

Figure IV-4. Immunohistochemical staining of FFPE porcine aorta with anti-calponin (A and B), anti-caldesmon (C and D), anti-smoothelin (E and F), and anti-non-muscle MHC (G and H) using ImmPRESS. Serial sections from HT animals (B, D, and F) and NT animals (A, C, and E). The lumen is at the right of the micrographs.

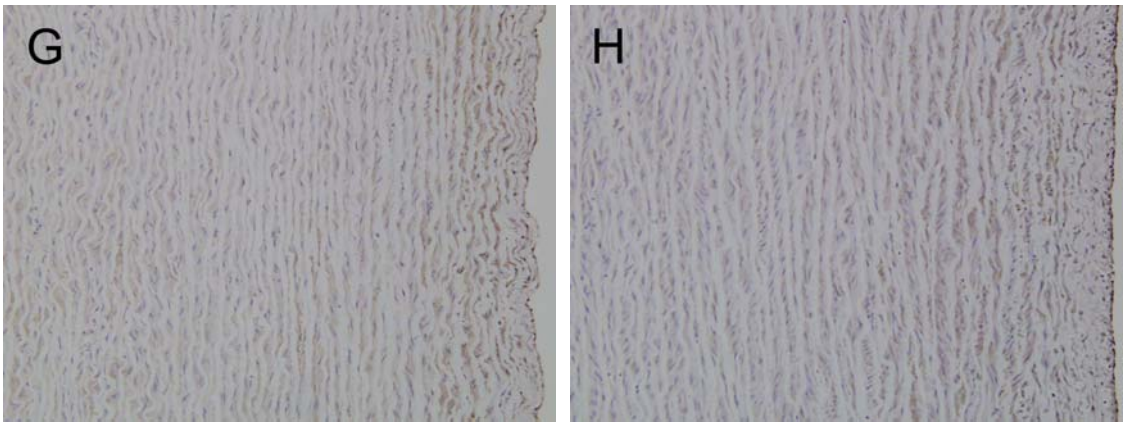

Figure IV-4 (Continued)

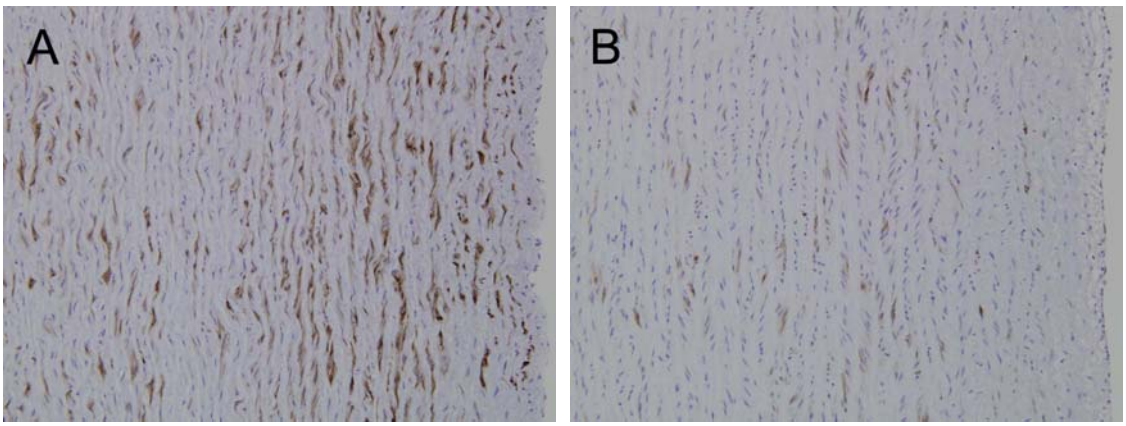

Figure IV-5. Immunohistochemical staining of FFPE porcine aorta with anti-desmin (A and B) using ImmPRESS. Serial sections from HT animals (B) and NT animals (A). The lumen is at the right of the micrographs.

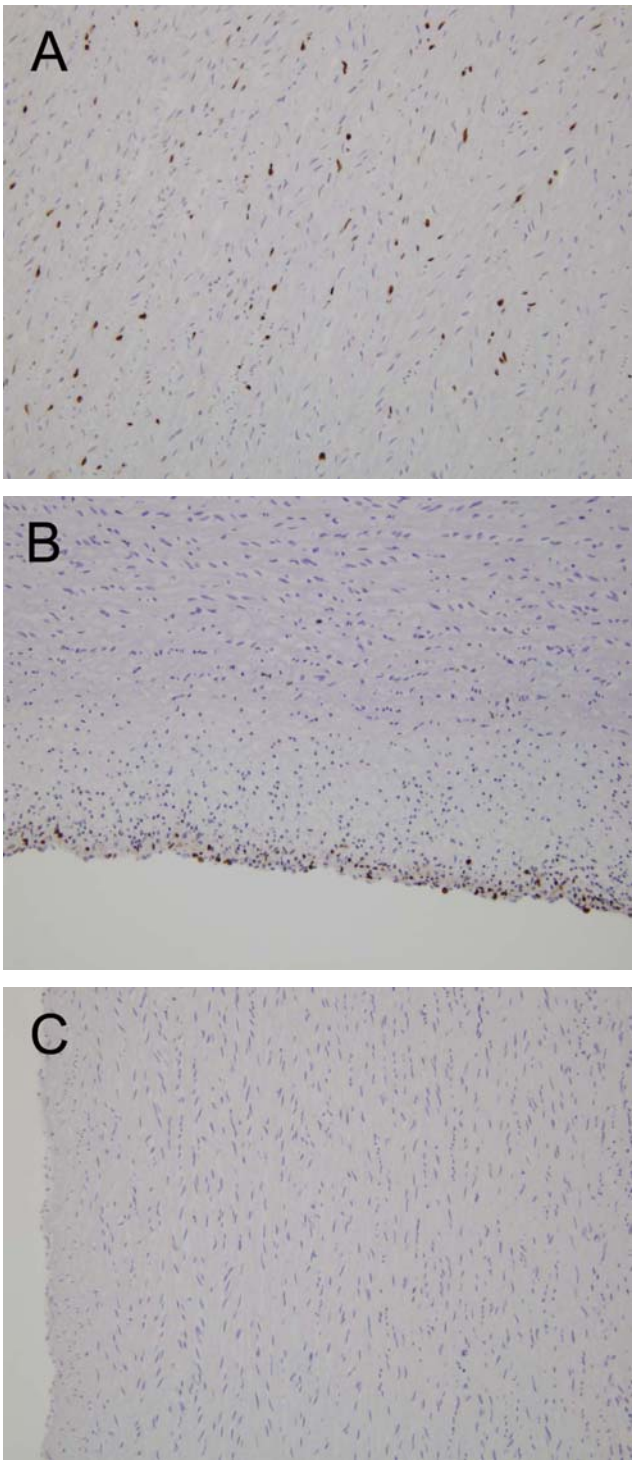

Figure IV-6. Immunohistochemical staining of FFPE porcine aorta with anti-ki-67 using ImmPRESS.

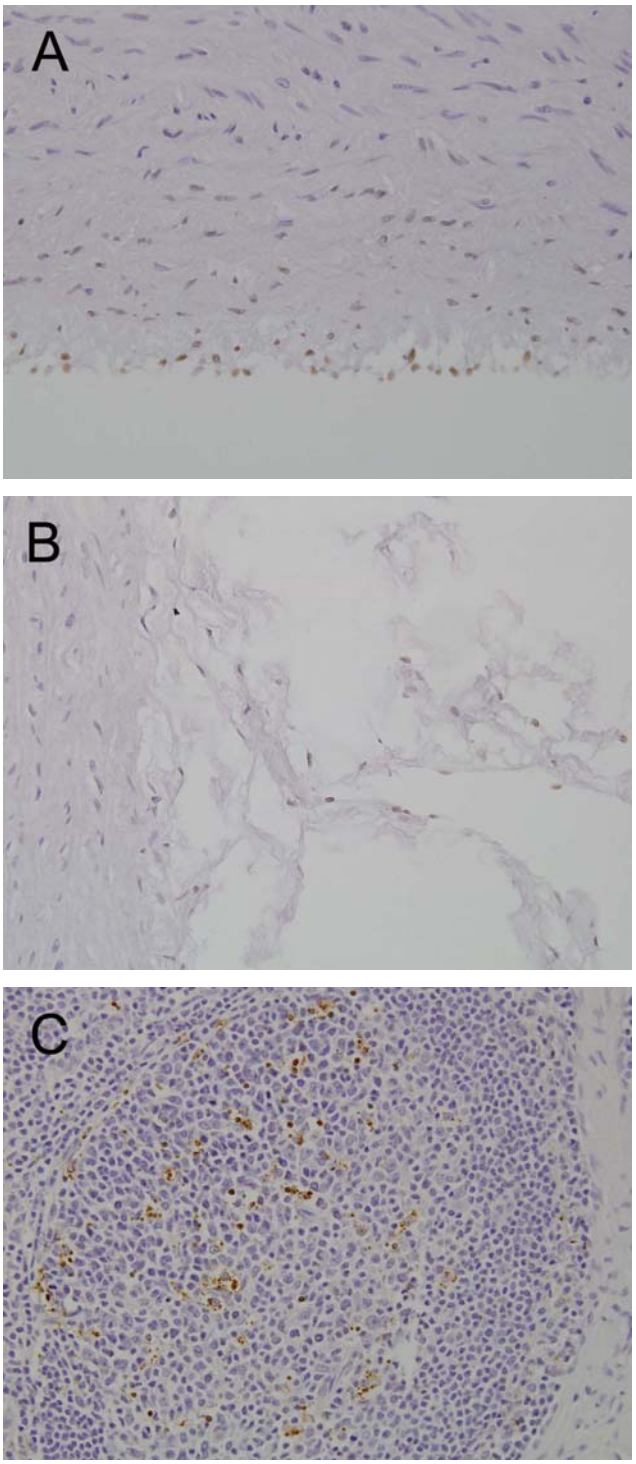

Figure IV-7. Detection of apoptosis by TUNEL assay. The aorta sections from HT animals showing apoptosis in intima (A) and adventitia (B). The lymph node from a NT pig was used as the control tissue to optimize the procedure of pretreatment. Cells undergoing apoptosis in the germinal center showed positive stain.

TABLE IV-2. Immunohistochemical Findings in Aortic Media of Hypertensive Pigs

No	Treatment	IT	Calponin (IM/MM/OM)	Caldesmon (IM/MM/OM)	Non-M MHC (IM/MM/OM)	Smlin (IM/MM/OM)	Desmin (IM/MM/OM)
1	2H	-	+/+/+	++/++/++	+/±/+		±/±/±
2	2H	+	+/+/+	++/+/++	±/±/±		+/±/±
3	2H	±	+/±/+	++/+/++	±/+/±	++/+/++	+/±/+
4	2H	+	+/+/+	+/+/+	+/±/±	+/±/±	±/±/±
5	2H	-	+/+/+	++/++/++	+/+/+	++/++/++	±/±/±
6	2H	-	++/+/++	++/+/++	+/+/+	+/+/+	+/±/±
7	2H	-	++/+/+			++/++/++	+/+/±
12	4H	±	+/+/+	+/+/+	±/+/+	±/++/++	±/+/±
13	4H	+	+/+/+	+/+/+	±/+/±	++/++/++	+/±/±
14	4H	±			±/+/±	++/+/+	+/±/±
15	4H	+	+/+/+	++/+/+	+/±/±	++/+/±	±/±/±
16	4H	±	+/+/+	±/±/±	±/±/±	+/++/+	+/±/±
17	4H	±	++/+/+	++/+/+	±/+/+	+/++/±	+/±/±
18	4H	±	++/+/++	++/+/++		++/+/+	+/±/±
23	6H	-	++/+/+	++/+/+	++/++/++	+/+/±	±/±/-
24	6H	±	+/+/++	±/±/+	+/±/±	+/±/+	±/+/±
25	6H	-	++/+/+	+/±/±	+/+/+	++/±/±	+/-/-
26	6H	+	++/+/++	++/+/++	±/+/+	++/+/+	+/±/±
27	6H	+	++/+/+	++/+/++		+/±/±	±/-/-
28	6H	+	++/+/+	++/+/+	±/+/±	++/++/++	+/±/±
32	8H	+	±/±/±	±/±/±	+/±/±		±/±/±
33	8H	+	+/+/+	±/+/±	±/±/±	±/+/±	+/±/±
34	8H	+	++/+/+	+/+/+	±/+/+	±/+/+	+/±+±
35	8H	+	+/+/+	++/+/+	±/+/+	±/+/±	±/±/±
36	8H	+			±/±/±	+/+/±	+/±/±
37	8H	±	++/+/++	+/+/+	+/+/+	++/±/++	+/±/±

Intensity of staining was scored from ++ (strong staining) to – (absence of staining) with the order: ++ > + > ± > -. IT: intimal thickening; Non-M MHC: non-muscle myosin heavy chain; Smlin: Smoothelin; IM: inner media; OM: outer media

TABLE IV-3. Immunohistochemical Findings in Aortic Media of Surgical and True Control Pigs

No	Treatment	IT	Calponin (IM/MM/OM)	Caldesmon (IM/MM/OM)	Non-M MHC (IM/MM/OM)	Smlin (IM/MM/OM)	Desmin (IM/MM/OM)
1	2N	-	+/+/+	++/++/++	+/±/±		±/±/±
2	2N	-			±/+/±		+/±/±
3	2N	+				±/±/+	+/±/±
4	2N	-	+/+/+	++/++/++	±/±/±	+/++/++	+/±/±
5	4N	-	+/+/+	+/+/+			+/±/+
6	4N	-	+/+/++	++/++/++			±/±/±
7	4N	-			+/+/+	+/++/+	+/±/±
8	4N	-			+/+/+	++/++/++	+/±/±
9	6N	-				++/++/++	±/±/±
10	6N	-	+/+/+	++/++/++	±/±/±	++/++/+	
11	6N	-	++/+/++	++/++/++	+/±/±		+/±/±
12	8N	-			±/±/±		±/±/±
13	8N	±				++/±/+	+/±/±
14	8N	+	+/+/+	++/+/+			+/+/+
15	8N	±	+/+/+	+/+/±	+/±/+	+/±/±	+/±/±
16	SC	-					±/-/±
17	SC	-					+/±/±
18	SC	-					±/-/±
19	UC	-					+/±/±
20	UC	-					+/±/+

See footnotes to Table IV-3.

DISCUSSION

We used a porcine aortic coarctation model to study pressure-induced G&R. The porcine aorta represents a better model for studying potential stress-induced G&R than rodent arteries since the many lamellae enable us to study possible spatial changes, or gradient expressions, across the vessel wall. The porcine vasculature is also more similar to that of humans in comparison with mouse or rat models[69], whose aorta contains only 4-6 elastic laminae.

Sans and Moragas used mathematical morphologic analyses to study the structure of the human aortic media in normotensive and hypertensive patients[70]. Consistent with their finding, the interlamellar distance was larger in the inner media than in the outer media and this difference was even more exaggerated in hypertensive animals. The decreasing interlamellar distance from the inner to the outer media found in normotensive patients may indicate a stress gradient through the wall thickness, although the inclusion of residual stress in the stress calculation supports an even distribution of tensile stress[43]. On the other hand, while they did not find significant changes in elastic lamina thickness across the aortic wall, the elastic lamina in the inner media of HT appeared to be thicker than in the outer media and in counterparts in NT. The increased tensile stress due to elevated blood pressure may affect mostly the inner media and thus result in significant matrix protein deposition in this area.

Examination of potential spatial and temporal changes in SMC differentiation in experimental hypertension can be valuable for tracing structural changes during vascular remodeling. Bearing in mind that the expression of a protein may be regulated by its own

specific mechanism, we used immunohistochemistry to examine the expression of a battery of SMC-specific markers, including calponin, caldesmon, non-muscle MHC, desmin, and smoothelin. Information from immunohistochemistry should be examined in parallel to histological staining such as VVG, however, which provides more structural details. Similarly, immunostaining for different antigens should be evaluated together to provide a more complete picture of phenotypical changes.

We found an increased number of nuclei staining for Ki-67 in the intima and media in many HT pigs. Contrary to our hypothesis, the stained nuclei appeared to be distributed evenly across the vessel wall. This may suggest that the stress distribution across the aortic wall renormalized within the first two weeks of hypertension or that some autocrine mechanism makes medial SMCs respond in concert. The latter seems preferred because our findings on matrix deposition suggested a stress gradient through the aortic wall thickness. The first two weeks seemed to be a key period for hypertensive aortic G&R since the highest of cell proliferation (Ki-67) and collagen (I) production (SP1.D8) was observed in the 2-week HT. It has been shown that the growth response of SMC to hypertension can be hypertrophy and/or hyperplasia[7]. Further morphometrical analysis of nuclei number per unit area of cross section could determine if hypertrophy was also involved[71]. Orton and colleagues also showed hyperplasia in media cells; instead of using immunohistochemistry for Ki-67 or PCNA, they used bromodeoxyuridine (BrdU)-labeling to index cell proliferation[72]. Although extra work (i.e., intravenous injection) needs to be performed for BrdU labeling, it allows one to determine the kinetics by doing pulse-chase labeling and it also provides information

with regard to the direction of proliferation[73].

In a bovine pulmonary hypertension model, Wohrley and colleagues showed that proliferation occurred almost exclusively in meta-vinculin-negative SMCs, which suggests an expansion of a specific SMC phenotype[74]. Based on our data for Ki-67, procollagen (I), and the SMC differentiation markers, however, it seemed that SMCs expressing contractile proteins can also proliferate and actively synthesize extracellular matrix proteins. This phenomenon suggested that phenotypic modulation, defined as a transition between contractile and synthetic phenotypes, played a role in this adaptive process.

In contrast to staining patterns for other SMC differentiation markers, some medial SMCs lacked expression of smoothelin and desmin; this may indicate subtle differences in SMC populations. Double-staining of immunohistochemistry for these two markers and Ki-67 may provide further information. On the other hand, to describe the possible spectrum of phenotypically distinct SMCs that may co-exist in the aortic media in our animal model, more specific SMC differentiation markers are desired (e.g., smooth muscle myosin heavy chain isotypes, SM1 and SM2). Alternatively, we may try markers (not necessarily SMC differentiation markers) reported to be responsive to stress/strain or growth factors.

The expression pattern of SMC differentiation markers in the aortic media was varied slightly along the circumference. This may result from different circumferential strains/stresses along the circumference. Indeed, due to the tethering of the aorta to the spine, the aorta does not deform uniformly along the circumference in a cardiac cycle[75].

In order to study the effect of the elevated blood pressure while eliminating the contributions of non-uniform expansion of the vessel, comparisons should focus on a specific portion of the aortic wall, e.g., the anterior wall, which has been shown to stretch maximally in a cardiac cycle. In addition, hypertension may cause more severe consequences in the anterior aortic wall than in the posterior wall.

The staining intensity was stronger near the boundaries between the intima, media, and adventitia probably due to the longitudinal orientation of SMCs in these regions. Generally, proteins of contractile apparatus align along the long axis of spindle-shaped SMCs. Therefore, in the aortic cross section, SMCs with longitudinal orientations may be immunostained stronger for these proteins due to their higher density in the thickness of the sections.

Quantification of possible patterns of in situ protein expressions will be elucidated further by digital image analysis of tissue sections in Dr. S. Liu's group (Department of Computer Science) at Texas A&M University. The down- or up-regulation of SMC differentiation markers found by immunohistochemistry should be complemented with quantitative data from Western Blot and/or RT-PCR, which will be carried out in Dr. Wilson's group (Department of Medical Physiology). Although immunohistochemistry reveals local distributions in proteins, in situ hybridization provides supplemental information with regard to the mRNA level of the protein as well as the type of cell contributing to the synthesis. Thus, combined immunohistochemistry and in situ hybridization may also prove helpful in the future.

As the intensity of elevated pressure and the frequency of pulse cannot be

manipulated in this model, attention needs to be paid to variations between animals as well as the pressure profiles of each animal during the experiment. Constriction of occluder affects the local hemodynamics, causing turbulence (e.g. eddies) downstream of the occluder, which may also complicate the interpretation of results from distal sections. Because of the possible involvement of hormonal and nervous stimuli in an animal model, establishment of an *ex vivo* organ culture system may provide complementary data to describe pressure-induced G&R.

The long-term objective of this study is to understand G&R of arteries in response to an altered mechanical environment and to elucidate the underlying mechanisms. Toward this end, there is a need to develop a mathematical model of pressure-induced G&R. The information obtained in this study can facilitate the development of such a model by kinetic analysis, which in turn may aid in the design of new treatment strategies to prevent maladapted G&R in hypertension and help provide directions for tissue engineering of vascular grafts.

CHAPTER V

CHANGES IN INTIMA OF AORTA IN A PIG COARCTATION MODEL

INTRODUCTION

Although hypertension is a risk factor for atherosclerosis, the precise mechanisms by which hypertension induces or aggravates atherosclerosis remain unknown. Based on the response to injury hypothesis, atherosclerosis is regarded as a chronic inflammatory response by the arterial wall that is initiated by some form of injury to the endothelium[76]. Indeed, endothelial injury[77] or dysfunction (e.g., altered NO production[78] and an associated increased permeability[79] and monocyte adhesion[80]) has been found in hypertension and likely plays an important role in the initiation of plaque formation.

In a monkey aortic-coarctation model[81], the arteries proximal to the coarcted site showed focal thickening of the intima. If further subjected to a hypercholesterolemic diet, the hypertensive monkey developed severe atherosclerotic lesions. It is worth nothing that the distribution of the atherosclerotic lesions appeared to be the same as that of the intimal lesions in the hypertensive only monkey. Using a combined hypercholesterolemia and hypertension rabbit model, Xu et al.[82] reported that hypertension induced a differential distribution of gene expression for collagen I and III whereas hyperlipidemia alone associated with an upregulation of tropoelastin gene expression, which is closely associated with the formation of foam cell lesions.

It is conceivable that the formation of a neointima may predispose atheroma formation. Nevertheless, a variety of events including bypass grafting surgery[83], balloon

angioplasty[84,85], and hypertension[81] cause endothelial injury and intimal thickening. Unfortunately the reasons for such thickening are not well known. An understanding of how intimal thickening happens may provide clues to prevent atherosclerosis.

We hypothesize that malfunctioning endothelial cells produce extracellular matrix proteins in the subendothelial space and thereby contribute to the intimal thickening. Moreover, the deposition of extracellular proteins under the endothelial layer may provide a suitable space for smooth muscle cell (SMC) migration and proliferation.

Heat shock protein 47 (Hsp47) is a collagen-specific molecular chaperon involved in the intracellular processing, folding, and assembly of procollagens[86]. Residing in endoplasmic reticulum, Hsp47 transiently binds to newly synthesized procollagen and dissociates from it before it is transported to the Golgi complex. Hsp47 knockout mice, which are defective in collagen synthesis, display abnormally oriented epithelial tissues and ruptured blood vessels and die before 11.5 day postcuitos[87]. In humans and experimental models, regardless of the tissue site or organ, induction of Hsp47 expression is always noted in fibrotic processes. In the vascular system, Hsp47 is found in the fibrous cap of human atheroma along with the expression of procollagen type I; it is regulated by TGF-β1 or FGF-2[88].

Soon after release into the extracellular space, first the amino propeptides and then the carboxyl propeptides are cleaved from procollagen type I[89,90]. Therefore, antibodies to the amino-terminus or carboxyl-terminus of procollagen type I, which only bind to intracellular procollagen type I, can be used to detect sites of active collagen type I deposition. This approach has been used to study vascular remodeling[91].

Positive staining in immunohistochemistry for Hsp47 or procollagen type I also indicates sites of active collagen synthesis. Immunohistochemical examination of cross sections of the aorta proximal to the occluder used to induce hypertension, particularly for Hsp47 and procollagen type I, may provide insight into sources of the accumulated matrix proteins in the neointima.

METHODS

Animal Model. Our aortic coarctation model for studying hypertension in the mini-pig is described in detail elsewhere[38]. Briefly, a balloon-expandable occluder is pre-filled with a 50% dextrose solution, placed over a Gor-Tex soft tissue patch sheet, and secured with suture around the aorta proximal to the diaphragm. The occluder is connected via stiff tubing to a vascular access port that is placed subcutaneously in the neck, which allows the occluder to be inflated or deflated in the conscious animal. An indwelling pressure transducer is placed within the internal thoracic artery or right carotid artery and connected to an implanted telemetry unit. Arterial pressure and heart rate can then be recorded continuously, but are typically recorded for 30 s every 2 h. The mean arterial pressure is defined as the diastolic pressure plus one-third the difference between systolic and diastolic pressure, and a daily average mean arterial pressure is used to track the condition of each animal.

To initiate hypertension, the aorta was coarcted approximately 1 week after surgery by adding small amounts of dextrose to the occluder over a 7 to 10 day period until the mean arterial pressure reached or exceeded 150 mmHg. Data were collected from a total of 46 mature (7 to 16 month old) male mini-pigs: 20 normotensive (NT) controls and 26 hypertensive (HT). Specifically, aortas were harvested from true controls ($n = 5$) without an occluder, from normotensive animals at 2 ($n = 4$), 4 ($n = 4$), 6 ($n = 3$), and 8 ($n = 4$) weeks following a sham surgery wherein an occluder was implanted but not inflated, and from hypertensive animals at 2 ($n = 7$), 4 ($n = 7$), 6 ($n = 6$), and 8 ($n = 6$) weeks after the animal reached its target mean arterial pressure (> 150 mmHg). All

animal care and use was approved by the University Laboratory Animal Care Committee at Texas A&M University.

Preparation of Paraffin Sections. Segments of aorta 3+ cm proximal and distal to the occluder that was used to induce the coarctation, and hence hypertension, were dissected free of perivascular tissue. The segments were fixed by immersing in 4% fresh paraformaldehyde for one hour at room temperature, dehydrated through a series of graded alcohols overnight, and embedded in paraffin to enable examination of cross sections. Five micron serial sections were cut using a microtome. Finally, control tissues (e.g. spleen and skeletal muscle from normotensive pigs) where handled and processed in a similar way.

Histology and Immunohistochemistry. Sections were deparaffinized in pure xylene, rehydrated through a series of graded alcohols and rinsed in phosphate buffered saline (PBS). Sections were stained with standard H&E for general morphology, Herovici's polychrome stain for delineating collagens[92] or immuno-stained for a panel of antibodies (Table V-2). Immunohistochemistry was carried out at room temperature in a humidity chamber to reduce evaporation. To unmask the antigen site, heat-induced epitope retrieval or enzymatic digestion were applied (appendix C). The optimal retrieval methods were tested for each antibody (Table V-2). After antigen retrieval, the slides were incubated with 3% H_2O_2 for twenty minutes to block endogenous peroxidase and rinsed in PBS. Slides were incubated in blocking serum for 30 minutes to prevent non-specific staining. Optimal dilution for each antibody was found by titering. Sections were incubated with an appropriately diluted primary antibody for 1 hour at room

temperature. After washing in PBS, the diluted biotinylated secondary antibody was applied to the sections, incubated for 30 minutes, and again washed in PBS. Sections were then incubated with streptavidin-peroxidase conjugate for 30 minutes, washed, and incubated with DAB substrate (Vector laboratories) for 3-5 minutes in dark until achieving the desired staining intensity. For simultaneous demonstration of two antigens in the same section, the section was incubated with the first primary antibody followed by ABC procedures with the addition of 0.02% $NiCl_2$ to the DAB substrate. This stains the first antigen black. The section was then incubated with the second primary antibody followed by ABC procedures using the DAB reaction without $NiCl_2$, giving a brown product. The slides were rinsed in tap water, couterstained with hematoxylin, dehydrated, and finally coverslipped with Permount (Fisher Scientific). Concerning the standardization and reproducibility for future image analysis, the sections were cut in the same thickness and stained in the same batch (or the same day if the former is not possible).

Antibodies: Table V-1 shows the antibodies, the vendors, the pretreatment needed to unmask the epitope, and the optimal dilutions.

TABLE V-1. Primary Antibodies Used in Intimal Immunohistochemistry

Antibody	Source	Pretreatment	dilution
SMC differentiation markers			
SM myosin heavy chain (SMMS-1)	Dako	1 mM EDTA, pH 8, MW 30%, 5 min*2	1:1000
Desmin (DE-R-11)	Dako	1 mM EDTA, pH 8, MW 30%, 5 min*2	1:200
Calponin (CALP)	Dako	1 mM EDTA, pH 8, MW 30%, 5 min*2	1:500
Caldesmon (N5/22)	Chemicon	1 mM EDTA, pH 8, MW 30%, 5 min*2	1:2500
Smoothelin (R4A)	Abcam	1 mM EDTA, pH 8, MW 30%, 5 min*2	1:50
SMemb (3H2)	Abcam	None	1:25,000
Cell proliferation			
Ki-67 (MIB-1)	Dako	1 mM EDTA, pH 8, MW 30%, 5 min*2	1:200
Collagen synthesis			
Hsp47 (M16.10A1)	Stressgen	1 mM EDTA, pH 8, MW 30%, 5 min*2	1:4000
Carboxyl-terminal propeptide of type I collagen (SP1.D8)	DSHB	Trypsin, 20 min, RT	1:300
Amino-terminal propeptide of type I collagen (PCIDG10)	Chemicon	Pronase, 20 min, RT	1:750

DSHB: Developmental Studies Hybridoma Bank, University of Iowa

Lectin staining. Dewaxed, rehydrated sections were soaked in EDTA solution (1 mM, pH=8.0) and cooked in pressure cooker for two minutes to unmask the epitope. After quenching the endogenous peroxidase and blocking non-specific binding sites, the sections were incubated with biotinylated lectin from *Dolichos Biflorus* (DBA)(Vector Laboratories, CA). The detection system was the same as that used in the immunohistochemistry.

RESULTS

Neointima development. Whereas the intima in normotensive pigs (sham-operated and non-operated) did not show remarkable changes, prominent neo-intimal formation was found in the aorta proximal to the occluder in most hypertensive animals (Figure V-1). The formation of a neointima increased with the progression of the hypertension (Table V-1). In four among six 8-week hypertensive pigs, focal atheroma formation was also observed in the luminal surface (Figure V-2). The neointima seemed to develop irreversibly.

Expression of Hsp47 and procollagen. From the immunohistochemistry of Hsp47 (Figure V-3A, 3B), we found in the intimal lesions an active synthesis of collagen undergoing in the endothelial cells. Immunostaining with procollagen specifically localized the active sites of collagen synthesis to the endothelial cells (ECs). In parallel to Hsp47 expression, the procollagen type I appeared to be produced by the ECs.

With the optimal dilution of primary antibodies, the staining intensity of procollagen was stronger in the aortic media proximal to the occluder in hypertensive animals than that in the normotensive animal. This variation of staining intensity was small among the hypertensive groups; the strongest staining was found in 8-wk hypertensive animals, however.

Smooth muscle cell markers. A variety of SMC and EC markers were used to elucidate the origin of the intimal cells in our model. The staining intensity of calponin was stronger in aortic EC of HT pigs than in NT pigs. It appeared that intimal cells also stained for calponin (Figure V-4). Figure V-5 shows that the aortic ECs in both NT and

HT pigs did not stain for caldesmon. Also, while medial SMCs were all positive, the intimal cells did not stain for caldesmon. Figure V-6 revealed that smoothelin reactivity only existed in aortic medial SMCs, not in aortic ECs in either NT or HT and not in intimal cells in HT. The intimal cells expressed non-muscle myosin heavy chain (MHC), which was also found in the medial SMCs and EC (Figure V-7).

Endothelial cells markers. Von Willebrand factor (factor VIII-related antigen) and CD-31 are generally employed as endothelial cell markers. Unfortunately, porcine aortic endothelial cells have been reported to not or weakly express von Willebrand factor[93]; their expression was inconsistently detected in our study (not shown). On the other hand, the anti-human CD-31 antibody (DakoCytomation, CA) did not cross react with porcine tissue (demonstrated using unfixed frozen section). Thus, DBA lectin staining and immunostaining for eNOS were used to identify the endothelial cells. Figure V-8A shows that eNOS-stained cells appeared to infiltrate into the thickened intima. The diffusing pattern of DBA staining similarly suggested that endothelial cells may have migrated into the subendothelial space (Figure V-8B).

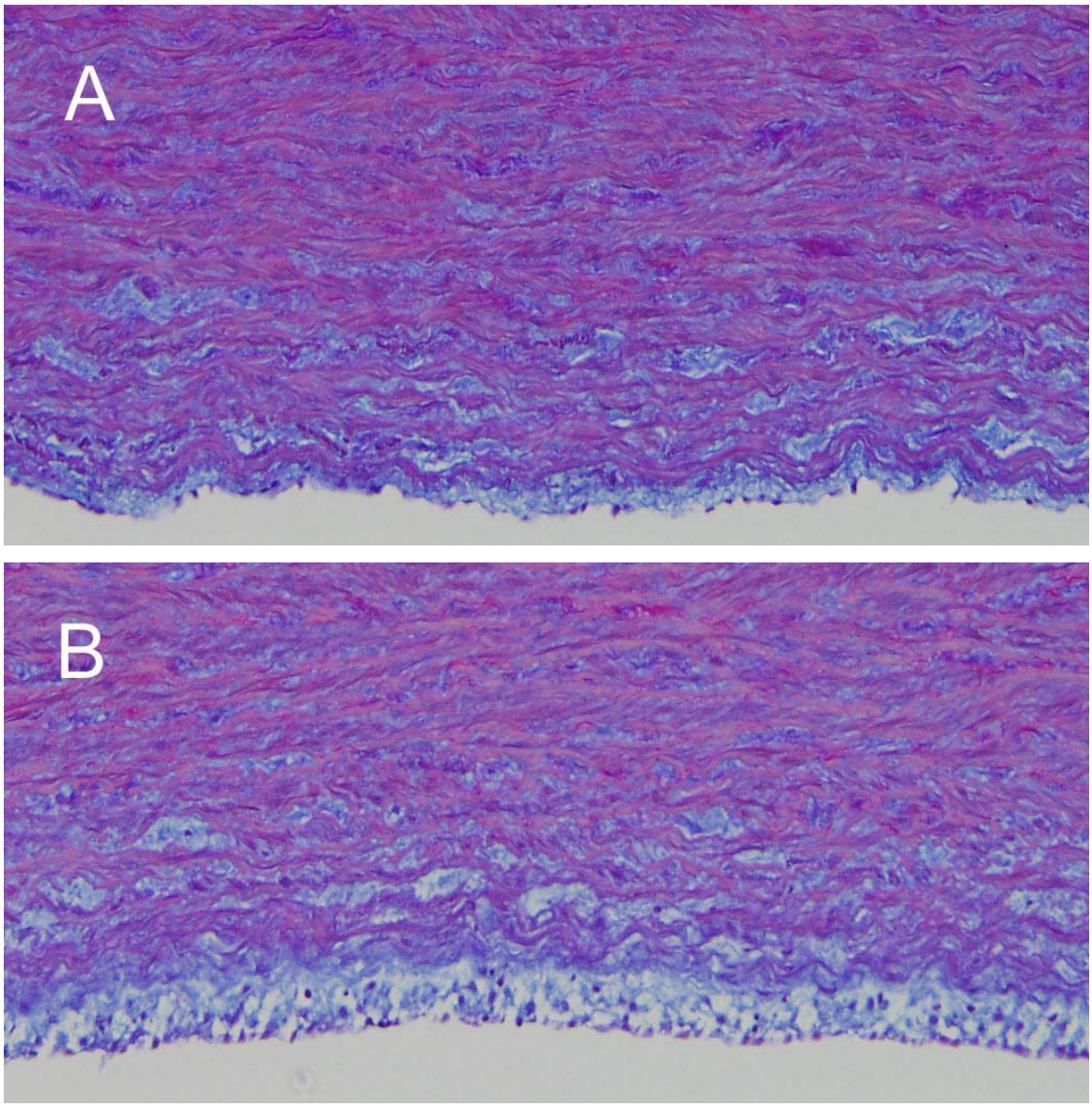

Figure V-1. Herovici's polychromic staining of aortic intima of NT (A) and HT (B) pigs. This staining has been claimed to be able to distinguish precollagen (blue) from mature collagen (red)[92].

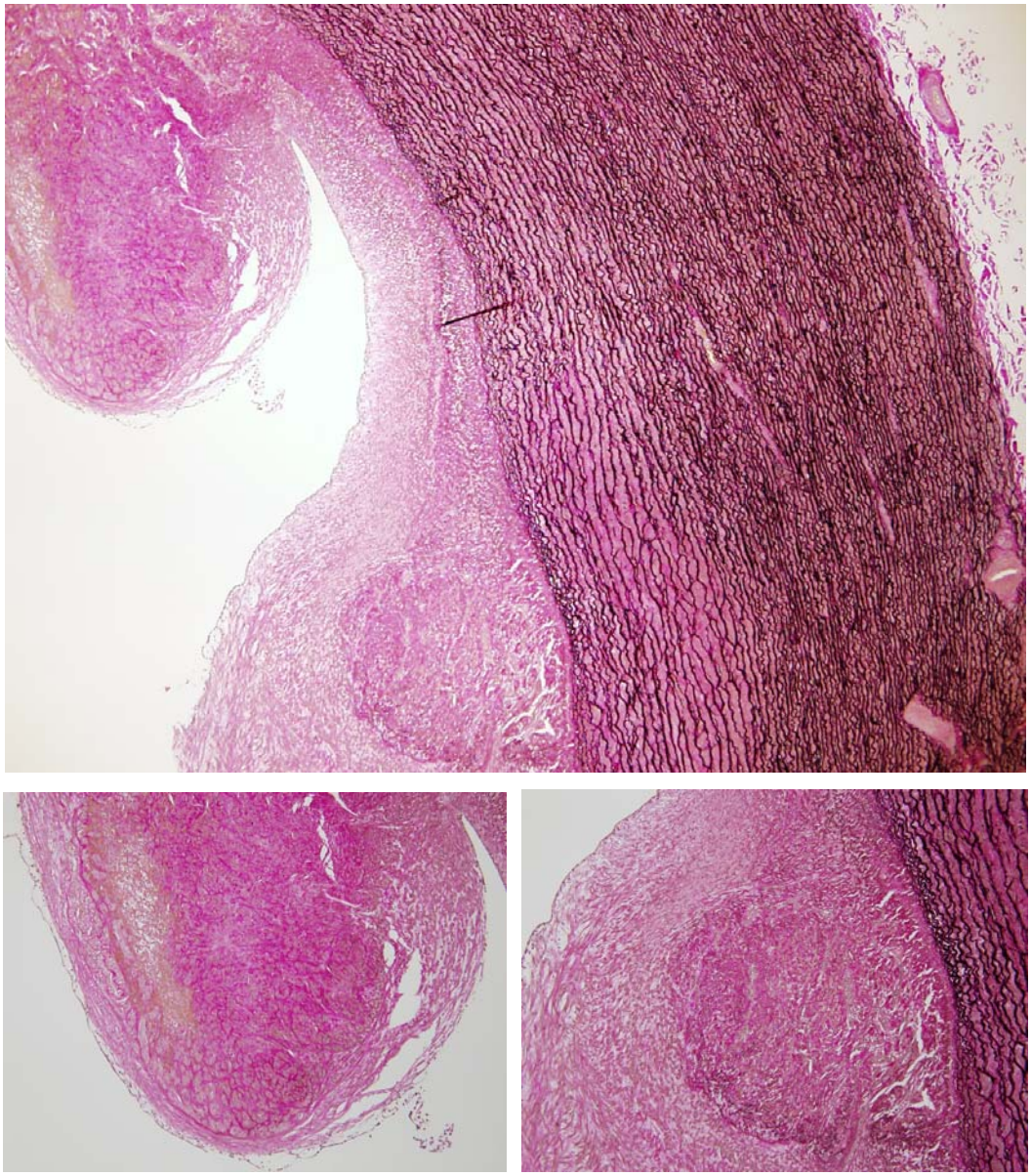

Figure V-2. Representative microphotography of VVG-stained sections of the aorta from an 8-week HT pig. Focal atheroma was found in the luminal surface. Note also that the inner media appeared to be very different from the outer media.

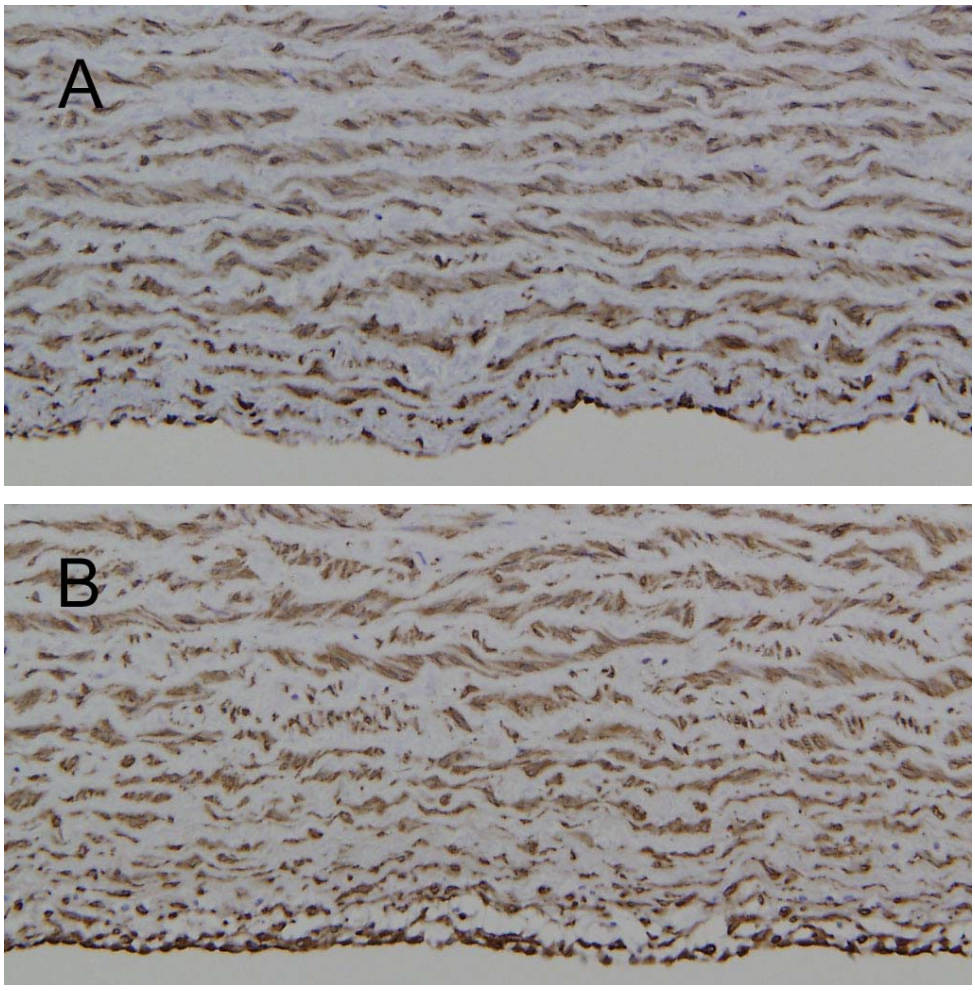

Figure V-3. Immunohistochemical staining of FFPE porcine aorta with anti-Hsp47 (A and B), anti-procollagen (C and D) using ImmPRESS. Serial sections from HT animals (B and D) and NT animals (A and C). The lumen is at the bottom of the micrographs.

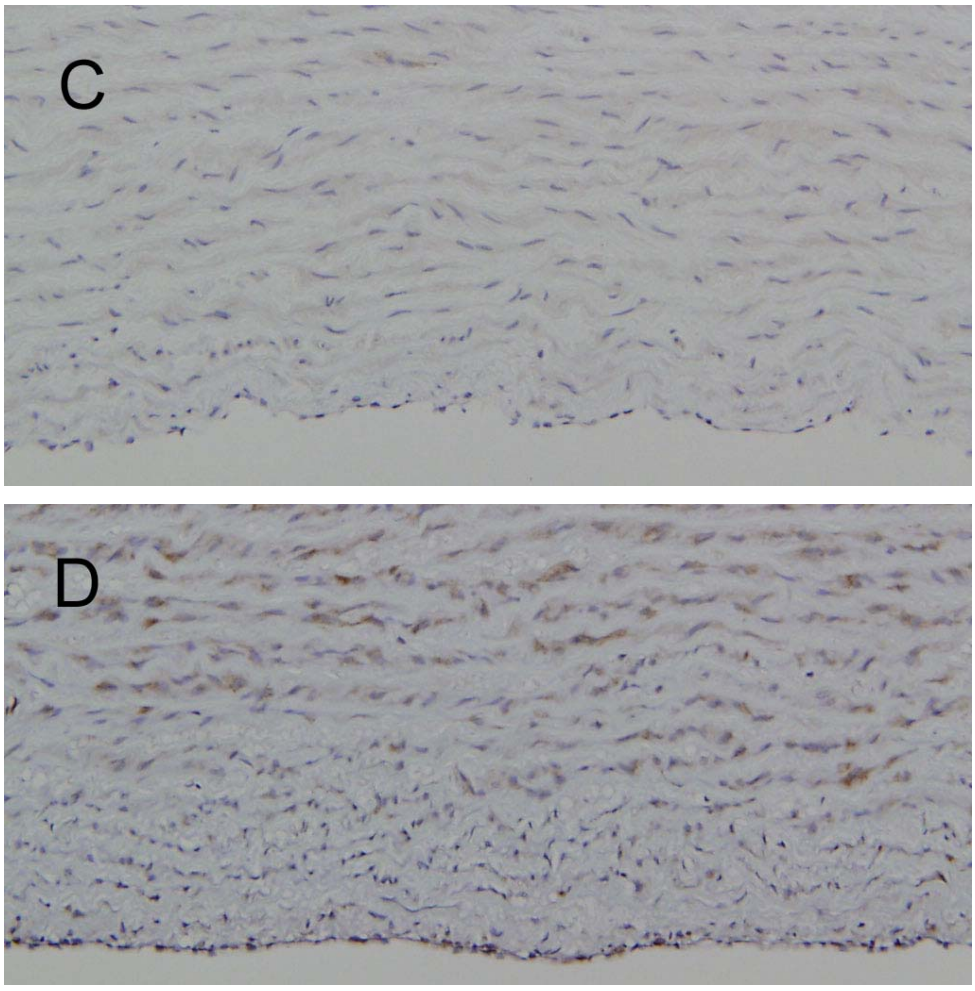

Figure V-3 (Continued)

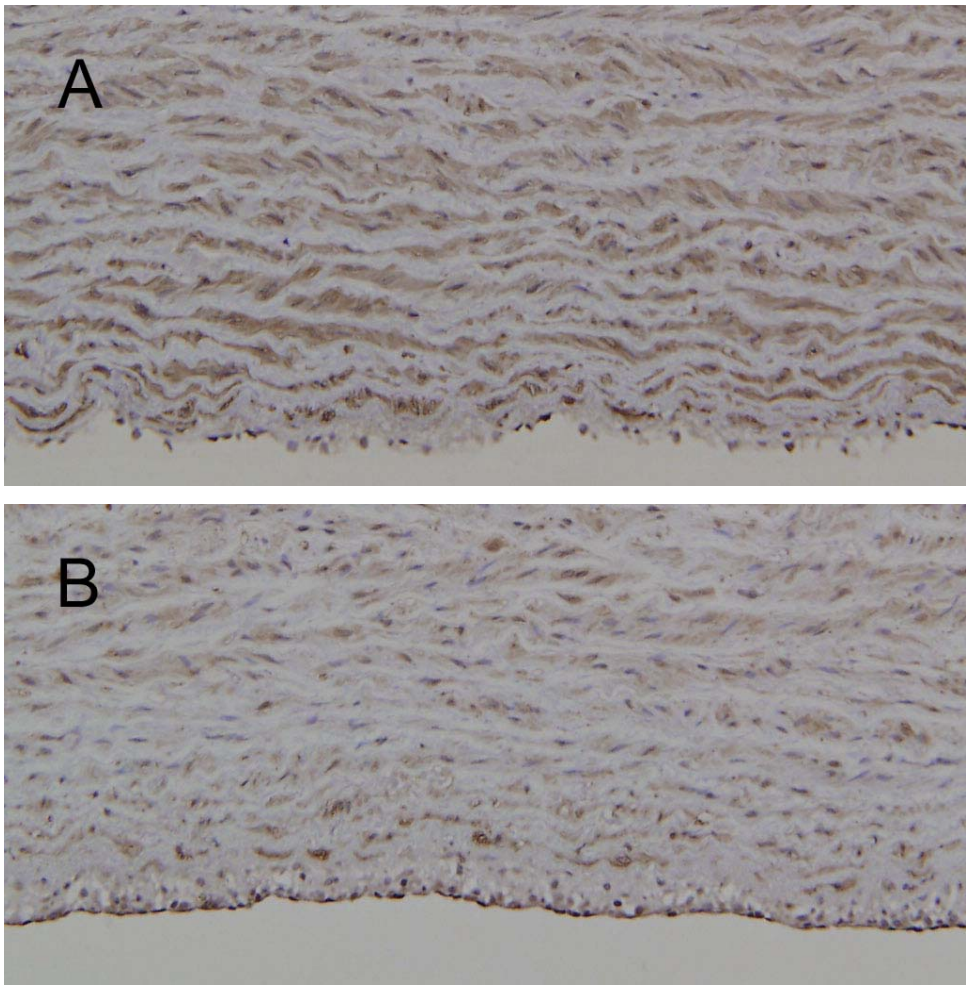

Figure V-4. Immunohistochemical staining of FFPE porcine aorta with anti-calponin (A and B), anti-caldesmon (C and D), anti-smoothelin (E and F), and anti-non-muscle MHC (G and H) using ImmPRESS. Serial sections from HT animals (B, D, F, and H) and NT animals (A, C, E, and G). The lumen is at the bottom of the micrographs.

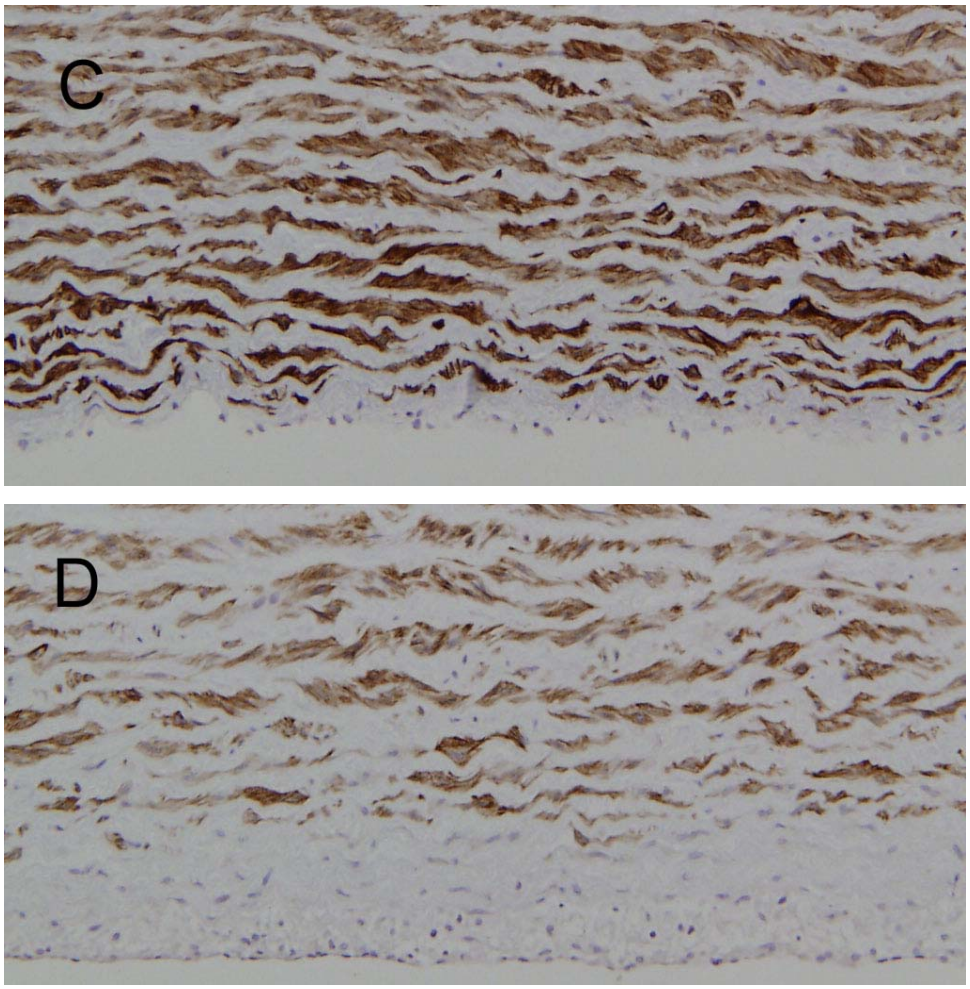

Figure V-4 (Continued)

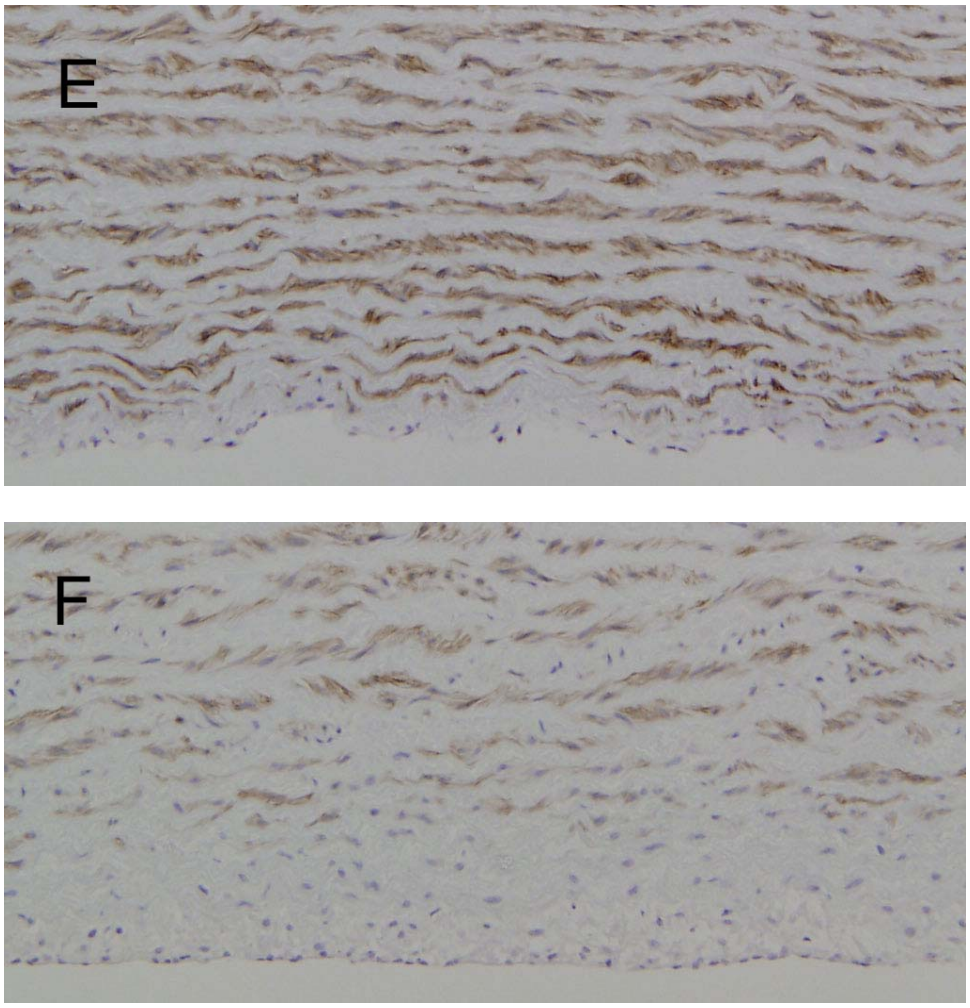

Figure V-4 (Continued)

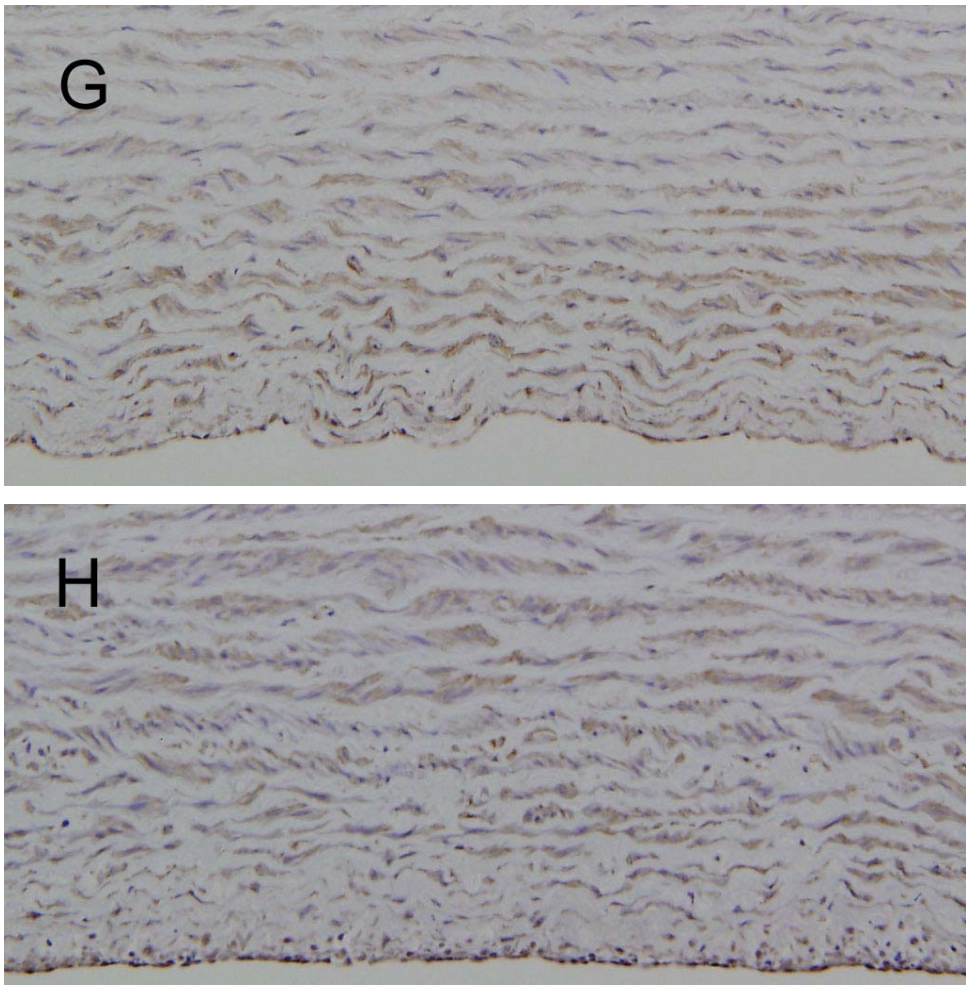

Figure V-4 (Continued)

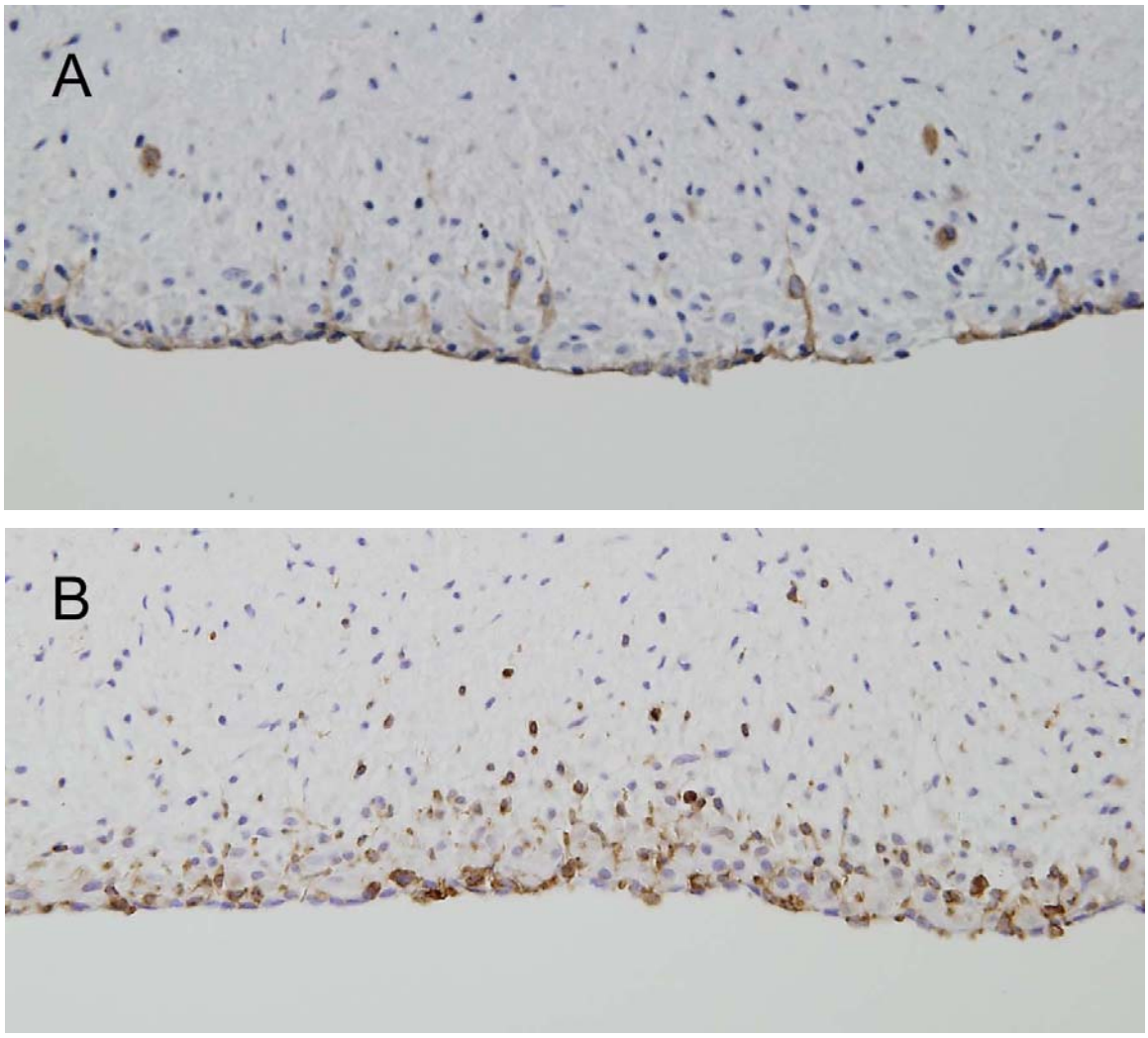

Figure V-5. Immunohistochemical staining of FFPE porcine aorta with anti-eNOS (A) using imPRESS and lectin staining for DBA using ABC (B). eNOS stained the endothelial cell; it revealed the infiltration of endothelial cells into the neointima.

TABLE V-2. Immunohistochemical Findings in Aortic Intima of Hypertensive Pigs

No	Treatment	IT	Ki-67 (EC/IC)	TUNEL (EC/IC)	Calp (EC/IC)	Cald (EC/IC)	Smemb (EC/IC)	Smlin (EC/IC)	Desm (EC/IC)
1	2H	-	-/na	/na	+/na	-/na	+/na	/na	-/na
2	2H	+	+/+		+/+	-/-	+/+		-/-
3	2H	±	-/-		+/-	-/-	+/+	-/-	-/-
4	2H	+	+/+		+/+	-/-	+/+	-/-	-/-
5	2H	-	-/na	/na	+/na	-/na	+/na	-/na	-/na
6	2H	-	-/na	/na	±/na	-/na	+/na	-/na	-/na
7	2H	-	-/na	/na	+/na		+/na	-/na	-/na
12	4H	±			+/+	+/±	+/+	-/-	-/-
13	4H	+			+/+	+/±	+/+	-/-	-/-
14	4H	±					+/±	-/-	-/-
15	4H	+			+/-	+/-	+/±	-/-	-/-
16	4H	±			+/+	+/±	±/±	-/-	-/-
17	4H	±			+/+	+/±	±/-	-/-	-/-
18	4H	±			+/+	+/±		-/-	-/-
23	6H	-	-/na	/na	+/na	+/na	+/na	-/na	-/na
24	6H	±			+/-	+/-	+/±	-/-	-/-
25	6H	-	-/na	/na	+/na	+/na	+/na	-/na	-/na
26	6H	+			+/-	+/±	+/+	-/-	-/-
27	6H	+			+/±	+/+		-/-	-/-
28	6H	+			+/±	+/+	+/±	-/-	-/-
32	8H	+			+/-	+/±	+/±		-/-
33	8H	+			+/±	+/±	+/±	-/-	-/-
34	8H	+			+/+	+/+	±/-	-/-	-/-
35	8H	+			+/±	+/+	±/-	-/-	-/±
36	8H	+					+/+	-/-	-/-
37	8H	±			+/-	+/±	+/+	-/-	-/-

Intensity of staining was scored from ++ (strong staining) to – (absence of staining) with the order: ++ > + > ± > -. IT: intimal thickening; Non-M MHC: non-muscle myosin heavy chain; Smlin: Smoothelin; EC: endothelial cell; IC: intimal cell.

TABLE V-3. Immunohistochemical Findings of Aortic Intima of Surgical and True Control Pigs

No	Treatment	IT	Ki-67 (EC/IC)	TUNEL (EC/IC)	Calp (EC/IC)	Cald (EC/IC)	Smemb (EC/IC)	Smlin (EC/IC)	Desm (EC/IC)
1	2N	-	-/na	/na	+/na	+/na	+/na		-/na
2	2N	-	-/na	/na					-/na
3	2N	+	+/+					-/-	-/-
4	2N	-	-/na	/na	+/na	+/na	-/na	-/na	-/na
5	4N	-		/na	+/na	+/na			-/na
6	4N	-		/na	+/na	+/na			-/na
7	4N	-		/na			+/na	-/na	-/na
8	4N	-		/na			+/na	-/na	-/na
9	6N	-	-/na	/na				-/na	-/na
10	6N	-	-/na	/na	±/na	±/na	+/na	-/na	
11	6N	-	-/na	/na	+/na	+/na	+/na		-/na
12	8N	-	-/na	/na			+/na		-/na
13	8N	±						-/-	-/-
14	8N	+			+/-	+/±			-/-
15	8N	±			±/±	±/±	+/±	-/-	-/-
16	SC	-	-/na	-/na					-/na
17	SC	-	-/na	-/na					-/na
18	SC	-	-/na	-/na					-/na
19	UC	-	-/na	-/na					-/na
20	UC	-	-/na	-/na					-/na

See footnotes to Table V-1. SC: Control animals with telemetry implanted but not occluder. UC: Un-operated control animals.

DISCUSSION

Wall stress and stretch higher than homeostatic levels, produced by persistent elevated intraluminal pressure, have been hypothesized to be major contributing factors to the localization of atherosclerotic lesions[94]. Increased wall stress and stretch cause endothelial injury, lipid accumulation, and SMC proliferation, all of which are essential steps in atherogenesis[94]. The intimal thickening observed in this study may likewise be due to the increased wall stress and stretch proximal to the occluder and may predispose atheroma formation.

Consistent with intimal thickening found proximal to coarctations in human aorta[95], a neointima also developed in the aorta proximal to the occluder in most HT pigs. In contrast to prior findings that the intimal SMCs were non-proliferating[95], however, we found Ki-67 staining in the intimal cells. In another study, neointima formation was induced by balloon endothelial denudation, and numerous Ki-67 stained cells were found in the intima within two weeks although at four weeks they were seen only rarely in the surface layer of the intima[85]. The missing proliferating cells in the coarctation model[95] may be due to data collection at the wrong time; this emphasizes the importance of knowing time courses of these changes.

That the endothelial cells in the intimal lesions stained with Hsp47 and procollagen indicated that the endothelium may be an active matrix producer contributing to neointima formation. It was shown as early as 1978 that pig aortic endothelial cells can synthesize, in addition to basement membrane type collagen (type IV), the interstitial collagens (type I and III)[96]. The type I collagen was found to promote phenotypic

transition of cultured SMCs from a contractile to a synthetic state[97]. That is, the subendothelial deposition of type I collagen created a suitable space for SMC migration, proliferation, and for their synthesis of matrix. Beside the possible contribution of EC released matrix proteins, the secretion of a soluble mediators by dysfunctioning, injured, or proliferating endothelial cells has also been found to stimulate intimal cell proliferation either directly or indirectly in the organ culture experiments[98].

To further clarify if the secreted collagen was laid down in the subendothelial space, the composition of the extracellular matrix in the neointima needs to be determined specifically by immunohistochemistry for collagen (type I and III).

Numerous cells embedded with in large quantities of extracellular matrix proteins were observed in the neointima. The origin of the intimal cells has elicited numerous debates, and many hypotheses have been proposed[99]. In the previous chapter, immunohistochemistry was used to study SMC differentiation in the media. Referring to Tables IV-3 and IV-4, we found that endothelial cells also express calponin, SM22α, and non-muscle MHC which are differentiation markers for the contractile phenotype of SMC. Similar results have been reported by Borrione and colleagues who found that ECs expressed non-muscle MHC[100]. Other differentiation markers claimed to be exclusively expressed in SMCs (e.g. calponin, metavinculin, and MHC isoforms) have also been found in pericytes and platelets[101,102]. More interestingly, the intimal cells showed an expression pattern for SMC differentiation markers similar to that for the endothelial cells. The infiltration of eNOS-stained cells into subendothelial layer may suggest transdifferentiation of ECs into intimal cells, which has been demonstrated during

embryonic development[103,104] and primary cultures of mature vascular endothelial cells[105].

In this study, an alternative hypothesis for the formation of a neointima has been introduced and validated in our coarctation model. The endothelial cells in HT may contribute to intimal thickening in two ways. They produce collagen type I, which appears to be released into the subendothelial space; on the other hand, they may transdifferentiate into SMCs in the neointima.

CHAPTER VI

DESIGN OF A UNIAXIAL TISSUE CULTURE DEVICE

INTRODUCTION

Circumferential tensile stress has been recognized to play a key role in growth and remodeling of arterial media; the media tends to restore the homeostatic stress by increasing its thickness when the stress field is altered. Stretching cultured SMCs has provided great insight into the possible mechanism[106-108]. Alternatively, experimental animal models of hypertension also give valuable information on the effects of tensile stress. An advantage of cultured cell systems is the easy access of cell lines, if primary culture is not required, and the ease of controlling culture conditions (e.g., media components, pH, and temperature). That the cells were grown on two-dimensional surfaces, however, is different from their *in situ* living environment with the exception of the endothelial cells. Animal models provide the most realistic environment to study cells, tissues, or organs. The main drawback of this system, however, is the complexity in the animal body; e.g., the neural-hormonal contributions sometimes complicate the data interpretation. Organ culture systems, in contrast, preserve cell-cell and cell-ECM interactions in controllable culture conditions, and thereby represent another outstanding tool for studying the mechanotransduction involved in medial growth and remodeling.

We hypothesize that the circumferential stress is the main mechanical force causing medial thickening in hypertension. The isolated effect of circumferential stress on the G&R of a vessel wall is unclear despite intensive study of cultured vascular cells

under cyclic strains. To study the effect of circumferential stress alone, a uni-axial stretcher, which is capable of stretching aortic ring segments, was designed and built.

Uni-axial stretching mimics the circumferential stretching in the vessel wall, albeit in the absence of axial loads. The oscillating movement, translated from a cam driven by a gear motor, provides the cyclic stretching to the attached aortic ring segment. The magnitude of the stretch is adjusted by the original length or the axis offset of the cam whilst the frequency of the stretching is maintained at 1 Hz by controlling the power input of the motor. The device can apply cyclic or static strains to the specimen to study the effects of pulsatility.

With intact cell-cell and cell-ECM interactions, mechanotransduction can be examined more realistically. For example, one could focus on protein expression of egr-1 and fos-1 to investigate the immediate mechanotransduction. Long-term organ culture can be maintained for studies of medial growth and remodeling, including cell death/proliferation and turnover of the structural proteins. The time course of the changes can be recorded.

METHODS

Stretcher. The uni-axial stretcher (Figure VI-1) was built partly with reference to Yost[109]. It was made of materials proved to be non-toxic to cells and capable of autoclaving. Polycarbonate was chosen to build the chamber for its good optical qualities and high melting point. Poly-ether-etherketone (PEEK) and polytetrafluorethylene (PTFE) were also used to build the parts inside the chamber concerned with easy modification, longevity under cyclic heating and cooling, and their special material properties. The joints of the chamber were sealed with High Temperature RTV Silicone (Permatex part #81409) and Nylon screws were used to assemble the chamber; these were done to prevent cracking of the polycarbonate during autoclave. Four latches were used to tighten the lid. Between the lid and the chamber is an o-ring of 1/4" diameter. The gear motor can be removed so that the culturing chamber can be autoclaved easily; the moisture can shorten its life. The motor is driven by an AC power supply.

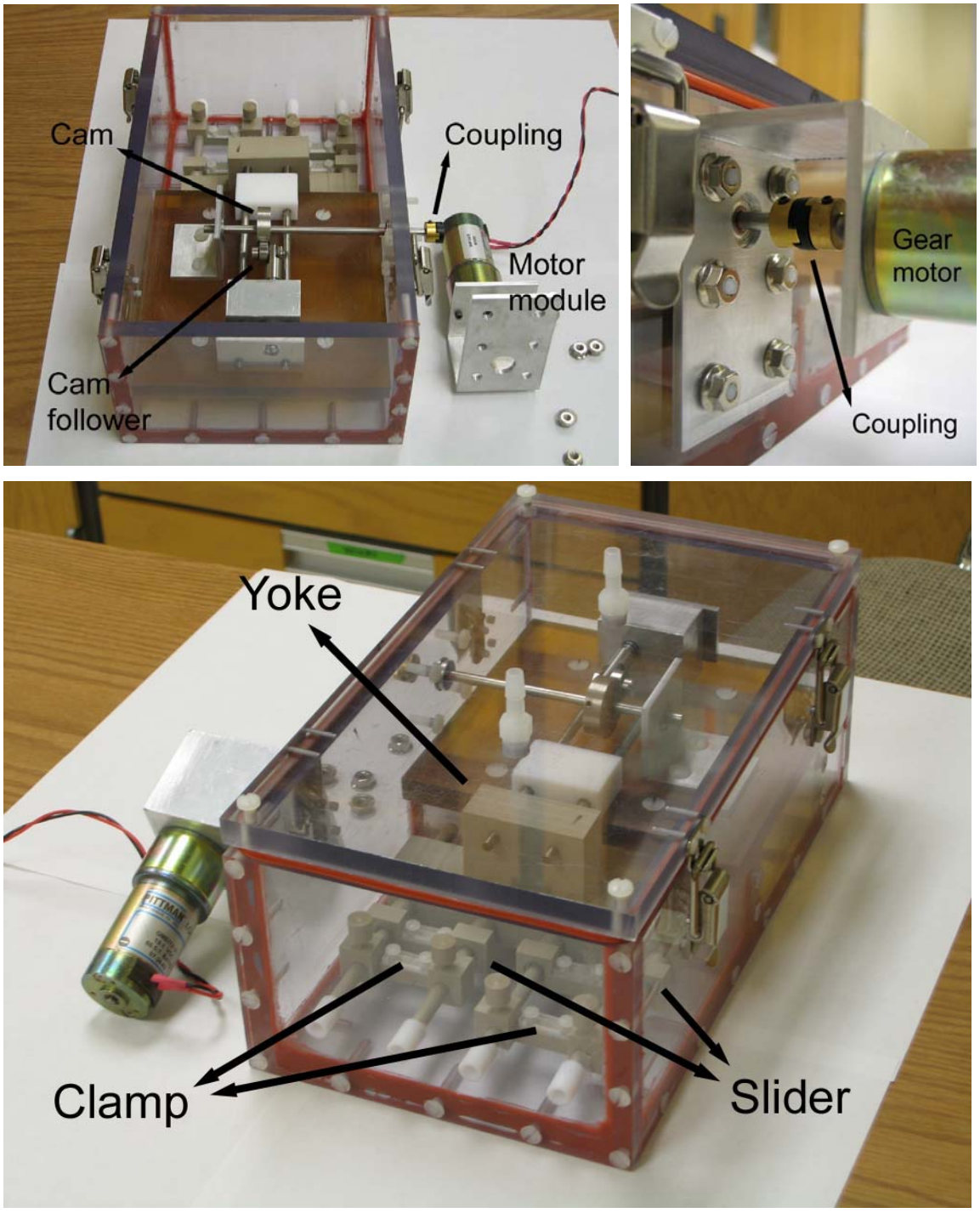

Figure VI-1. Experimental apparatus for uni-axial stretching of the aorta.

FUTURE WORK

Preparation of frozen sections. The aortic ring segments will be fixed in fresh 4% paraformaldehyde at RT for one hour and soaked in 10% sucrose PBS solution until fully immersed. The tissues will then be embedded in optimal cutting temperature (OCT) compound in plastic molds and snap-frozen in isopentane cooled by liquid nitrogen. Sections (7 μm) will be cut in cryostat at -20°C and attached to the Superfrost Plus slides (Fisher Scientific). The slides will be air-dried for 20 minutes. Before immuno- or histological staining, OCT will be removed by washing in 70% alcohol for several times.

Histology and immunohistochemistry. Immunohistochemistry for egr-1 and NFκ-B will be conducted to examine the *in situ* early gene activations at the onset of stretching. The matrix protein deposition and the potential changes in wall thickness will be evaluated by histological staining (H&E, PSR, and VVG).

Elastin degradation. The culture medium will be analyzed for the metabolites of the matrix proteins to examine their turnover. Medium levels of elastin-peptides, a maker of elastolysis, will be determined using an inhibition type of enzyme-linked immunosorbent assay (ELISA). The assay is performed by incubating 110 μL each of antiserum and antigen dilutions (e.g., cultured medium and standards) in round-bottom microtiter wells to equilibrium (> 8 hr) at 4°C. The competition reaction mixture is then transferred to plates coated with human aortic elastin (100 ng/well) and incubated for 30 min at 4°C. After rinsing away the unbound antibodies, the peroxidases-goat-antirabbit IgG is added and incubated for 1 hr. O-phenylenediamine is used as a substrate. The optical density at 492mm is read with a spectrophotometer. The concentrations of

elastin-peptide are calculated from a standard curve using quadratic regression analysis.

Collagen synthesis and degradation: We will measure medium levels of carboxyterminal propeptide of procollagen type I (PIP) and pyridinoline crosslinked telopeptide domain of collagen type I (CITP) as a marker of type I collagen synthesis and degradation, respectively. Medium levels of PIP and CITP is determined by the radioimmunoassay (RIA) methods using antisera specifically directed against the carboxy-terminal peptide procollagen type I and the carboxy-terminal telopeptide of collage type I, respectively. The assay is performed by incubating 100 μL aliquots of antigen dilution (e.g., cultured medium and standards) with 200 μL of tracer solution (^{125}I-labeled PIP or ^{125}I-labeled CITP, about 50000 cpm) and 200 μL of diluted antiserum against PIP (or CITP) in a microcentrifuge tube for 2 hours at 37°C. Then 500 μL of the solid-phase secondary-antibody suspension is added to each tube and vortex-mixed. After 30 minutes at RT, the bound fraction is separated by centrifugation (2000g, 15 mins, 4°C). The supernatant containing the unbound tracer is decarded and the radioactivity of the precipitate containing the bound tracer is counted with a Gamma counter.

Bromodeoxyuridine (BrdU) labeling: The aortic ring segment will be exposed to 10^{-5} M BrdU in the medium for 3-6 hours. The tissue will then be either fixed immediately or fixed after another 24 hours of culturing in a new medium containing no BrdU. Either frozen sections or paraffin sections will be prepared. Possible incorporation of BrdU into the cells will be demonstrated by immunohistochemical staining for BrdU.

EXPECTED RESULTS AND LIMITATIONS

Instead of trying to mimic the complicated physiological environment, the purpose of this novel device is to study the isolated effect of tensile stress on the G&R of the aorta. The center portion of the segment will be dissected for analysis while the area near the clamps is avoided. Due to the natural curvature of the arterial wall, stretching the aorta uni-axially in a plane may cause bending, that is the extension of tissue in the inner wall and compression in the outer wall. We will thus focus on the middle media, in which the geometry remains close to its normal state when the segment is stretched. Actually, it may be interesting to compare the G&R occurring in the inner and outer walls. Attention also needs to be paid to the absence of axial loading, which has been shown to play an important role in arterial G&R. Similarly, the flow-induced endothelial contribution to the G&R is also overlooked in this system. Nevertheless, the endothelial cells will be subjected to circumferential stretch and the effect of endothelial denudation can be tested. We have made every effort in designing this device (e.g., sealing the shaft), to minimize the chance of contamination, which is essential for long-term G&R. In addition, to maintain long-term viability of an organ *ex vivo* for G&R to happen, the culture conditions, especially culture medium, have to be well selected.

This novel device can also be used to uni-axially stretch cell-seeded membranes with minor modifications, and will be proved to be useful in study mechanotransduction at both tissue and cellular levels.

CHAPTER VII

CONCLUSIONS AND RECOMENDATIONS

Through decades of research, we have gained much more understanding of the cardiovascular system, what it consists of, how it functions, and how it deteriorates due to aging or diseases. Not until recently, however, has the emergence of soft tissue biomechanics allowed us to investigate deeper the biological responses in such a dynamic, complicated mechanical environment. Indeed, a better description of the mechanical environment at cell, tissue, and organ levels is important to elucidate the mechanobiology involved in, say, hypertension-induced G&R. In this study, we found changes in mechanical property of the basilar artery as well as its histology due to the development of hypertension. With multiple cell markers, we revealed the SMC phenotypic modulation in the aortic media due to hypertension and its relation to cell proliferation and matrix protein deposition. The primary findings are listed as follows:

1. The pressure-stretch curves for the basilar artery were influenced greatly by the choice of reference configuration. The axial stretch at which the cyclic inflation tests were carried out also affected the pressure-stretch curves (i.e., mechanical behavior).
2. Although changes in inner radius, outer radius, media area and luminal area were not significant in hypertensive basilar arteries, the wall thickness and the ratio of inner radius to wall thickness were greater in the hypertensive basilar artery than in the normotensive artery.

3. Both structural stiffness and material stiffness were increased for hypertensive basilar arteries. The circumferential stress in the media of hypertensive basilar artery was normalized by two week after induction of hypertension, comparable to that of normotensive basilar artery.
4. The increased aortic medial thickness observed in hypertensive animals compared to normotensive pigs was due to hyperplasia of SMCs and accumulation of extracellular matrix proteins, which were accompanied by a phenotypic modulation of SMCs. The increased interlamellar thickness, collagen fibers, and the thickness of elastic lamina found in the inner media of hypertensive animals may be associated with the gradient of stress decreasing into the outer media. SMC proliferation, if any, was found to be evenly distributed across the media, however. In cases showing increased proliferation and matrix protein synthesis, the SMC contractile markers were down-regulated whereas the SMC synthetic markers were up-regulated.
5. The turnover rate of endothelial cells subjected to hypertension increased. Proliferation of intimal cells appeared to be independent to that of media SMC cells.
6. The endothelial cells appeared to actively synthesize collagen in the hypertensive aorta. The neosynthesized collagen (I) may release into subendothelial space and contribute to the thickening of the intima.
7. It appeared that the vascular remodeling of basilar artery and aorta has almost completed in two weeks either in study of mechanical properties of the basilar arteries or in study of spatial and temporal changes in SMC phenotypic heterogeneity. We may try a closer time point such as one-week and see if these changes happen as early

as one week. The medial degeneration-like lesions found in the same group of pig suggested that eight week is close to the limit of this model.

Finally, although much has been learned in this study, the complexity of the response of different vascular beds due to hypertension is great, and much remains to be done. For example, listed here are five immediate needs that should be pursued:

1. Information about the composition of the arterial wall and the potential staining patterns needs to be extracted from (immuno-)histological sections in both the basilar artery and aorta, which when coupled with stress-strain data could lead to a constituent-based constitutive relation for arterial mechanical behavior and could provide clues of targets for medical treatments. The time course of changes needs to be analyzed.
2. The neointimal formation induced by hypertension may accelerate atherosclerosis if combined with other risk factors. More information about the origin of the neointimal cells and how they are activated is needed, bearing in mind that the underlying mechanism may vary depending on differences between injury-models.
3. Migration of cells, either ECs or SMCs, requires degradation of the basement membrane. The turnover of basement membrane, which may involve MMPs, should be investigated for more clues in neointima formation.
4. Besides the direct influence of stress, autocrine/paracrine regulations involving growth factors such as PDGF, TGF-β1, and FGF are likely to play a part in the medial G&R and the neointima formation. Knowledge of spatial and temporal expression of

the key growth factors due to the development of hypertension will prove useful in medical intervention.

5. Our novel pig aortic coarctation model allows us to reverse the hypertension. Since the adaptation appeared to finish quickly, it is critical to know if the G&R is reversible by lowering the blood pressure. If not, the last minute before which the G&R is still reversible is of importance.

Clearly, much awaits for us to discover.

REFERENCES

1. Gartner LP, Hiatt JL. *Color Textbook of Histology*. 2 ed. Philadelphia, PA: Saunders; 2001.
2. Wolinsky H, Glagov S. Structural basis for the static mechanical properties of the aortic media. *Circ Res*. 1964;14:400-13.
3. Dobrin PB. Distribution of lamellar deformations: implications for properties of the arterial media. *Hypertension*. 1999;33:806-10.
4. Pastor PN, Makuc DM, Reuben C, Xia H. Chartbook on trends in the health of American. In: *Health, United States, 2002*. Hyattsville, Maryland: National Center for Health Statistics; 2002.
5. Cherry DK, Woodwell DA. National ambulatory medical care survey: 2000 summary. In: *Advance Data from Vital and Health Statistics*. Hyattsville, Maryland: National Center for Health Statistics; 2002.
6. Gariepy J, Massonneau M, Levenson J, Heudes D, Simon A. Evidence for in vivo carotid and femoral wall thickening in human hypertension. Groupe de Prevention Cardio-vasculaire en Medecine du Travail. *Hypertension*. 1993;22:111-8.
7. Owens GK, Rabinovitch PS, Schwartz SM. Smooth muscle cell hypertrophy versus hyperplasia in hypertension. *Proc Natl Acad Sci U S A*. 1981;78:7759-63.
8. Laviades C, Varo N, Fernandez J, Mayor G, Gil MJ, Monreal I, Diez J. Abnormalities of the extracellular degradation of collagen type I in essential hypertension. *Circulation*. 1998;98:535-40.
9. Armentano R, Megnien JL, Simon A, Bellenfant F, Barra J, Levenson J. Effects of hypertension on viscoelasticity of carotid and femoral arteries in humans. *Hypertension*. 1995;26:48-54.
10. Cardillo C, Kilcoyne CM, Waclawiw M, Cannon RO, 3rd, Panza JA. Role of endothelin in the increased vascular tone of patients with essential hypertension. *Hypertension*. 1999;33:753-8.
11. Triggle CR. Reactivity and sensitivity changes of blood vessels in hypertension. In: Lee RMKW, ed. *Blood vessel changes in hypertension: structure and function*. Boca Raton, FL: CRC press; 1988:22-44.
12. Johnson PC. The myogenic response. In: *Handbook of physiology. The cardiovascular system. Vascular smooth muscle.* Bethesda, MD: Am. Physiol. Soc.; 1981:409-442.
13. Williams B. Mechanical influences on vascular smooth muscle cell function. *J Hypertens*. 1998;16:1921-9.
14. Negoro N, Kanayama Y, Haraguchi M, Umetani N, Nishimura M, Konishi Y, Iwai J, Okamura M, Inoue T, Takeda T. Blood pressure regulates platelet-derived growth factor A-chain gene expression in vascular smooth muscle cells in vivo. An autocrine mechanism promoting hypertensive vascular hypertrophy. *J Clin Invest*. 1995;95:1140-50.

15. Xu C, Lee S, Singh TM, Sho E, Li X, Sho M, Masuda H, Zarins CK. Molecular mechanisms of aortic wall remodeling in response to hypertension. *J Vasc Surg*. 2001;33:570-8.
16. Fath KA, Alexander RW, Delafontaine P. Abdominal coarctation increases insulin-like growth factor I mRNA levels in rat aorta. *Circ Res*. 1993;72:271-7.
17. Anwar A, Delafontaine P. Hypertension increases insulin-like growth factor binding protein-4 mRNA levels in rat aorta. *Hypertension*. 1994;24:679-85.
18. Owens GK, Reidy MA. Hyperplastic growth response of vascular smooth muscle cells following induction of acute hypertension in rats by aortic coarctation. *Circ Res*. 1985;57:695-705.
19. Xu C, Zarins CK, Bassiouny HS, Briggs WH, Reardon C, Glagov S. Differential transmural distribution of gene expression for collagen types I and III proximal to aortic coarctation in the rabbit. *J Vasc Res*. 2000;37:170-82.
20. Xu C, Zarins CK, Glagov S. Gene expression of tropoelastin is enhanced in the aorta proximal to the coarctation in rabbits. *Exp Mol Pathol*. 2002;72:115-23.
21. Chesler NC, Ku DN, Galis ZS. Transmural pressure induces matrix-degrading activity in porcine arteries ex vivo. *Am J Physiol*. 1999;277:H2002-9.
22. Owens GK. Regulation of differentiation of vascular smooth muscle cells. *Physiol Rev*. 1995;75:487-517.
23. Stenmark KR, Mecham RP. Cellular and molecular mechanisms of pulmonary vascular remodeling. *Annu Rev Physiol*. 1997;59:89-144.
24. Sartore S, Chiavegato A, Franch R, Faggin E, Pauletto P. Myosin gene expression and cell phenotypes in vascular smooth muscle during development, in experimental models, and in vascular disease. *Arterioscler Thromb Vasc Biol*. 1997;17:1210-5.
25. Sobue K, Hayashi K, Nishida W. Expressional regulation of smooth muscle cell-specific genes in association with phenotypic modulation. *Mol Cell Biochem*. 1999;190:105-18.
26. Kocher O, Gabbiani G. Cytoskeletal features of normal and atheromatous human arterial smooth muscle cells. *Hum Pathol*. 1986;17:875-80.
27. Glukhova MA, Frid MG, Koteliansky VE. Developmental changes in expression of contractile and cytoskeletal proteins in human aortic smooth muscle. *J Biol Chem*. 1990;265:13042-6.
28. Takahashi K, Hiwada K, Kokubu T. Isolation and characterization of a 34,000-dalton calmodulin- and F-actin-binding protein from chicken gizzard smooth muscle. *Biochem Biophys Res Commun*. 1986;141:20-6.
29. Gimona M, Herzog M, Vandekerckhove J, Small JV. Smooth muscle specific expression of calponin. *FEBS Lett*. 1990;274:159-62.
30. Sobue K, Sellers JR. Caldesmon, a novel regulatory protein in smooth muscle and nonmuscle actomyosin systems. *J Biol Chem*. 1991;266:12115-8.
31. Walsh MP. The Ayerst Award Lecture 1990. Calcium-dependent mechanisms of regulation of smooth muscle contraction. *Biochem Cell Biol*. 1991;69:771-800.
32. Rush DS, Tan J, Baergen RN, Soslow RA. h-Caldesmon, a novel smooth muscle-specific antibody, distinguishes between cellular leiomyoma and

endometrial stromal sarcoma. *Am J Surg Pathol*. 2001;25:253-8.
33. Miettinen MM, Sarlomo-Rikala M, Kovatich AJ, Lasota J. Calponin and h-caldesmon in soft tissue tumors: consistent h-caldesmon immunoreactivity in gastrointestinal stromal tumors indicates traits of smooth muscle differentiation. *Mod Pathol*. 1999;12:756-62.
34. Aikawa M, Sivam PN, Kuro-o M, Kimura K, Nakahara K, Takewaki S, Ueda M, Yamaguchi H, Yazaki Y, Periasamy M, et al. Human smooth muscle myosin heavy chain isoforms as molecular markers for vascular development and atherosclerosis. *Circ Res*. 1993;73:1000-12.
35. van der Loop FT, Schaart G, Timmer ED, Ramaekers FC, van Eys GJ. Smoothelin, a novel cytoskeletal protein specific for smooth muscle cells. *J Cell Biol*. 1996;134:401-11.
36. van der Loop FT, Gabbiani G, Kohnen G, Ramaekers FC, van Eys GJ. Differentiation of smooth muscle cells in human blood vessels as defined by smoothelin, a novel marker for the contractile phenotype. *Arterioscler Thromb Vasc Biol*. 1997;17:665-71.
37. Wehrens XH, Mies B, Gimona M, Ramaekers FC, Van Eys GJ, Small JV. Localization of smoothelin in avian smooth muscle and identification of a vascular-specific isoform. *FEBS Lett*. 1997;405:315-20.
38. Fossum TW, Baltzer WI, Miller MW, Aguirre M, Whitlock D, Solter P, Makarski LA, McDonald MM, An MY, Humphrey JD. A novel aortic coarctation model for studying hypertension in the pig. *J Invest Surg*. 2003;16:35-44.
39. Ling P, Taber LA, Humphrey JD. Approach to quantify the mechanical behavior of the intact embryonic chick heart. *Ann Biomed Eng*. 2002;30:636-45.
40. Whittaker P, Kloner RA, Boughner DR, Pickering JG. Quantitative assessment of myocardial collagen with picrosirius red staining and circularly polarized light. *Basic Res Cardiol*. 1994;89:397-410.
41. Pickering JG, Boughner DR. Fibrosis in the transplanted heart and its relation to donor ischemic time. Assessment with polarized light microscopy and digital image analysis. *Circulation*. 1990;81:949-58.
42. Tanaka M, Fujiwara H, Onodera T, Wu DJ, Hamashima Y, Kawai C. Quantitative analysis of myocardial fibrosis in normals, hypertensive hearts, and hypertrophic cardiomyopathy. *Br Heart J*. 1986;55:575-81.
43. Humphrey JD. *Cardiovascular Solid Mechanics: Cells, Tissues, and Organs*. New York: Springer-Verlag; 2002.
44. Winquist RJ, Bohr DF. Structural and functional changes in cerebral arteries from spontaneously hypertensive rats. *Hypertension*. 1983;5:292-7.
45. Cox RH. Comparison of arterial wall mechanics using ring and cylindrical segments. *Am J Physiol*. 1983;244:H298-303.
46. Vinall PE, Simeone FA. Whole mounted pressurized in vitro model for the study of cerebral arterial mechanics. *Blood Vessels*. 1987;24:51-62.
47. Nagasawa S, Handa H, Okumura A, Naruo Y, Moritake K, Hayashi K. Mechanical properties of human cerebral arteries. Part 1: Effects of age and vascular smooth muscle activation. *Surg Neurol*. 1979;12:297-304.

48. Hayashi K, Handa H, Nagasawa S, Okumura A, Moritake K. Stiffness and elastic behavior of human intracranial and extracranial arteries. *J Biomech*. 1980;13:175-84.
49. Hajdu MA, Baumbach GL. Mechanics of large and small cerebral arteries in chronic hypertension. *Am J Physiol*. 1994;266:H1027-33.
50. Matsumoto T, Hayashi K. Mechanical and dimensional adaptation of rat aorta to hypertension. *J Biomech Eng*. 1994;116:278-83.
51. Strandgaard S, Paulson OB. Cerebral blood flow in untreated and treated hypertension. *Neth J Med*. 1995;47:180-4.
52. Rachev A, Stergiopulos N, Meister JJ. A model for geometric and mechanical adaptation of arteries to sustained hypertension. *J Biomech Eng*. 1998;120:9-17.
53. Gleason RL, Humphrey JD. A mixture model of arterial growth and remodeling in hypertension: altered muscle tone and tissue turnover. *J Vasc Res*. 2004;41:352-63.
54. Humphrey JD, Wilson E. A potential role of smooth muscle tone in early hypertension: a theoretical study. *J Biomech*. 2003;36:1595-601.
55. Lodi CA, Ursino M. Hemodynamic effect of cerebral vasospasm in humans: a modeling study. *Ann Biomed Eng*. 1999;27:257-73.
56. Mangiarua EI, Lee RM. Morphometric study of cerebral arteries from spontaneously hypertensive and stroke-prone spontaneously hypertensive rats. *J Hypertens*. 1992;10:1183-90.
57. Wolinsky H. Response of the rat aortic media to hypertension. Morphological and chemical studies. *Circ Res*. 1970;26:507-22.
58. Clark JM, Glagov S. Structural integration of the arterial wall. I. Relationships and attachments of medial smooth muscle cells in normally distended and hyperdistended aortas. *Lab Invest*. 1979;40:587-602.
59. Kamiya A, Togawa T. Adaptive regulation of wall shear stress to flow change in the canine carotid artery. *Am J Physiol*. 1980;239:H14-21.
60. Frid MG, Printesva OY, Chiavegato A, Faggin E, Scatena M, Koteliansky VE, Pauletto P, Glukhova MA, Sartore S. Myosin heavy-chain isoform composition and distribution in developing and adult human aortic smooth muscle. *J Vasc Res*. 1993;30:279-92.
61. Giuriato L, Scatena M, Chiavegato A, Tonello M, Scannapieco G, Pauletto P, Sartore S. Non-muscle myosin isoforms and cell heterogeneity in developing rabbit vascular smooth muscle. *J Cell Sci*. 1992;101 (Pt 1):233-46.
62. Samaha FF, Ip HS, Morrisey EE, Seltzer J, Tang Z, Solway J, Parmacek MS. Developmental pattern of expression and genomic organization of the calponin-h1 gene. A contractile smooth muscle cell marker. *J Biol Chem*. 1996;271:395-403.
63. Duband JL, Gimona M, Scatena M, Sartore S, Small JV. Calponin and SM 22 as differentiation markers of smooth muscle: spatiotemporal distribution during avian embryonic development. *Differentiation*. 1993;55:1-11.
64. Hungerford JE, Hoeffler JP, Bowers CW, Dahm LM, Falchetto R, Shabanowitz J, Hunt DF, Little CD. Identification of a novel marker for primordial smooth

muscle and its differential expression pattern in contractile vs noncontractile cells. *J Cell Biol*. 1997;137:925-37.

65. Johansson B, Eriksson A, Ramaekers F, Thornell L. Smoothelin in adult and developing human arteries and myocardium. *Histochem Cell Biol*. 1999;112:291-9.
66. Fridez P, Zulliger M, Bobard F, Montorzi G, Miyazaki H, Hayashi K, Stergiopulos N. Geometrical, functional, and histomorphometric adaptation of rat carotid artery in induced hypertension. *J Biomech*. 2003;36:671-80.
67. Negoescu A, Lorimier P, Labat-Moleur F, Drouet C, Robert C, Guillermet C, Brambilla C, Brambilla E. In situ apoptotic cell labeling by the TUNEL method: improvement and evaluation on cell preparations. *J Histochem Cytochem*. 1996;44:959-68.
68. Avolio A, Jones D, Tafazzoli-Shadpour M. Quantification of alterations in structure and function of elastin in the arterial media. *Hypertension*. 1998;32:170-5.
69. Johnson GJ, Griggs TR, Badimon L. The utility of animal models in the preclinical study of interventions to prevent human coronary artery restenosis: analysis and recommendations. On behalf of the Subcommittee on Animal, Cellular and Molecular Models of Thrombosis and Haemostasis of the Scientific and Standardization Committee of the International Society on Thrombosis and Haemostasis. *Thromb Haemost*. 1999;81:835-43.
70. Sans M, Moragas A. Mathematical morphologic analysis of the aortic medial structure. Biomechanical implications. *Anal Quant Cytol Histol*. 1993;15:93-100.
71. Olivetti G, Melissari M, Marchetti G, Anversa P. Quantitative structural changes of the rat thoracic aorta in early spontaneous hypertension. Tissue composition, and hypertrophy and hyperplasia of smooth muscle cells. *Circ Res*. 1982;51:19-26.
72. Orton EC, LaRue SM, Ensley B, Stenmark K. Bromodeoxyuridine labeling and DNA content of pulmonary arterial medial cells from hypoxia-exposed and nonexposed healthy calves. *Am J Vet Res*. 1992;53:1925-30.
73. Jamal A, Bendeck M, Langille BL. Structural changes and recovery of function after arterial injury. *Arterioscler Thromb*. 1992;12:307-17.
74. Wohrley JD, Frid MG, Moiseeva EP, Orton EC, Belknap JK, Stenmark KR. Hypoxia selectively induces proliferation in a specific subpopulation of smooth muscle cells in the bovine neonatal pulmonary arterial media. *J Clin Invest*. 1995;96:273-81.
75. Draney MT, Arko FR, Alley MT, Markl M, Herfkens RJ, Pelc NJ, Zarins CK, Taylor CA. Quantification of vessel wall motion and cyclic strain using cine phase contrast MRI: in vivo validation in the porcine aorta. *Magn Reson Med*. 2004;52:286-95.
76. Ross R. The pathogenesis of atherosclerosis: a perspective for the 1990s. *Nature*. 1993;362:801-9.
77. Svendsen E, Tindall AR. Raised blood pressure and endothelial cell injury in rabbit aorta. *Acta Pathol Microbiol Scand [A]*. 1981;89:325-34.

78. Bouloumie A, Bauersachs J, Linz W, Scholkens BA, Wiemer G, Fleming I, Busse R. Endothelial dysfunction coincides with an enhanced nitric oxide synthase expression and superoxide anion production. *Hypertension*. 1997;30:934-41.
79. Limas C, Westrum B, Limas CJ. The evolution of vascular changes in the spontaneously hypertensive rat. *Am J Pathol*. 1980;98:357-84.
80. Tropea BI, Huie P, Cooke JP, Tsao PS, Sibley RK, Zarins CK. Hypertension-enhanced monocyte adhesion in experimental atherosclerosis. *J Vasc Surg*. 1996;23:596-605.
81. Hollander W, Madoff I, Paddock J, Kirkpatrick B. Aggravation of atherosclerosis by hypertension in a subhuman primate model with coarctation of the aorta. *Circ Res*. 1976;38:63-72.
82. Xu C, Zarins CK, Pannaraj PS, Bassiouny HS, Glagov S. Hypercholesterolemia superimposed by experimental hypertension induces differential distribution of collagen and elastin. *Arterioscler Thromb Vasc Biol*. 2000;20:2566-72.
83. Yamada T, Shiraishi R, Taki K, Nakano S, Tokunaga O, Itoh T. Immunohistochemical and ultrastructural examination of smooth muscle cells in aortocoronary saphenous vein grafts. *Angiology*. 1997;48:381-90.
84. Malik N, Francis SE, Holt CM, Gunn J, Thomas GL, Shepherd L, Chamberlain J, Newman CM, Cumberland DC, Crossman DC. Apoptosis and cell proliferation after porcine coronary angioplasty. *Circulation*. 1998;98:1657-65.
85. Aoyagi M, Yamamoto M, Azuma H, Niimi Y, Tajima S, Hirakawa K, Yamamoto K. Smooth muscle cell proliferation, elastin formation, and tropoelastin transcripts during the development of intimal thickening in rabbit carotid arteries after endothelial denudation. *Histochem Cell Biol*. 1997;107:11-7.
86. Nagata K. Hsp47: a collagen-specific molecular chaperone. *Trends Biochem Sci*. 1996;21:22-6.
87. Nagai N, Hosokawa M, Itohara S, Adachi E, Matsushita T, Hosokawa N, Nagata K. Embryonic lethality of molecular chaperone hsp47 knockout mice is associated with defects in collagen biosynthesis. *J Cell Biol*. 2000;150:1499-506.
88. Rocnik E, Chow LH, Pickering JG. Heat shock protein 47 is expressed in fibrous regions of human atheroma and is regulated by growth factors and oxidized low-density lipoprotein. *Circulation*. 2000;101:1229-33.
89. Morris NP, Fessler LI, Weinstock A, Fessler JH. Procollagen assembly and secretion in embryonic chick bone. *J Biol Chem*. 1975;250:5719-26.
90. Davidson JM, McEneany LS, Bornstein P. Intermediates in the limited proteolytic conversion of procollagen to collagen. *Biochemistry*. 1975;14:5188-94.
91. Botney MD, Liptay MJ, Kaiser LR, Cooper JD, Parks WC, Mecham RP. Active collagen synthesis by pulmonary arteries in human primary pulmonary hypertension. *Am J Pathol*. 1993;143:121-9.
92. Herovici C. A polychrome stain for differentiating precollagen from collagen. *Stain Technology*. 1963;38:204-205.
93. Giddings JC, Jarvis AL, Bloom AL. Differential localisation and synthesis of porcine factor VIII related antigen (VIIIR:AG) in vascular endothelium and in

endothelial cells in culture. *Thromb Res*. 1983;29:299-312.
94. Thubrikar MJ, Robicsek F. Pressure-induced arterial wall stress and atherosclerosis. *Ann Thorac Surg*. 1995;59:1594-603.
95. Jimenez M, Daret D, Choussat A, Bonnet J. Immunohistological and ultrastructural analysis of the intimal thickening in coarctation of human aorta. *Cardiovasc Res*. 1999;41:737-45.
96. Barnes MJ, Morton LF, Levene CI. Synthesis of interstitial collagens by pig aortic endothelial cells in culture. *Biochem Biophys Res Commun*. 1978;84:646-53.
97. Yamamoto M, Yamamoto K, Noumura T. Type I collagen promotes modulation of cultured rabbit arterial smooth muscle cells from a contractile to a synthetic phenotype. *Exp Cell Res*. 1993;204:121-9.
98. Koo EW, Gotlieb AI. Endothelial stimulation of intimal cell proliferation in a porcine aortic organ culture. *Am J Pathol*. 1989;134:497-503.
99. Zalewski A, Shi Y, Johnson AG. Diverse origin of intimal cells: smooth muscle cells, myofibroblasts, fibroblasts, and beyond? *Circ Res*. 2002;91:652-5.
100. Borrione AC, Zanellato AM, Giuriato L, Scannapieco G, Pauletto P, Sartore S. Nonmuscle and smooth muscle myosin isoforms in bovine endothelial cells. *Exp Cell Res*. 1990;190:1-10.
101. Turner CE, Burridge K. Detection of metavinculin in human platelets using a modified talin overlay assay. *Eur J Cell Biol*. 1989;49:202-6.
102. Takeuchi K, Takahashi K, Abe M, Nishida W, Hiwada K, Nabeya T, Maruyama K. Co-localization of immunoreactive forms of calponin with actin cytoskeleton in platelets, fibroblasts, and vascular smooth muscle. *J Biochem (Tokyo)*. 1991;109:311-6.
103. Arciniegas E, Ponce L, Hartt Y, Graterol A, Carlini RG. Intimal thickening involves transdifferentiation of embryonic endothelial cells. *Anat Rec*. 2000;258:47-57.
104. DeRuiter MC, Poelmann RE, VanMunsteren JC, Mironov V, Markwald RR, Gittenberger-de Groot AC. Embryonic endothelial cells transdifferentiate into mesenchymal cells expressing smooth muscle actins in vivo and in vitro. *Circ Res*. 1997;80:444-51.
105. Frid MG, Kale VA, Stenmark KR. Mature vascular endothelium can give rise to smooth muscle cells via endothelial-mesenchymal transdifferentiation: in vitro analysis. *Circ Res*. 2002;90:1189-96.
106. Leung DY, Glagov S, Mathews MB. Cyclic stretching stimulates synthesis of matrix components by arterial smooth muscle cells in vitro. *Science*. 1976;191:475-7.
107. Wilson E, Mai Q, Sudhir K, Weiss RH, Ives HE. Mechanical strain induces growth of vascular smooth muscle cells via autocrine action of PDGF. *J Cell Biol*. 1993;123:741-7.
108. O'Callaghan CJ, Williams B. Mechanical strain-induced extracellular matrix production by human vascular smooth muscle cells: role of TGF-beta(1). *Hypertension*. 2000;36:319-24.

109. Yost MJ, Simpson D, Wrona K, Ridley S, Ploehn HJ, Borg TK, Terracio L. Design and construction of a uniaxial cell stretcher. *Am J Physiol Heart Circ Physiol*. 2000;279:H3124-30.

APPENDIX A
LEAST SQUARES SOLUTIONS FOR DEFORMATION GRADIENT

Basically, tracking three markers provides sufficient information to determine a 2-D deformation gradient $\mathbf{F}$ mapping a line element $\Delta\mathbf{X}$ in the referential configuration β_0 to the corresponding line element $\Delta\mathbf{x}$ in the deformed configuration β, i.e. $\Delta\mathbf{x} = \mathbf{F}\Delta\mathbf{X}$. Details can be found in Ling[39]. Briefly, in a triplet, *A*, *B*, and *C* refer to the markers in the reference configuration, whereas *a*, *b*, and *c* are in any deformed configuration. The three markers define two independent vectors (i.e., $\mathbf{V}_{\mathbf{AB}}$, $\mathbf{V}_{\mathbf{AC}}$ in the reference configuration, $\mathbf{v}_{\mathbf{ab}}$, and $\mathbf{v}_{\mathbf{ac}}$ in the deformed configuration). Assuming that the same $\mathbf{F}$ maps $\mathbf{V}_{\mathbf{AB}}$ and $\mathbf{V}_{\mathbf{AC}}$ in the reference configuration to $\mathbf{v}_{\mathbf{ab}}$ and $\mathbf{v}_{\mathbf{ac}}$ in the current configuration, respectively. That is,

$$\mathbf{v}_{\mathbf{ab}} = \mathbf{F}\cdot\mathbf{V}_{\mathbf{AB}} \Rightarrow \begin{bmatrix} \mathbf{x}_\mathbf{a} - \mathbf{x}_\mathbf{b} \\ \mathbf{y}_\mathbf{a} - \mathbf{y}_\mathbf{b} \end{bmatrix} = \begin{bmatrix} \mathbf{F}_{11} & \mathbf{F}_{12} \\ \mathbf{F}_{21} & \mathbf{F}_{22} \end{bmatrix} \begin{bmatrix} \mathbf{X}_\mathbf{A} - \mathbf{X}_\mathbf{B} \\ \mathbf{Y}_\mathbf{A} - \mathbf{Y}_\mathbf{B} \end{bmatrix}$$

$$\mathbf{v}_{\mathbf{ac}} = \mathbf{F}\cdot\mathbf{V}_{\mathbf{AC}} \Rightarrow \begin{bmatrix} \mathbf{x}_\mathbf{a} - \mathbf{x}_\mathbf{c} \\ \mathbf{y}_\mathbf{a} - \mathbf{y}_\mathbf{c} \end{bmatrix} = \begin{bmatrix} \mathbf{F}_{11} & \mathbf{F}_{12} \\ \mathbf{F}_{21} & \mathbf{F}_{22} \end{bmatrix} \begin{bmatrix} \mathbf{X}_\mathbf{A} - \mathbf{X}_\mathbf{C} \\ \mathbf{Y}_\mathbf{A} - \mathbf{Y}_\mathbf{C} \end{bmatrix}$$

These relations yield four equations of four unknown: $\mathbf{F}_{11}$, $\mathbf{F}_{11}$, $\mathbf{F}_{11}$, $\mathbf{F}_{11}$, which exists an exact solution.

However, what if more than three markers are available for analysis? Least square solution which represents an approach to best-fit the data in an overdetermined system thus comes to our minds. We shall demonstrate its feasibility by looking at the following example.

If the deformation gradient $\mathbf{F}$ is independent of $\mathbf{X}$ for the body of interest (i.e., homogeneous deformation), $\mathbf{x}$ can be given by

$$\mathbf{x} = \mathbf{F}\mathbf{X} + \mathbf{c}$$

where vector $\mathbf{c}$ represents a rigid translation of the whole body. Therefore, for marker *A*, we can express its deformed position vector in the matrix form as follows:

$$\begin{bmatrix} \mathbf{x}_\mathbf{a} \\ \mathbf{y}_\mathbf{a} \end{bmatrix} = \begin{bmatrix} \mathbf{F}_{11} & \mathbf{F}_{12} \\ \mathbf{F}_{21} & \mathbf{F}_{22} \end{bmatrix} \begin{bmatrix} \mathbf{X}_\mathbf{A} \\ \mathbf{Y}_\mathbf{A} \end{bmatrix} + \begin{bmatrix} \mathbf{c}_1 \\ \mathbf{c}_2 \end{bmatrix}$$

We can rearrange the matrix operation:

$$\begin{bmatrix} \mathbf{x_a} \\ \mathbf{y_a} \end{bmatrix} = \begin{bmatrix} \mathbf{X_A} & \mathbf{Y_A} & 0 & 0 & 1 & 0 \\ 0 & 0 & \mathbf{X_A} & \mathbf{Y_A} & 0 & 1 \end{bmatrix} \begin{bmatrix} \mathbf{F_{11}} \\ \mathbf{F_{12}} \\ \mathbf{F_{21}} \\ \mathbf{F_{22}} \\ \mathbf{c_1} \\ \mathbf{c_2} \end{bmatrix}$$

For instance, if we have six markers in track, we can expand the matrix easily. The subscript refers to the markers.

$$\begin{bmatrix} \mathbf{x_a} \\ \mathbf{y_a} \\ \mathbf{x_b} \\ \mathbf{y_b} \\ \mathbf{x_c} \\ \mathbf{y_c} \\ \mathbf{x_d} \\ \mathbf{y_d} \\ \mathbf{x_e} \\ \mathbf{y_e} \\ \mathbf{x_f} \\ \mathbf{y_f} \end{bmatrix} = \begin{bmatrix} \mathbf{X_A} & \mathbf{Y_A} & 0 & 0 & 1 & 0 \\ 0 & 0 & \mathbf{X_A} & \mathbf{X_A} & 0 & 1 \\ \mathrm{X_B} & \mathbf{Y_B} & 0 & 0 & 1 & 0 \\ 0 & 0 & \mathbf{X_B} & \mathbf{Y_B} & 0 & 1 \\ \mathbf{X_C} & \mathbf{Y_C} & 0 & 0 & 1 & 0 \\ 0 & 0 & \mathbf{X_C} & \mathbf{Y_C} & 0 & 1 \\ \mathbf{X_D} & \mathbf{Y_D} & 0 & 0 & 1 & 0 \\ 0 & 0 & \mathbf{X_D} & \mathbf{Y_D} & 0 & 1 \\ \mathbf{X_E} & \mathbf{Y_E} & 0 & 0 & 1 & 0 \\ 0 & 0 & \mathbf{X_E} & \mathbf{Y_E} & 0 & 1 \\ \mathbf{X_F} & \mathbf{Y_F} & 0 & 0 & 1 & 0 \\ 0 & 0 & \mathbf{X_F} & \mathbf{Y_F} & 0 & 1 \end{bmatrix} \begin{bmatrix} \mathbf{F_{11}} \\ \mathbf{F_{12}} \\ \mathbf{F_{21}} \\ \mathbf{F_{22}} \\ \mathbf{c_1} \\ \mathbf{c_2} \end{bmatrix} \quad \text{or} \quad [\mathbf{b}] = [\mathbf{A}][\mathbf{Y}]$$

where $[\mathbf{b}]$ is $\begin{bmatrix} \mathbf{x_a} \\ \mathbf{y_a} \\ \mathbf{x_b} \\ \mathbf{y_b} \\ \mathbf{x_c} \\ \mathbf{y_c} \\ \mathbf{x_d} \\ \mathbf{y_d} \\ \mathbf{x_e} \\ \mathbf{y_e} \\ \mathbf{x_f} \\ \mathbf{y_f} \end{bmatrix}$, $[\mathbf{A}]$ is $\begin{bmatrix} \mathbf{X_A} & \mathbf{Y_A} & 0 & 0 & 1 & 0 \\ 0 & 0 & \mathbf{X_A} & \mathbf{X_A} & 0 & 1 \\ \mathrm{X_B} & \mathbf{Y_B} & 0 & 0 & 1 & 0 \\ 0 & 0 & \mathbf{X_B} & \mathbf{Y_B} & 0 & 1 \\ \mathbf{X_C} & \mathbf{Y_C} & 0 & 0 & 1 & 0 \\ 0 & 0 & \mathbf{X_C} & \mathbf{Y_C} & 0 & 1 \\ \mathbf{X_D} & \mathbf{Y_D} & 0 & 0 & 1 & 0 \\ 0 & 0 & \mathbf{X_D} & \mathbf{Y_D} & 0 & 1 \\ \mathbf{X_E} & \mathbf{Y_E} & 0 & 0 & 1 & 0 \\ 0 & 0 & \mathbf{X_E} & \mathbf{Y_E} & 0 & 1 \\ \mathbf{X_F} & \mathbf{Y_F} & 0 & 0 & 1 & 0 \\ 0 & 0 & \mathbf{X_F} & \mathbf{Y_F} & 0 & 1 \end{bmatrix}$, and $[\mathbf{Y}]$ is $\begin{bmatrix} \mathbf{F_{11}} \\ \mathbf{F_{12}} \\ \mathbf{F_{21}} \\ \mathbf{F_{22}} \\ \mathbf{c_1} \\ \mathbf{c_2} \end{bmatrix}$.

Basically, to be able to solve six unknowns (4 from $\mathbf{F}$ and 2 from $\mathbf{c}$), it requires only six equations, that is, three markers. Apparently we have more than we need. Still we can get a least square solution by calculating the pseudo-inverse of $[\mathbf{A}]$; i.e., $[\mathbf{Y}] = pinv[\mathbf{A}][\mathbf{b}]$.

Following is a Matlab® code for calculating the deformation gradient and the

associated principal Green strains based on position vectors of six markers in the deformed configuration and reference configuration.

```
% R6r('reference_f','current_f', r1,r2,r3,r4,r5,r6, p1,p2,p3,p4,p5,p6)
% For a homogeneous deformation => x = FX + c, where x is the position vector in the current
configuration,
% X that in the reference configuration, F the deformation gradient, and c a constant vector.

function R6r(ref_file, cur_file, r1,r2,r3,r4,r5,r6, p1,p2,p3,p4,p5,p6)

X=load(ref_file);
X0=X(1,:);
% 1st row in reference data
ZeroF=X(1,26);
% The force in the reference configuration should be zero; used as a simple calibration.

A=zeros(12,6);

A(1,1)=X0(2*r1-1);A(1,2)=X0(2*r1);A(1,5)=1.0;
A(2,3)=X0(2*r1-1);A(2,4)=X0(2*r1);A(2,6)=1.0;
A(3,1)=X0(2*r2-1);A(3,2)=X0(2*r2);A(3,5)=1.0;
A(4,3)=X0(2*r2-1);A(4,4)=X0(2*r2);A(4,6)=1.0;
A(5,1)=X0(2*r3-1);A(5,2)=X0(2*r3);A(5,5)=1.0;
A(6,3)=X0(2*r3-1);A(6,4)=X0(2*r3);A(6,6)=1.0;
A(7,1)=X0(2*r4-1);A(7,2)=X0(2*r4);A(7,5)=1.0;
A(8,3)=X0(2*r4-1);A(8,4)=X0(2*r4);A(8,6)=1.0;
A(9,1)=X0(2*r5-1);A(9,2)=X0(2*r5);A(9,5)=1.0;
A(10,3)=X0(2*r5-1);A(10,4)=X0(2*r5);A(10,6)=1.0;
A(11,1)=X0(2*r6-1);A(11,2)=X0(2*r6);A(11,5)=1.0;
A(12,3)=X0(2*r6-1);A(12,4)=X0(2*r6);A(12,6)=1.0;

Data=load(cur_file);

[n,m]=size(Data);   % n= the number of rows, m= the number of columns

for i=1:n
   B(1)= Data(i,p1*2-1);B(2)= Data(i,p1*2);
   B(3)= Data(i,p2*2-1);B(4)= Data(i,p2*2);
   B(5)= Data(i,p3*2-1);B(6)= Data(i,p3*2);
   B(7)= Data(i,p4*2-1);B(8)= Data(i,p4*2);
   B(9)= Data(i,p5*2-1);B(10)= Data(i,p5*2);
   B(11)= Data(i,p6*2-1);B(12)= Data(i,p6*2);

   Y=pinv(A)*B;       %Y(1)=F11, Y(2)=F12, Y(3)=F21 ,Y(4)=F22, Y(5)=c1, Y(6)=c2

   C(1,1)=Y(1)^2+Y(3)^2;                %C_11
   C(2,2)=Y(2)^2+Y(4)^2;                %C_22
   C(1,2)=Y(1)*Y(2)+Y(3)*Y(4);               %C_12
   C(2,1)=C(1,2);
   Out(i,1)=0.5*(Y(1)^2+Y(3)^2-1.0);                %E_11
   Out(i,2)=0.5*(Y(2)^2+Y(4)^2-1.0);                %E_22
   Out(i,3)=0.5*(Y(1)*Y(2)+Y(3)*Y(4));            %E_12
   Out(i,4)=Data(i,25);                             %Pressure
   Out(i,5)=Data(i,26);                 %Force

   [V,D]=eig(C);
   inv1(i)=trace(C)-2;
   inv2(i)=det(C)-1;

   Vec(i,1)=acos(V(1,1));
```

```
    Vec(i,2)=asin(V(2,1));
    Vec(i,3)=acos(V(1,2));
    Vec(i,4)=asin(V(2,2));

    if (Vec(i,1)<0.7854)|(2.3562<Vec(i,1))  % theta < pi/4 or 3pi/4 < theta
        Val(i,1)=D(1,1);    % axial
        Val(i,2)=D(2,2);    % tangential
    else
        Val(i,2)=D(1,1);
        Val(i,1)=D(2,2);
    end
end

R1=(sqrt(Val(:,1)))';   % U = sqrt(C)
R2=(sqrt(Val(:,2)))';
E1=((Val(:,1))'-1)/2;      % R^2 = 2E+1
E2=((Val(:,2))'-1)/2;
P=(Out(:,4))';
F=(Out(:,5))'-ZeroF;

figure(1);

subplot(3,3,3);
plot(P,R1);
axis([0 125 1 1.35]);
xlabel('Pressure (mmHg)');
ylabel('Principal stretch 1');
ps1=[P;R1];
out_f1=strcat(cur_file,'.rr1');  % Name the output file
dlmwrite(out_f1,ps1,'\t');

subplot(3,3,6);
plot(P,R2);
axis([0 125 1 1.35]);
xlabel('Pressure (mmHg)');
ylabel('Principal stretch 2');
ps2=[P;R2];
out_f2=strcat(cur_file,'.rr2');  % Name the output file
dlmwrite(out_f2,ps2,'\t');

subplot(3,3,2);
plot(P,E1);
axis([0 125 0 0.35]);
xlabel('Pressure (mmHg)');
ylabel('Principal strain 1');
Strain1=[P;E1];
out_f3=strcat(cur_file,'.re1');  % Name the output file
dlmwrite(out_f3,Strain1,'\t');

subplot(3,3,5);
plot(P,E2);
axis([0 125 0 0.35]);
xlabel('Pressure (mmHg)');
ylabel('Principal strain 2');
Strain2=[P;E2];
out_f4=strcat(cur_file,'.re2');  % Name the output file
dlmwrite(out_f4,Strain2,'\t');

subplot(3,3,1);
plot(Out(:,4),Out(:,1));
axis([0 125 0.0 0.35]);
xlabel('Pressure (mmHg)');
ylabel('Exx');
```

```
subplot(3,3,4);
plot(Out(:,4),Out(:,2));
axis([0 125 0 0.35]);
xlabel('Pressure (mmHg)');
ylabel('Eyy');

subplot(3,3,7);
plot(Out(:,4),Out(:,3));
axis([0 125 -0.15 0.15]);
xlabel('Pressure (mmHg)');
ylabel('Exy');

subplot(3,3,8);
plot(P,F);
axis([0 125 0 5]);
xlabel('Pressure (mmHg)');
ylabel('Force');
ps1=[P;F];
out_f1=strcat(cur_file,'.f');   % Name the output file
dlmwrite(out_f1,ps1,'\t');

subplot(3,3,9);
plot(Out(:,4),Vec(:,1)/3.14159*2);
axis([0 125 0 2]);
xlabel('Pressure (mmHg)');
ylabel('theta');

figure(2);

subplot(2,1,1);
plot(P,inv1);
axis([0 125 0 1.5]);
xlabel('Pressure (mmHg)');
ylabel('tr(C)-2');
ps1=[P;inv1];
out_f1=strcat(cur_file,'.inv1');   % Name the output file
dlmwrite(out_f1,ps1,'\t');

subplot(2,1,2);
plot(P,inv2);
axis([0 125 0 1.5]);
xlabel('Pressure (mmHg)');
ylabel('det(C)-1');
ps2=[P;inv2];
out_f2=strcat(cur_file,'.inv2');   % Name the output file
dlmwrite(out_f2,ps2,'\t');

clear all;
```

APPENDIX B

GENERAL INFORMATION OF EXPERIMENTAL ANIMALS

TABLE B-1. Clinical Details of Hypertensive Pigs

No	Euth. Date (yy-mm-dd)	Treatment	Age (month)	Weight (kg)	Averaged MAP (mmHg)	Pulse Pressure (mmHg)
1	03-01-08	2H	10	37	158	52
2	03-03-24	2H	9	37	158	57
3	03-04-25	2H	12	30	152	36
4	04-05-05	2H	7	40	156	56
5	04-06-25	2H	8	42	155	40
6	04-10-01	2H	10	36	153	51
7	04-10-28	2H	11	50	145	46
12	02-09-25	4H	11	41	182	62
13	02-11-25	4H	13	46	167	38
14	02-12-04	4H	15	41	167	49
15	02-12-11	4H	9	41	179	57
16	03-01-29	4H	11	31	173	66
17	03-02-21	4H	12	36	153	44
18	04-10-25	4H	11	48	175	60
23	03-05-21	6H	7	32	147	44
24	03-06-09	6H	9	40	179	37
25	03-06-18	6H	10	33	174	49
26	04-03-31	6H	9	50	188	58
27	04-04-07	6H	10	52	161	58
28	04-11-30	6H	12	34	154	49
32	03-04-02	8H	13	34	159	41
33	03-04-18	8H	11	40	185	41

TABLE B-1 (Continued)

No	Euth. Date (yy-mm-dd)	Treatment	Age (month)	Weight (kg)	Averaged MAP (mmHg)	Pulse Pressure (mmHg)
34	03-05-02	8H	11	42	174	56
35	03-06-11	8H	9	34	205	67
36	04-02-25	8H	9	104	203	69
37	04-11-02	8H	13	50	161	60

TABLE B-2. Clinical Details of Surgical and True Control Pigs

No	Euth. Date	Treatment	Age (month)	Weight (kg)	Averaged MAP (mmHg)	Pulse Pressure (mmHg)
1	02-08-29	2N	10	43	131	31
2	04-06-14	2N	8	42	123	28
3	04-06-16	2N	8	32	134	49
4	04-08-31	2N	10	30	128	38
5	02-11-13	4N	13	39	N/A	
6	04-02-11	4N	9	110	141	37
7	04-06-21	4N	8	34	135	41
8	04-08-04	4N	10	32	129	48
9	03-02-12	6N	11	30	134	28
10	04-06-30	6N	8	40	120	39
11	05-03-12	6N	10	36	118	36
12	03-03-26	8N	12	26	130	40
13	03-05-07	8N	11	37	138	44
14	03-08-28	8N	16	34	134	41
15	03-11-21	8N	13	55	133	43
16	04-02-18	SC	8	80	132	38
17	04-03-03	SC	10	110	125	32
18	04-03-10	SC	9	35	N/A	N/A
19	03-08-26	UC	10	40	140	33
20	04-11-15	UC	12	32	N/A	N/A

SC: surgery control; UC: un-operated control; N/A: not available.

APPENDIX C

PROTOCOL FOR VERHOEFF'S VAN-GIESON (VVG) STAIN

Solutions:

Verhoeff's Elastic Stain: Stable for 2-3 weeks

Prepare fresh each time. **Add in order and mix between additions**:
A – 120 mL; B – 80 mL; C – 40 mL

A. 2 % Hematoxylin in 95 % ethanol

Hematoxylin	20 g
95 % ethanol	1000 mL

B. Acidified ferric chloride

$FeCl_3 \cdot 6H_2O$	12.4 g
Distilled water	495 mL
Conc. HCl	5 mL

C. Iodine: 2 % I_2 in 4 % KI aq. solution

I_2	5 g
KI	10 g
Distilled water	250 mL

1 % Ferric Chloride: Dilute from 10% ferric chloride. (25:225)

10 % Ferric Chloride (store in the refrigerator)

$FeCl_3 \cdot 6H_2O$	50.0 g
Distilled water	500 mL

5 % Sodium thiosulfate

Sodium Thiosulfate	12.5 g
Distilled water	250 mL

Van Gieson's solution

1 % aqueous acid fuchsin	15 mL
Saturated aq. picric acid	235 mL

Add some solid picric acid to assure saturation. (allow to stand 24 hours before use)

Procedure:

1. Deparaffinize sections and hydrate to dH_2O.
2. Place sections in Verhoeff's elastic stain for 60 min.
3. Wash in a few changes of dH_2O until the water becomes clear.
4. Differentiate in 1% ferric chloride solution. (Generally 10 dips are sufficient for FRESH solutions.) Check microscopically. Elastic fibers are black and sharply fined; the background is gray. If the sections are differentiated too far, restain.
5. Rinse in dH_2O twice to dilute the ferric chloride ASAP.
6. Place in 5% sodium thiosulfate solution for 1 min.

7. Rinse in dH_2O.
8. Wash in running tap water for 5 min.
9. Counterstain with van Gieson's solution for 1 min (Note: Do not prolong staining as picric acid will differentiate the elastic stain further)
10. Dehydrate rapidly in four changes of absolute alcohol (1st: 20 dips; 2nd: 30 dips; 3rd: 1 min; 4th: 1 min), clear in xylene, and mount in Permount. (Note: prolonged immersion in alcohol will slowly extract picric acid, but not acid fuchsine; end up losing one color)

Result:

Elastic fibers and nuclei – blue-black to black; collagen – red; other tissue elements – yellow.

APPENDIX D

PROTOCOL FOR PICRO-SIRIUS RED (PSR) STAIN

Solutions:

0.2 % Phosphomolybdic Acid (stable for 6 months)

Phosphomolybdic acid	0.5 g
Distilled water	250 mL

0.1 % picro-Sirius red in saturated picric acid solution

Sirius red F3BA (C.I. 35780)	0.5 g
Saturated aq. picric acid	500 mL

Add some solid picric acid to assure saturation. (allow to stand 24 hours before use)

Procedure:

11. Deparaffinize sections and hydrate to dH_2O. (Thorough washing of sections prior to staining is essential. Rehydration, i.e., adsorption of water molecules by the charged groups of tissue structures, causes swelling, which permits the large Sirius red F3BA molecule to penetrate connective tissue fibers)
12. Place sections in 0.2% phosphomolybdic acid for 1 min.
13. Rinse in dH_2O.
14. Place sections in 0.1% picro-Sirius red F3BA solution for 60 min.
15. Dehydrate rapidly in four changes of absolute alcohol (1st: 20 dips; 2nd: 30 dips; 3rd: 1 min; 4th: 1 min), clear in xylene, and mount in Permount. (Note: prolonged immersion in alcohol will slowly extract picric acid)

Result:

Stains fibrillar collagen (I) and (III):
Under normal light – collagen: red
Under polarized light – Collagen (I): yellow; collagen (III) green

Note: For the study of collagens (II) and (III), it is essential to use an intense light.

APPENDIX E
PROTOCOL FOR ANTIGEN RETRIEVAL

Formalin fixation forms protein cross-links that usually mask the antigenic sites in the tissues, causing weak or false negative staining of immunohistochemistry. This issue can largely be resolved by performing antigen retrieval (AR) prior to incubation of primary antibody. For example, the sections can undergo heat-induced epitope retrieval (HIER) to unmask the antigenic sites. Unfortunately, no universal protocol works for all antigens; trial and error is thus necessary to determine the optimal AR condition for each antigen. Two types of procedures are regularly employed on formalin-fixed paraffin-embedded (FFPE) sections to reveal the antigenic sites: HIER and enzymatic digestion.

HIER. Three retrieval solutions were tried: (1) 1 mM EDTA solution (pH=8.0), (2) 10 mM citrate buffer (pH=6.0), and (3) 10 mM Tris buffer with 1 mM EDAT (pH=9.0). Heat could either be provided by microwave or pressure cooker. Generally, 2*5-minute microwaving or 2-minute pressure cooking will do the job. The slides were allowed to cool for 20 min after these treatments.

Enzymatic digestion. Five enzymes were tried: (1) trypsin (Sigma) at 37°C, (2) pepsin (Dako) at 37°C, (3) pronase (Dako) at room temperature, (4) proteinase K (Dako) at room temperature, and (5) proteolytic enzyme (Dako) at room temperature. The incubation time must be determined for each antigen.

APPENDIX F
PROTOCOL FOR IMMUNOHISTOCHEMISTRY

1. Block endogenous peroxidase by incubating the sections in 0.3% H_2O_2 methanol solution for 20 minutes.
2. Block nonspecific sites by incubating the sections in normal serum for 30 minutes.
3. Drain off the solution on the sections. DO NOT rinse. (The interactions between blocking serum and the nonspecific sites are weak.)
4. Incubate the sections for one hour with appropriately diluted primary antibody.
5. Wash slides with PBS for several times.
6. Incubate the sections for 30 minutes with universal biotinylated secondary antibody.
7. Wash slides with PBS for several times.
8. Incubate the sections for 30 minutes with streptavidin-horseradish peroxidase (HRP) conjugate (Vector Laboratories, CA).
9. Wash the slides with PBS for several times.
10. Incubate the sections in DAB substrate (Vector Laboratories, CA) until achieving desired stain intensity. Generally, 3-5 minutes are sufficient.
11. Rinse the sections in tap water.
12. Counterstain with Mayer's Hematoxylin (5 dips).
13. Dehydrate through graded alcohol series (95%→100%→100%→100%; 2 min for each step with agitation), clear in xylene (twice; 5 min each). Coverslip with Permount (Fisher Scientific) Alternatively, apply Crystal/Mount (Biomeda) to the tissue section. Place the slides at 20-37°C for 1-2 hours. Slides with hardened Crystal/Mount can be post-mounted and coverslipped in Permount.

VITA

Name: Jin-Jia Hu

Address: Texas A&M University
Biomedical Engineering Department
337 Zachry Engineering Center
College Station, TX 77840

Email Address jjhu1127@hotmail.com

Collegiate Education:

Institution	Major	Degree	Date of Graduation
Texas A&M University	Biomedical Engineering	Ph. D.	2005
National Taiwan University	Chemical Engineering	M. S.	1998
National Taiwan University	Chemical Engineering	B. S.	1994